In vitro reprogramming of glial cells from adult dorsal root ganglia into nociceptor-like neurons

In vitro Reprogrammierung von Gliazellen aus adulten Spinalganglien in Nozizeptor-ähnliche Neurone

Doctoral thesis for a doctoral degree
at the Graduate School of Life Sciences,
Julius-Maximilians-Universität Würzburg,
Section **Neuroscience**
submitted by

Annemarie Schulte
from
Damme

Würzburg 2022

Submitted on: ……..……..

Office stamp

Members of the Thesis Committee

Chairperson:	**Prof. Dr. Markus Sauer**
Primary Supervisor:	**Prof. Dr. Heike Rittner**
Supervisor (Second):	**PD Dr. Robert Blum**
Supervisor (Third):	**Prof. Dr. Erhard Wischmeyer**

Table of contents

Abstract

Plexus injury often occurs after motor vehicle accidents and results in lifelong disability with severe neuropathic pain. Surgical treatment can partially restore motor functions, but sensory loss and neuropathic pain persist. Regenerative medicine concepts, such as cell replacement therapies for restoring dorsal root ganglia (DRG) function, set high expectations. However, up to now, it is unclear which DRG cell types are affected by nerve injury and can be targeted in regenerative medicine approaches.

This study followed the hypothesis that satellite glial cells (SGCs) might be a suitable endogenous cell source for regenerative medicine concepts in the DRG. SGCs originate from the same neural crest-derived cell lineage as sensory neurons, making them attractive for neural repair strategies in the peripheral nervous system. Our hypothesis was investigated on three levels of experimentation. First, we asked whether adult SGCs have the potential of sensory neuron precursors and can be reprogrammed into sensory neurons *in vitro*. We found that adult mouse DRG harbor SGC-like cells that can still dedifferentiate into progenitor-like cells. Surprisingly, expression of the early developmental transcription factors Neurog1 and Neurog2 was sufficient to induce neuronal and glial cell phenotypes. In the presence of nerve growth factor, induced neurons developed a nociceptor-like phenotype expressing functional nociceptor markers, such as the ion channels TrpA1, TrpV1 and $Na_V1.9$. In a second set of experiments, we used a rat model for peripheral nerve injury to look for changes in the DRG cell composition. Using an unbiased deep learning-based approach for cell analysis, we found that cellular plasticity responses after nerve injury activate SGCs in the whole DRG. However, neither injury-induced neuronal death nor gliosis was observed. Finally, we asked whether a severe nerve injury changed the cell composition in the human DRG. For this, a cohort of 13 patients with brachial plexus injury was investigated. Surprisingly, in about half of all patients, the injury-affected DRG showed no characteristic DRG tissue. The complete entity of neurons, satellite cells, and axons was lost and fully replaced by mesodermal/connective tissue. In the other half of the patients, the basic cellular entity of the DRG was well preserved. Objective deep learning-based analysis of large-scale bioimages of the “intact” DRG showed no loss of neurons and no signs of gliosis.

This study suggests that concepts for regenerative medicine for restoring DRG function need at least two translational research directions: reafferentation of existing DRG units or full replacement of the entire multicellular DRG structure. For DRG replacement, SGCs of the adult DRG are an attractive endogenous cell source, as the multicellular DRG units could possibly be rebuilt by transdifferentiating neural crest-derived sensory progenitor cells into peripheral sensory neurons and glial cells using Neurog1 and Neurog2.

Zusammenfassung

Plexusläsionen treten häufig nach Verkehrsunfällen auf und führen zu lebenslangen Einschränkungen mit starken neuropathischen Schmerzen. Eine operative Behandlung kann die motorischen Funktionen teilweise wiederherstellen, dennoch bleiben Verlust der Sensorik und neuropathische Schmerzen bestehen. Ansätze der regenerativen Medizin, wie z. B. Zellersatztherapien zur Wiederherstellung der Funktion der Spinalganglien, wecken hohe Erwartungen. Bislang ist jedoch vollkommen unklar, welche Zelltypen der Spinalganglien von der Nervenverletzung betroffen sind und bei Ansätzen der regenerativen Medizin gezielt eingesetzt werden sollten.

Hier war die Hypothese, dass Satellitengliazellen (SGCs) eine geeignete endogene Zellquelle für Ansätze der regenerativen Medizin in den Spinalganglien sein könnten. SGCs und sensorische Neurone stammen von denselben Stammzellen der Neuralleiste ab, was SGCs für neurale Reparaturstrategien im peripheren Nervensystem attraktiv macht. Unsere Hypothese wurde auf drei Ebenen experimentell untersucht.

Zuerst stellten wir die Frage, ob adulte SGCs das Potenzial haben, neuronale Vorläufermerkmale anzunehmen und *in vitro* in sensorische Neuronen reprogrammiert werden können. Hierbei zeigte sich, dass Spinalganglien der Maus adulte SGC-ähnliche Zellen beherbergen, die sich in vorläuferähnliche Zellen dedifferenzieren können. Überraschenderweise war die Expression der frühen entwicklungsrelevanten Transkriptionsfaktoren Neurog1 und Neurog2 ausreichend, um neuronale und gliale Phänotypen zu induzieren. In Anwesenheit des Neurotrophins NGF (nerve growth factor) entwickelten die induzierten Neurone einen Nozizeptor-ähnlichen Phänotyp, der funktionelle Marker für Nozizeptoren wie die Ionenkanäle TrpA1, TrpV1 und $Na_V1.9$ exprimierte.

In einer zweiten Reihe von Experimenten haben wir in einem Rattenmodell für periphere Nervenverletzungen Veränderungen in der Zellzusammensetzung von Spinalganglien untersucht. Mithilfe eines objektiven Deep Learning basierten Ansatzes zur Bildanalyse fanden wir im gesamten DRG SGCs, die auf Nervenverletzungen mit einer hohen zellulären Plastizität reagierten. Es wurde jedoch weder ein verletzungsbedingter neuronaler Verlust noch eine Gliose beobachtet.

Schließlich untersuchten wir, ob eine schwere Nervenverletzung die Zellzusammensetzung in menschlichen Spinalganglien verändert. Dazu wurde eine Kohorte von 13 Patienten mit einer Verletzung des *Plexus brachialis* untersucht. Überraschenderweise zeigte sich in verletzten Spinalganglien bei etwa der Hälfte aller Patienten kein Spinalgangliengewebe mehr. Die gesamte Einheit aus Neuronen, Satellitengliazellen und Axonen war verloren und vollständig durch mesodermales Bindegewebe ersetzt. Bei der anderen Hälfte der Patienten war die grundlegende zelluläre Einheit des Spinalganglions gut erhalten. Eine objektive, auf Deep

Learning basierende Analyse von großflächigen Mikroskopiebildern des "intakten" Spinalganglions zeigte keinen Verlust von Neuronen und keine Anzeichen von Gliose.
Diese Studie legt nahe, dass zur Wiederherstellung der Funktionen des Spinalganglions mindestens zwei translationale Forschungsrichtungen der regenerativen Medizin erforderlich sind: Reafferenzierung bestehender Spinalganglion-Einheiten oder vollständiger Ersatz der gesamten multizellulären Spinalganglion-Struktur. Für den Ersatz des Spinalganglions sind SGCs des adulten Spinalganglions eine plausible endogene Zellquelle. Die multizellulären Einheiten des Spinalganglions könnten möglicherweise durch eine Neurog1- und Neurog2-induzierte Transdifferenzierung von sensorischen Vorläuferzellen der Neuralleiste in periphere sensorische Neuronen und Gliazellen wiederaufgebaut werden.

1 Introduction

Chronic pain is a major public health problem. In Germany, 23 million people suffer from chronic pain and for 7 million people, the pain has a significant impact on their lives (Hauser et al. 2014). A subgroup of these patients endures neuropathic pain, which is defined as “pain caused by a lesion or disease of the somatosensory nervous system”. Neuropathic pain often transits from acute to chronic because healing and regeneration of the peripheral nervous system are limited. Thus, about 7-8% of the European population suffers from chronic neuropathic pain. The significance of chronic pain is now considered in the ICD-11, which includes entities like chronic neuropathic pain and chronic postsurgical pain.

In general, neuropathic pain is generated by primary sensory afferents (Sommer et al, 2018). Primary sensory afferents are comprised of C-, Aδ- and Aβ fibers (Basbaum *et al*, 2009). C- and Aδ fibers react to noxious stimuli, while Aβ fibers respond to stretch, indentation, or vibration. In a simplistic overview, nociceptors are ascribed to C- and Aδ fibers, and mechano- and proprioceptors to Aβ fibers, although the reality is far more complex (Crawford & Caterina, 2020). Across species, there are different sensory neuron subtypes, each with unique expression patterns, functions, and contributions to chronic pain (Kupari *et al*, 2021; Usoskin *et al*, 2015). Especially nociceptors generate neuropathic pain because their activity and excitability directly influence how strongly impulses are transmitted to the central nervous system (CNS) (Cummins *et al*, 2007; Kleggetveit *et al*, 2012).

Another fundamental principle of nociceptive and pathological pain is the involvement of inflammatory processes (Ji et al, 2016). This can trigger a higher spontaneous action potential firing of nociceptors but can also cause increased responsiveness to pain-inducing irritants (Ji et al., 2016; Martin et al, 2018). Although inflammatory processes and activation of nociceptors play a crucial role in certain pain syndromes, the etiology of neuropathic pain after traumata and peripheral nerve lesions is not well understood.

Traumata or accidents can cause severe neuropathic pain. For instance, traffic accidents with motorcycles can cause a plexus injury, such as dorsal root avulsion (Figure 1).

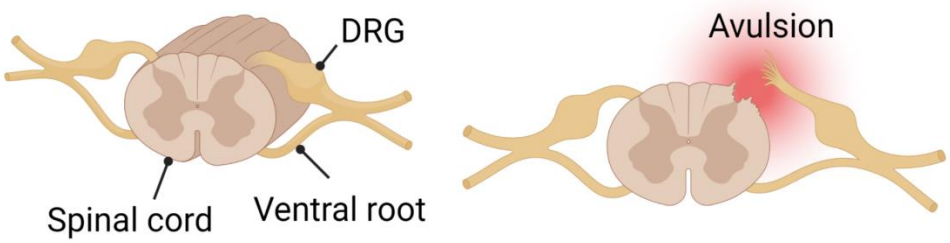

Figure 1. Scheme of DRG and spinal cord showing dorsal root avulsion. Created with BioRender.com.

Although plexus injuries occur rarely, it is no less of a burden for patients, as plexus damage inevitably leads to functional limitations and severe neuropathic pain with lifelong disability (Haldane *et al*, 2022). Treatment of this loss of neuronal function is particularly difficult as surgery often alleviates only motoric dysfunction but not sensory loss or chronic neuropathic pain. Indeed, 76 % of patients still suffer from chronic pain after brachial plexus injury surgery (Rasulić *et al*, 2017). Reasons for this might be the lack of sensory input and ectopic firing in the dorsal horn, regenerating axons from non-avulsed roots (Bertelli & Ghizoni, 2010), or the loss of peripheral sensory neurons in the DRG (Teixeira *et al*, 2015). Better understanding of the pathophysiology is needed so that new molecular treatment options, such as pathfinding strategies, or regenerative medicine (Aldskogius & Kozlova, 2021; Hoeber *et al*, 2015), can be developed.

In preclinical models of peripheral nerve injury, the contribution of neuronal loss in the DRG to neuropathic pain is controversial. After sciatic nerve axotomy, a significant loss of neurons was observed, peaking at 30-35% loss after 2-4 weeks (Kuo *et al*, 2005; McKay Hart *et al*, 2002). However, neuronal loss is not seen in other preclinical models (Schulte *et al*, 2022c), raising the question of whether neuronal loss after peripheral nerve injury is more likely to be a model-specific effect, dependent on severity and location of the injury (Menorca *et al*, 2013). Furthermore, it is questionable how the loss of DRG neurons, particularly nociceptors, may contribute to neuropathic pain. Genetic ablation of nociceptors could fully abrogate neuropathic pain, even months after spared nerve injury (SNI) (Gangadharan *et al*, 2022), which rather indicates the opposite. The study also showed that allodynia was driven by structural plasticity, abnormal terminal connectivity, and malfunction of nociceptors during reinnervation of affected areas (Cranfill & Luo, 2022).

For restoring sensory functions, regeneration of different motor, sensory and nociceptive elements of the nervous system impaired after injury could be helpful (Rodríguez *et al*, 2004). Despite the ambiguities whether neurons persist or are lost after injury, research follows the idea to replace potentially lost neurons. For neuronal replacement concepts, three approaches are investigated: transplantation of neuronal progenitor cells (NPCs), recruitment of neuronal cells from neural stem cells, or reprogramming (transdifferentiation) of body-own cells from a local cell source (Gascon *et al*, 2017; Grade & Götz, 2017). As integration of transplanted cells is challenging and neural stem cells are unlikely to be found outside of the hippocampus in the human nervous system (Assinck *et al*, 2017; Ernst & Frisen, 2015), utilization of endogenous cells with plasticity potential might be more promising.

Endogenous replacement therapy is a well-known concept for regenerative medicine in the CNS. Here, astrocytes change their properties after injury, become reactive glial cells, and start to proliferate (gliosis) (Buffo *et al*, 2008). *In vitro*, fast-dividing astrocytes show properties of reactive glial cells and can be reprogrammed into different neuron subtypes (Blum *et al*,

2011; Dimou & Götz, 2014; Gascon *et al.*, 2017; Heinrich *et al*, 2010). Based on this *in vitro* research, it was also shown that *in vivo* reprogramming of astrocytes into subtype-specific neurons and integration into a functional system is possible (Bocchi & Götz, 2020; Li & Chen, 2016).

In the peripheral nervous system (PNS), it is less clear whether gliosis occurs and whether such glial cell reactivity can be used for regenerative purposes. In the DRG, two glial cell types are good candidates for regenerative medicine through reprogramming: the satellite glial cells (SGCs) or the Schwann cells. For Schwann cells, there is no good evidence for an atypical accumulation, focal proliferation (gliosis), or re-juvenilization (Jessen & Mirsky, 2019). However, at least SGCs show strong plasticity and reactivity after injury (Avraham *et al*, 2020; Gehrmann *et al*, 1991; Jager *et al*, 2020; Schulte *et al.*, 2022c). SGCs have some unique properties: They tightly envelop sensory neurons in the peripheral ganglia and control the neuronal microenvironment, similar to astrocytes in the CNS (Hanani & Spray, 2020). In response to neuronal stress and nerve damage, SGCs show increased expression of glial fibrillary acidic protein (GFAP) and apolipoprotein J (APOJ) (Avraham *et al.*, 2020; Woodham *et al*, 1989), and contribute to neuropathic pain (Kim *et al*, 2016; Liu *et al*, 2012; Warwick & Hanani, 2013). Moreover, SGCs show plasticity towards different subtypes, e.g., towards an SGC type enriched in immune-response genes (Avraham *et al*, 2021; Mapps *et al*, 2022).

Interestingly, SGCs might acquire neural progenitor-like properties in the course of an injury. Pluripotent and progenitor-like cells are found in both embryonic and adult DRG (Li *et al*, 2007; Ogawa *et al*, 2017; Tasdemir-Yilmaz *et al*, 2021) and might develop into neurons after injury (Gallaher *et al*, 2014; Muratori *et al*, 2015; Zhang *et al*, 2019). *In vitro*, SGCs show progenitor markers (Jager *et al*, 2022) and can be differentiated into sensory neurons (Wang *et al*, 2021). Their similarity to Schwann cell precursors (SCPs), possibly in a developmentally arrested state (George *et al*, 2018), and the common developmental origin of sensory neurons and SGCs (Newbern, 2015) makes them particularly useful for regeneration and transdifferentiation into sensory neurons (Milichko & Dyachuk, 2020).

Reprogramming and differentiation into specific cell types are classically conducted with induced pluripotent stem cells (iPSCs) (Takahashi & Yamanaka, 2006). From them, also sensory neurons can be made, which is mainly done to study molecular mechanisms that contribute to pain *in vitro*. Human sensory neurons can be induced with small molecule inhibitors (Chambers *et al*, 2012; Eberhardt *et al*, 2015). However, iPSC-derived sensory neurons show considerable heterogeneity in their genetic profile (Schwartzentruber *et al*, 2018). This high variability leads to a high n-number needed to detect disease-related effects with moderately large effect sizes (Schwartzentruber *et al.*, 2018), which is hardly scalable in disease modeling studies.

An alternative is the forced expression of transcription factors in iPSCs, which has also been used for reprogramming strategies toward sensory neurons (Holzer *et al*, 2022; Nickolls *et al*, 2020). Transcription factor expression was even sufficient to directly reprogram fibroblasts into sensory, possibly nociceptor-like neurons (Blanchard *et al*, 2015; Wainger *et al*, 2015; Xiao *et al*, 2020). In these experiments, forced viral expression of the transcription factors Neurog1, Neurog2 (neurogenins), and/or Brn3a was sufficient to induce sensory neuron phenotypes (Blanchard *et al.*, 2015; Holzer *et al.*, 2022). These transcription factors play a central role in sensory neuron development and seem to be especially useful for generating more homogenous sensory neuron populations (Lallemend & Ernfors, 2012; Nickolls *et al.*, 2020).
The rise of single-cell sequencing techniques has been particularly helpful in determining which transcription factors might be useful for reprogramming. Sequencing changed our understanding of the developmental and cellular profiles of neurons in the DRG (Sharma *et al*, 2020; Usoskin *et al.*, 2015). During development, two waves of neurogenesis give rise to sensory neurons (Anderson, 1999). Neurog2 is mainly expressed in the first wave, and Neurog1 in the second wave, although there is also a phase where both overlap (Faure *et al*, 2020). In a later developmental phase, Brn3a and Islet1 expression induce sensory neuron differentiation. This includes the activity of transcription factors of the Runx family (Dykes *et al*, 2011; Newbern, 2015). Runx1, together with signaling via the nerve growth factor receptor TrkA, controls the cell type specification of peptidergic and nonpeptidergic nociceptors (Figure **2**) (Chen *et al*, 2006; Inoue *et al*, 2008; Kobayashi *et al*, 2012; Kramer *et al*, 2006). Furthermore, Prdm12, another transcription factor, is necessary for the development of nociceptive neurons by regulating TrkA expression (Bartesaghi *et al*, 2019; Desiderio *et al*, 2019). TrkA signaling is known to promote the differentiation of subtypes of sensory neurons (Sharma *et al.*, 2020).

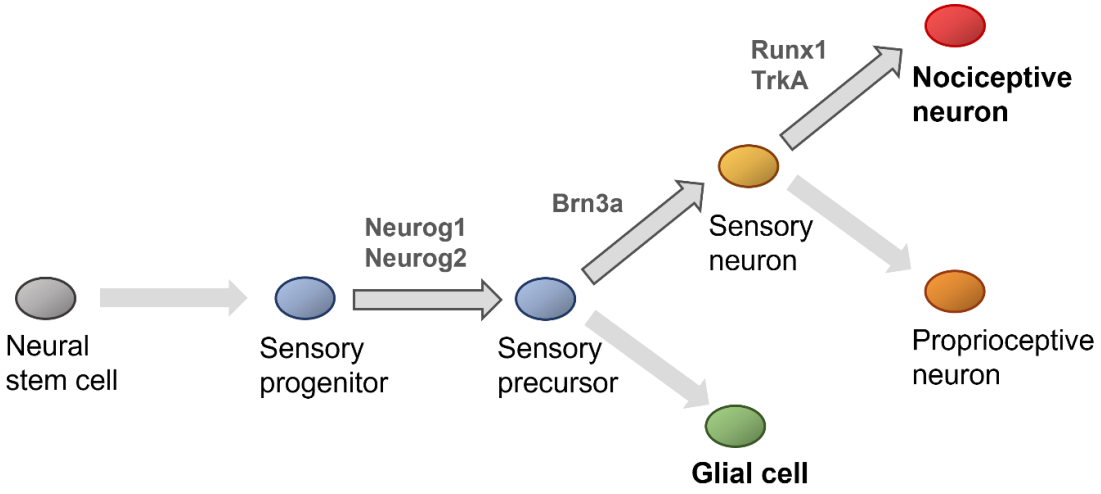

Figure 2. Scheme of nociceptor development. Neural stem cells develop into sensory progenitors. The transcription factors Neurog1 and Neurog2 drive the early differentiation into sensory precursors, and Brn3a expression further induces sensory neurons. Alternatively, sensory precursors can differentiate into peripheral glial cells. Differentiation of sensory neurons into nociceptive neurons is induced through Runx1 and TrkA expression.

2 Aim of the thesis

Rationale: Severe neuropathic pain after extensive injury, e.g., plexus avulsion, is a huge burden for affected patients. Therefore, new therapy options are needed. Neuronal replacement could be one approach to restore the somatosensory system and thereby normal nociception. SGCs and sensory neurons both originate from a common neural crest stem cell (Newbern, 2015). SGCs from adult DRG show properties of progenitor cells *in vitro* and cellular plasticity after peripheral injury *in vivo* (Avraham *et al.*, 2021; George *et al.*, 2018; Jager *et al.*, 2022; Schulte *et al.*, 2022c). This makes them an interesting starting point for regenerative medicine.

Hypothesis: In this thesis, we followed the hypothesis that SGCs from DRG are a suitable endogenous cell source for regenerative medicine. SGCs from adult DRG rejuvenate in cell culture and acquire hallmarks of sensory neuron progenitors. These dedifferentiated glial cells should have neural stem cell-like properties and thereby serve as a prospective cell source for regenerative medicine. *In vivo*, we hypothesized that SGCs are activated and proliferate (gliosis) after nerve injury and that neurons are lost in the DRG, so SGC-derived neurons may be useful for neuronal replacement.

Our **experiments** were organized on three levels. First, we aimed to genetically reprogram SGC-like cells into nociceptors *in vitro* by utilizing their progenitor-like properties and developmental origin. Secondly, we investigated changes in the DRG composition in a rat model for peripheral nerve injury. Lastly, we analyzed the human DRG of 13 patients affected by brachial plexus injury for SGC- and neuronal changes.

In summary, the study revealed the need for at least two translational research directions: reafferentation of existing DRG units in case no neurons are lost or otherwise a full replacement of the entire multicellular DRG structure. For DRG replacement, SGCs of the adult DRG are an attractive endogenous cell source. *In vitro*, SGCs showed high rejuvenation potential and could be reprogrammed into nociceptor-like neurons as well as glial cells using Neurog1 and Neurog2. *In vivo*, SGCs showed high plasticity after peripheral nerve injury but this is not associated with neuronal loss or significant cell division-triggered gliotic responses in the DRG tissue.

3 Materials and Methods

3.1 Materials

3.1.1 Chemicals, peptides, and recombinant proteins

Reagent	Source	Identifier
Adenosine 5′-triphosphate magnesium salt	Sigma-Aldrich	Cat#A9187
Allyl-isothiocyanate (AITC)	Sigma-Aldrich	Cat#36682
Aqua-Poly/Mount	Polyscienes Inc.	Cat#18606
B-27™ Supplement (50X), serum free	Gibco	Cat#17504044
β-Mercaptoethanol	Sigma-Aldrich	Cat#M7154
Capsaicin	Sigma-Aldrich	Cat#M2028
Cesium fluoride	Sigma-Aldrich	Cat#198323
Cesium hydroxide solution	Fluka	Cat#20995
DAPI	Sigma	Cat#32670
D(+)-Glucose-monohydrat	Merck	Cat#K38291142
DMEM, high glucose, GlutaMAX™ Supplement	Gibco	Cat#61965059
DMEM/F-12, GlutaMAX™ supplement	Gibco	Cat#31331028
Dimethylsulfoxide (DMSO)	Roth	Cat#4720
EDTA acid	Sigma-Aldrich	Cat#E6758
EGTA	Sigma-Aldrich	Cat#E3889
Epidermal growth factor human (EGF)	Sigma-Aldrich	Cat#E9644
Fetal calf serum (FCS)	Sigma-Aldrich	Cat#F7524
Fibroblast growth factor basic human (FGF)	Sigma-Aldrich	Cat#SRP6159
Guanosine 5′-triphosphate sodium salt hydrate	Sigma-Aldrich	Cat#G8877
HBSS, no calcium, no magnesium	Gibco	Cat#14170112
HEPES	Roth	Cat#HN77.4
Horse serum	Sigma-Aldrich	Cat#H1270
Liberase™ TH Research Grade	Sigma-Aldrich: Roche	Cat#5401135001
Liberase™ TM Research Grade	Sigma-Aldrich: Roche	Cat#5401119001
Lipofectamine 2000 Transfection Reagent	Thermo Fisher Scientific	Cat#11668019
Magnesium chloride hexahydrate	Merck	Cat#A914133
N-2 Supplement (100X)	Gibco	Cat#17502048
Natriumhydrogencarbonat	Merck	Cat#144-55-8
Nerve growth factor (NGF)	Sigma-Aldrich	Cat#N0513
Oregon Green 488 BAPTA-1 AM	Invitrogen	Cat#O-6807
Paraformaldehyde (PFA)	Merck	Cat#A11313
PBS, pH 7.4	Gibco	Cat#10010023
Penicillin-Streptomycin (Pen/Strep)	Thermo Fisher Scientific	Cat#15070063
Poly-L-lysine hydrobromide (PLL)	Sigma-Aldrich	Cat#P2636
Potassium dihydrogen phosphate	Merck	Cat#A850773
Sodium chloride	Sigma-Aldrich	Cat#31434
Sodium dihydrogen phosphate monohydrate	Merck	Cat#A723946
Triton X100	Sigma-Aldrich	Cat#T8787
TrypLE™ Express Enzyme (1X), phenol red	Gibco	Cat#12605010
Tween 20	Sigma-Aldrich	Cat#P1379

3.1.2 Media, solutions, and buffers

Medium/ Solution/ Buffer	Composition
DRG medium	450 ml DMEM/F-12, GlutaMAX™ supplement; 50 ml FCS; 5 ml Pen/Strep
Differentiation medium (serum free)	DMEM/F-12, GlutaMAX™ supplement; 1% Pen/Strep; 2% B-27 Supplement; 1% N-2 Supplement
HEK293 medium	450 ml DMEM, high glucose, GlutaMAX™ Supplement; 50 ml FCS; 5 ml Pen/Strep
EDTA 0.5 M	146.12 g in 1 l dH_2O, pH 8.0
EGTA 0.5 M	10 g in 47.54 ml dH_2O, pH 8.0
Liberase enzymes (TH/TM)	for 10 U/ml: dilute 5 mg in 2.6 ml dH_2O
PLL 0.1 %	dilute 0.1 % in dH_2O
Washing solution	1x PBS, 0.1% Triton X100, 0.1% Tween 20
Blocking solution	1x PBS, 10% horse serum, 0.1% Triton X100, 0.1% Tween 20
Extracellular current clamp solution	120 mM NaCl, 3 mM KCl, 2.5 mM $CaCl_2$, 1 mM $MgCl_2$, 30 mM HEPES, 15 mM D(+)-Glucose, adjust pH to 7.4 with NaOH, stored at 4°C
Extracellular voltage clamp solution	150 mM NaCl, 2 mM KCl, 1.5 mM $CaCl_2$, 1 mM $MgCl_2$, 10 mM HEPES, adjust pH to 7.4 with NaOH, stored at 4°C
HEPES-buffered ACSF	120 mM NaCl, 2.5 mM KCl, 1.2 mM $MgCl_2$, 2.4 mM $CaCl_2$, 1.2 mM NaH_2PO_4, 26 mM $NaHCO_3$, 10 mM D(+)-Glucose, 10 mM HEPES, adjust pH to 7.4 with NaOH
Intracellular current clamp solution	8 mM NaCl, 125 mM KCl, 1 mM $CaCl_2$, 1 mM $MgCl_2$, 0.4 mM Na_2-GTP, 4 mM Mg-ATP, 10 mM HEPES, 10 mM EGTA, adjust pH to 7.4 with KOH, stored at -20°C
Intracellular voltage clamp solution	35 mM NaCl, 105 mM CsF, 10 mM HEPES, 10 mM EGTA, adjust pH to 7.4 with CsOH, stored at 4°C
PFA 4% 500 ml	20 g Paraformaldehyde, 205 ml 0.2 M Na_2HPO_4, 45 ml 0.2 M $Na_2H_2PO_4$, adjust pH to 7.4
10x Phosphate-buffered saline (PBS)	1.37 M NaCl, 27 mM KCl, 100 mM Na_2HPO_4, 18 mM KH_2PO_4, adjust pH to 7.4

3.1.3 Antibodies

Antibody	Source	Identifier
Primary antibodies		
Rabbit polyclonal anti-Brn3a	Synaptic Systems	Cat#411 003, RRID:AB_2737037
Fibronectin mouse	Biomol	A117
Mouse monoclonal anti-Flag (DYKDDDDK)	Thermo Fisher Scienctific	Cat#MA1-91878, RRID:AB_1957945
Mouse monoclonal anti-GFAP	Synaptic Systems	Cat#173 011, RRID:AB_2232308
Rabbit anti-GFAP	Acris	Cat#DP014, RRID:AB_1001789
Chicken polyclonal anti-GFAP	Abcam	Cat#ab13970, RRID:AB_300798
Mouse monoclonal anti-HA.11 Epitope Tag	BioLegend	Cat#901501, RRID:AB_2565006
Chicken polyclonal anti-Map2	Abcam	Cat#ab5392, RRID:AB_2138153
Mouse monoclonal anti-c-Myc (9E10)	Santa Cruz	Cat#sc-40, RRID:AB_627268
Rabbit polyclonal anti-$Na_V1.9$ (T71n)	Our research group	(Subramanian *et al*, 2012)
Rabbit polyclonal anti-NG2 Chondroitin Sulfate Proteoglycan	Millipore	Cat#AB5320, RRID:AB_91789
Goat polyclonal anti-PDGFRβ	R&D Systems	Cat#AF1042, RRID:AB_2162633

Rabbit polyclonal anti-Peripherin	Chemicon	Cat#Ab1530
Rabbit polyclonal anti-Prdm12	Sigma	Cat#HPA043143, RRID:AB_10806379
Rabbit polyclonal anti-RFP	Rockland	Cat#600-401-379, RRID:AB_2209751
Mouse monoclonal anti-Runx1	Santa Cruz	Cat#sc-365644, RRID:AB_10843207
Mouse monoclonal anti-S100β	Sigma	Cat#S2532, RRID:AB_477499
Guinea pig anti-Sox10	Prof. Michael Wegner, Universität Erlangen, Germany	(Maka *et al*, 2005)
Goat polyclonal anti-Sox2 (Y-17)	Santa Cruz	Cat#sc-17320, RRID:AB_2286684
Rabbit polyclonal anti-TrkA	Merck	Cat#06-574, RRID:AB_310180
Rabbit polyclonal anti-TrpA1 rabbit	Novus	Cat#NB110-40763SS, RRID:AB_1291838
Goat polyclonal anti-VR1 (P-19)	Santa Cruz	Cat#sc-12498, RRID:AB_2241046
Mouse monoclonal anti-Tuj1	Neuromics	Cat#MO15013, RRID:AB_2737114
Rabbit polyclonal anti-βIII-Tubulin	Synaptic Systems	Cat#302 302 , RRID:AB_10637424
Secondary antibodies		
Alexa Fluor 488, Donkey anti-Mouse IgG (H+L) Highly Cross-Adsorbed	Thermo Fisher Scientific	Cat#A-21202 RRID:AB_141607
Alexa Fluor 488 AffiniPure Donkey Anti-Chicken IgY (IgG) (H+L)	Jackson ImmunoResearch	Cat#703-545-155 RRID:AB_2340375
Cy3-AffiniPure Donkey Anti-Mouse IgG (H+L)	Jackson ImmunoResearch	Cat#715-165-151 RRID:AB_2315777
Cy3-AffiniPure Donkey Anti-Rabbit IgG (H+L)	Jackson ImmunoResearch	Cat#711-165-152 RRID:AB_2307443
Cy3 AffiniPure Donkey Anti-Goat IgG (H+L)	Jackson ImmunoResearch	Cat#705-165-003 RRID:AB_2340411
Cy5-AffiniPure Donkey Anti-Goat IgG (H+L)	Jackson ImmunoResearch	Cat#705-175-147 RRID:AB_2340415
Cy5-AffiniPure Donkey Anti-Guinea Pig IgG (H+L)	Jackson ImmunoResearch	706-175-148 RRID:AB_2340462
Alexa Fluor 647-AffiniPure Donkey Anti-Chicken IgY (IgG) (H+L)	Jackson ImmunoResearch	Cat#703-605-155 RRID:AB_2340379
Cy5-AffiniPure Donkey Anti-Rabbit IgG (H+L)	Jackson ImmunoResearch	Cat#711-175-152 RRID:AB_2340607
Cy5-AffiniPure Donkey Anti-Mouse IgG (H+L)	Jackson ImmunoResearch	Cat#715-175-150 RRID:AB_2340819

3.1.4 Critical commercial assays

Resource	Source	Identifier
RNeasy Mini Kit	Qiagen	Cat#74104
Gel Extraction Kit	Monarch	Cat#T1020S
PCR & DNA Cleanup Kit	Monarch	Cat#T1030S
NucleoBond Xtra Midi EF, Midi kit	Machinery Nagel	Cat#740420.50
NucleoBond PC 10000 EF, Giga kit	Machinery Nagel	Cat#740548
Quick Blunting Kit	New England Biolabs	Cat#E1201

3.1.5 Oligonucleotides

Resource	Sequence
CAG sequencing primer, forward	5‘ – CCT GGG CAA CGT GCT GGT TAT T – 3’
IRES sequencing primer, reverse	5‘ – CCT CAC ATT GCC AAA AGA CG – 3‘
Ngn1 PCR primer, forward	5‘ – CTC GAT GCA GAT CTC GCC ACC ATG CCG GCA CCA CTT GAA ACC T – 3‘
Ngn1 PCR primer, reverse	5‘ – TCA CGT TTA AAC CTA TTA TCA GTG ATA CGG GAT GAA GCA – 3‘

3.1.6 Recombinant DNA

Table 1. Transfer plasmids for retroviral vectors based on the pSIN-CAG backbone.

Vector	Detailed construct	Source	
		Backbone; Enzyme	**Insert; Enzyme**
CAG-Ngn2-DsRed (#576)	CAG-Kozak-ATG-Flag-Ngn2-IRES-DsRed	(Heinrich *et al.*, 2010)	
CAG-(Pax6)-GFP (#582)	CAG-Kozak-ATG-(Pax6)-IRES-GFP	Zhao et al, 2006; RRID:Addgene 48201	
CAG-DsRed (#955)	CAG-IRES-DsRed	CAG-Ngn2-DsRed (#576); BamHI, PmeI	none
pEX-A128-Brn3a-Ngn2-Ngn1 (#976)	Kozak-ATG-Brn3a*-GSG-P2A-GSG-HA-GGSGG-Ngn2*-G^^SG-T2A-GSG-Myc-GGSGG-Ngn1*	gene synthesis, eurofins Genomics	
CAG-Brn3a-Ngn2-Ngn1 (#1013)	CAG-Kozak-ATG-Brn3a*-GSG-P2A-GSG-HA-GGSGG-Ngn2*-GSG-T2A-GSG-Myc-GGSGG-Ngn1*	CAG-Ngn2-DsRed (#576); BamHI, PmeI (blunt)	pEX-A128-Brn3a-Ngn2-Ngn1(#976); EcoRV (blunt)
CAG-Ngn1-dsRed (#1025)	CAG-Kozak-ATG-Ngn1*-IRES-DsRed	CAG-Ngn2-DsRed (#576); BamHI, PmeI	Ngn1 PCR ampliflied from pEX-A128-Brn3a-Ngn2-Ngn1(#976); BglII, PmeI
CAG-Runx1-GFP (#1038)	CAG-Kozak-ATG-HA-GSG-Runx1*-IRES-GFP	CAG-Pax6-GFP (#582); BamHI	pUCderivate-Runx1 (#1041); BglII
pUCderivate-Brn3a (#1040)	Kozak-ATG-Brna3*	gene synthesis, ATG:biosynthetics	

pUCderivate--Runx1 (#1041)	Kozak-ATG-HA-GSG-Runx1*	gene synthesis, ATG:biosynthetics	
pUCderivate-Ngn1 (#1042)	Kozak-ATG-Myc-GSG-Ngn1*	gene synthesis, ATG:biosynthetics	
CAG-Brn3a-GFP (#1043)	CAG-Kozak-ATG-Brn3a*-IRES-GFP	CAG-Pax6-GFP (#582); BamHI	pUCderivate-Brn3a (#1040); BamHI
CAG-Ngn1-GFP (#1044)	CAG-Kozak-ATG-Myc-GSG-Ngn1-*IRES-GFP	CAG-Pax6-GFP (#582); BamHI	pUCderivate-Ngn1 (#1042); BamHI
CAG-Brn3a-DsRed (#1045)	CAG-Kozak-ATG-Brn3a*-IRES-DsRed	CAG-Ngn2-DsRed (#576); BamHI, PmeI (blunt)	pUCderivate-Brn3a (#1040); BamHI (blunt)
CAG-Runx1-DsRed (#1051)	CAG-Kozak-ATG-HA-GSG-Runx1*-IRES-DsRed	CAG-Ngn2-DsRed (#576); BamHI, PmeI (blunt)	pUCderivate-Runx1 (#1041); BglII (blunt)
CAG-Brn3a-GFP (#1056)	CAG-Kozak-ATG-Brn3a*-IRES-GFP	CAG-Brn3a-DsRed (#1045); HindIII, NotI	CAG-Brn3a-GFP (#1043); HindIII, NotI (GFP exchanged)
pUCderivate-Ngn2-Ngn1 (#1057)	Kozak-ATG-Flag-GSG-Ngn2*-GSG-P2A-GSG-Myc-GGSGG-Ngn1*	gene synthesis, ATG:biosynthetics	
pUCderivate-Brn3a-Runx1 (#1058)	Kozak-ATG-Brn3a*-GSG-P2A-GGSGG-Runx1*	gene synthesis, ATG:biosynthetics	
CAG-Ngn2-Ngn1-DsRed (#1063)	CAG-Kozak-ATG-Flag-GSG-Ngn2*-GSG-P2A-GSG-Myc-GGSGG-Ngn1*-IRES-DsRed	CAG-Ngn2-DsRed (#576); BamHI, PmeI	pUCderivate-Ngn2-Ngn1 (#1057); BglII, EcoRV
CAG-Brn3a-Runx1-DsRed (#1064)	CAG-Kozak-ATG-Brn3a*-GSG-P2A-GGSGG-Runx1*-IRES-DsRed	CAG-Ngn2-DsRed (#576); BamHI, PmeI	pUCderivate-Brn3a-Runx1 (#1058); BglII, EcoRV, PvuI
pUCderivate-Brn3a-Ngn1 (#1065)	Kozak-ATG-Brn3a*-GSG-P2A-GSG-Myc-GGSGG-Ngn1*	gene synthesis, ATG:biosynthetics	
pUCderivate-Brn3a-Ngn2 (#1066)	Kozak-ATG-Brn3a*-GSG-P2A-GSG-Flag-GGSGG-Ngn2*	gene synthesis, ATG:biosynthetics	
CAG-Brn3a-Runx1-GFP (#1067)	CAG-Kozak-ATG-Brn3a*-GSG-P2A-GGSGG-Runx1*-IRES-GFP	CAG-Brn3a-GFP (#1056); BstXI, SfiI	CAG-Brn3a-Runx1-DsRed (#1064); BstXI, SfiI
CAG-Brn3a-Ngn1-DsRed (#1068)	CAG-Kozak-ATG-Brn3a*-GSG-P2A-GSG-Myc-GGSGG-Ngn1*-IRES-DsRed	CAG-Ngn2-DsRed (#576); BamHI, PmeI	pUCderivate-Brn3a-Ngn1 (#1065); BglII, EcoRV
CAG-Brn3a-Ngn2-DsRed (#1069)	CAG-Kozak-ATG-Brn3a*-GSG-P2A-GSG-Flag-GGSGG-Ngn2*-IRES-DsRed	CAG-Ngn2-DsRed (#576); BamHI, PmeI	pUCderivate-Brn3a-Ngn1 (#1065); BglII, EcoRV
pUCderivate-Prdm12 (#1080)	Kozak-ATG-Prdm12*	gene synthesis, ATG:biosynthetics	
CAG-Prdm12-DsRed (#1082)	CAG-Kozak-ATG-Prdm12*-IRES-DsRed	CAG-Ngn2-DsRed (#576); BamHI, PmeI (blunt)	pUCderivate-Prdm12 (#1080); EcoRV (blunt)

*codon-optimized

3.1.7 Selected consumables

Resource	Source	Identifier
10 mm glass coverslips	Marienfeld	Cat#0111500
Borosilicate glass	Science Products	Cat#GB 150-8P
Cell culture dish, 35 x 10 mm, four inner rings	greiner BIO-ONE	Cat#627170
Immersion oil	Olympus	Cat#IMMOIL-F30CC

3.1.8 Equipment

Resource	Source
Axio Imager M2	Zeiss
BX51WI upright microscope	Olympus
EPC10 USB patch-clamp amplifier	HEKA
IX81 microscope with Fluoview FV 1000	Olympus
pE-400	CoolLED
Minipuls 3 peristaltic pump	Gilson
Nanodrop Spectrophotometer ND1000	PeqLab Biotechnologie
Objective UPLAPO 20×	Olympus
Objective UPLFLN 20×	Olympus
Objective UPLFLN40×	Olympus
Objective UPLSAPO60×	Olympus
Osmometer Typ OM806	Vogel
P-97 micropipette puller	Sutter Instruments
Power supply for halogen lamp (TH4-200)	Olympus
Remote control SM7 / Keypad SM7	Luigs & Neumann
Rolera XR Mono fast 1394 CCD camera	Qimaging
sonifier water bath	Bandelin
Spectral detector FVD10 SPD	Olympus
Thermomixer comfort	Eppendorf

3.1.9 Software and algorithms

Resource	Source	Identifier
Adobe Photoshop CS5	Adobe Systems	RRID:SCR_014199
Anaconda Software Distribution	Anaconda Inc.	https://www.anaconda.com/
CellProfiler	Broad Institute	RRID:SCR_007358
Deepflash2	(Griebel *et al*, 2021)	
Fitmaster 2x91	HEKA Electronic	RRID:SCR_016233
ImageJ	WS Rasband, ImageJ, US National Institutes of Health	RRID:SCR_003070
PatchMaster v2x90	HEKA Electronic	RRID:SCR_000034
QuPath	(Bankhead *et al*, 2017)	RRID:SCR_018257
Stardist2D	(Schmidt *et al*, 2018)	
StreamPix 4	NORPIX	N/A
Zen Imaging Software Version 2.6	Carl Zeiss Microscopy GmbH	N/A

3.2 Methods

3.2.1 Vector design and retroviral production

To express transcription factors, self-inactivating retroviral vectors containing a chicken beta actin promoter (pSIN-CAG backbone (Zhao *et al*, 2006)) were cloned. Codon-optimized cDNA encoding corresponding transcription factors were produced by gene synthesis (Eurofins, ATG:biosynthetics GmbH). Transcription factor sequences were synthesized based on the protein Reference Sequence (RefSeq) of Mus musculus: neurogenin-1 (Neurog1, RefSeq: NP_035026.1); neurogenin-2 (Neurog2, RefSeq: NP_033848.1); POU domain, class 4, transcription factor 1 (Brn3a, RefSeq: NP_035273.3); runt-related transcription factor 1 isoform 1 (Runx1, RefSeq: NP_001104491.1); PR domain zinc finger protein 12 (Prdm12, RefSeq: NP_001116834.1). For bi- or tricistronic expression, inserts were linked with 2A fusion peptides (P2A: ATNFSLLKQAGDVEENPGP; T2A: EGRGSLLTCGDVEENPGP). For affinity detection, Flag (DYKDDDD), HA (YPYDVPDYA), and Myc (EQKLISEEDL) peptides were tagged to individual inserts. DNA cassettes were fused with GSG- and GGSGG-linker sequences. Red fluorescent protein (DsRed) or green fluorescent protein (GFP) served as transduction control and were expressed with the help of an IRES sequence. Constructs were cloned into CAG-DsRed (Heinrich *et al.*, 2010) and CAG-GFP (Zhao *et al.*, 2006) backbones; Neurog2 was already available in CAG-Ngn2-DsRed (Blum *et al.*, 2011). Detailed retroviral vector constructs with sources of backbone, insert, and used restriction enzymes are listed in Table 1. For validation, DNA inserts were sequenced by LGC Genomics (Berlin, Germany).

Viral vectors were produced in HEK293TN cells by co-transfection of the pCAG-expression plasmids and two helper plasmids with CMV-VSVG, and MMLV-CMV-gag-pol. Viral particles were purified by ultracentrifugation before application (Blum *et al.*, 2011).

3.2.2 Cell culture

3.2.2.1 Primary dorsal root ganglia cells

Primary DRG cell cultures were prepared from adult 4 to 6 weeks old wild-type mice as described before (Dib-Hajj *et al*, 2009; Martin *et al.*, 2018). Mice were sacrificed by CO_2 asphyxiation and cervical dislocation. DRG were collected in ice-cold HBSS. Isolated DRG were treated with 0.6 U/ml Liberase TH (Sigma-Aldrich) and 0.6 U/ml Liberase TM (Sigma-Aldrich) in EDTA ($3.\overline{3}$ mM) buffered DMEM. DRG were plated on poly-L-lysine (PLL)-coated 3.5 cm culture dishes. Cells were cultivated in DMEM/F12, GlutaMAX™ supplement (Gibco), 10% fetal calf serum (FCS), and 1% penicillin/streptomycin supplemented with 10 ng/ml EGF and FGF at 37°C, 5% CO_2 atmosphere. After 7 d in culture, RNA was isolated or cells were split, transduced with moloney murine leukemia virus (MMLV)-based retroviral vectors, and plated on poly-L-lysine-coated 10 mm glass coverslips (Marienfeld, Lauda-Königshofen,

Germany). For evaluation of reprogramming efficiency, cells were fixed 7 days post infection (dpi) and used for immunocytochemistry. To differentiate the infected cells, the medium was changed from 1 to 3 dpi in 50% increments to a serum-free differentiation medium containing DMEM/F12, GlutaMAX™ supplement (Gibco), B-27 and N-2 supplement, and 100 ng/ml nerve growth factor (NGF, Sigma). The differentiation medium was changed weekly.

3.2.2.2 HEK293 cells

Human embryonic kidney-293 (HEK293, # ACC 305) cells were cultivated in DMEM, high glucose, GlutaMAX™ Supplement (Gibco), 10% FCS, and 1% penicillin/streptomycin at 37°C in 5% CO_2. For testing of DNA plasmids, HEK293 cells were transfected using Lipofectamine 2000 (Invitrogen). Media was replaced after 24 h and cells were fixed 48 h after transfection for immunofluorescence analysis.

3.2.3 RNA isolation and bulk sequencing

For RNA isolation of 7 d old DRG cell cultures, the RNeasy Mini Kit (Qiagen) was used. Cells were washed once with PBS and lysed with the provided RLT buffer supplemented with 1% β-mercaptoethanol. The cell lysate was homogenized with a 0.7 x 30 mm syringe. RNA was eluted in 50 µl RNAse free water. RNA was bulk mRNA sequenced (custom-sequencing) in one batch by the Core Unit SysMed (University of Würzburg, Germany). Visualization of results was done in python.

3.2.4 Indirect immunofluorescence staining

Cells were fixed with 4 % paraformaldehyde (PFA) in phosphate buffer for 15 min at 37°C and stored in 1xPBS at 4°C when not directly processed. For cell permeabilization and blocking, cells were incubated with 10% horse serum, 0.1% Triton X100, and 0.1% Tween 20 in 1xPBS (blocking solution) for 1 h at RT. Primary antibodies in blocking solution were incubated for 2 h at RT. After washing the cells 8 times with 0.1% Triton X100, and 0.1% Tween 20 in 1xPBS (washing solution), secondary antibodies in a concentration of 0.5 µg/ml in blocking solution were incubated for 1.5 h at RT. Used antibodies are listed in 3.1.3. Cells were washed again with washing solution and 1xPBS, and nuclei were stained with 0.4 µg/ml DAPI in 1x PBS. Finally, cells were washed with 1xPBS, dipped in water, dried, and embedded in Aqua-Poly/Mount (Polysciences).

3.2.5 Microscopy

Immunocytochemical stainings and tile scans were captured with an Axio Imager M2 (Zeiss) using a Plan Apochromat 20x (air, numerical aperture (NA): 0.8). For higher resolution, an inverted Olympus IX81 microscope combined with an Olympus FV1000 confocal laser scanning system was used. Images were acquired with an FVD10 SPD spectral detector and diode lasers of 405, 473, 559, and 635 nm using an Olympus UPLAPO 20× (air, NA: 0.75), Olympus UPLFLN40× (oil, NA: 1.3), or UPLSAPO60× (oil, NA: 1.35). The pinhole setting represented one Airy disc. 12-bit greyscale images were processed with maximum intensity projection, adjusted in brightness and contrast, and merged into an RGB composite using ImageJ (Schneider *et al*, 2012). Final processing was done with Adobe Photoshop CS5.

3.2.6 Calcium imaging

Imaging of cytosolic calcium was performed with Oregon Green 488 BAPTA-1 AM (OGB1, Invitrogen). Cells were loaded with 5 µM OGB1 for 15 min at 37 °C in HEPES-buffered ACSF (artificial cerebrospinal fluid, 120 mM NaCl, 2.5 mM KCl, 1.2 mM $MgCl_2$, 2.4 mM $CaCl_2$, 1.2 mM NaH_2PO_4, 26 mM $NaHCO_3$, 10 mM Glucose, 10 mM HEPES). 5 mM OGB1 (in 20% pluronic/DMSO) was stored in small single-use aliquots.

The imaging setup for fast calcium imaging consisted of a BX51WI upright microscope (Olympus) equipped with a water-immersion objective (20× Olympus UPLFLN, NA 0.5) and a pE-4000 fluorescence illumination system (CoolLED). Images were captured at 5 Hz with a Rolera XR Mono fast 1394 CCD camera (Qimaging) controlled by the streaming software Streampix 4.0 (NorPix). A camera binning of 2×2 was used.

Cells expressing Ngn2-P2A-Ngn1-^{IRES}DsRed were imaged 14 and 15 dpi at room temperature in a plastic perfusion chamber in HEPES-buffered ACSF under continuous perfusion with the help of a Minipuls 3 peristaltic pump (speed of the perfusion pump: 15 A.U., purple tubing, Gilson). The DsRed signal excited by 550 nm wavelength was captured to identify infected cells. Changes in calcium signals (OGB1: 470 nm excitation) were imaged in response to 10 µM capsaicin (Sigma-Aldrich) and 100 µM allyl-isothiocyanate (AITC, Sigma-Aldrich). Capsaicin was applied for 10s through perfusion with the peristaltic pump, and 1 ml AITC was applied for 10s with a pipette.

3.2.7 Electrophysiology

For electrophysiological measurements of reprogrammed neurons, current-clamp and voltage-clamp recordings were performed in the whole-cell configuration at room temperature. Extracellular solution for current-clamp recordings contained (in mM): 120 NaCl, 3 KCl, 2.5 $CaCl_2$, 1 $MgCl_2$, 30 HEPES, 15 glucose (pH 7.4 with NaOH), and the intracellular solution

contained 125 KCl, 8 NaCl, 1 $CaCl_2$, 1 $MgCl_2$, 0.4 Na_2-GTP, 4 Mg-ATP, 10 EGTA, 10 HEPES (pH 7.3 with KOH) (Leipold *et al*, 2015). The extracellular solution used for voltage-clamp recordings contained (in mM): 150 NaCl, 2 KCl, 1.5 $CaCl_2$, 1 $MgCl_2$, 10 HEPES (pH 7.4 with NaOH) and was supplemented with 500 nM tetrodotoxin (TTX) to block TTX-sensitive sodium currents. For voltage-clamp recordings, the patch pipette was filled with a buffer composed of (in mM) 35 NaCl, 105 CsF, 10 EGTA, 10 HEPES (pH 7.3 with CsOH) (Leipold *et al.*, 2015). Reprogrammed (14-17 dpi) or naive (1-2 DIV) neurons were continuously perfused with the help of a Minipuls 3 peristaltic pump (speed of the perfusion pump: 3 A.U., purple tubing, Gilson). Pipettes with 2−4 MΩ resistances were pulled from borosilicate glass. Data were acquired using a HEKA EPC-10 USB patch-clamp amplifier controlled by the PatchMaster software (HEKA Electronic) at a sampling interval of 40 µs. Data were processed with Fitmaster (HEKA Electronic) and analyzed using python scripts (https://github.com/AmSchulte/Nociceptor).

3.2.7.1 Current-clamp recordings

After establishing the whole-cell configuration, cells were voltage-clamped at a holding potential of -60 mV and tested for functional ion channel expression by measuring inward and outward currents with a 50 ms test pulse to -20 mV and a 100 ms test pulse to 60 mV, respectively. The resting membrane potential (RMP) was measured at zero current injection immediately after switching to the current-clamp mode. Subsequently, cells were clamped to -60 mV using the low-frequency voltage clamp available in the PatchMaster software. Action potentials were evoked by a series of current injections increasing from 0 to 220 pA in steps of 20 pA. The duration of current injections was set to 3 ms to evoke single action potentials or to 300 ms to trigger trains of action potentials. Data were low-pass filtered at 3 kHz. An action potential was regarded as such if the maximal amplitude exceeded 0 mV and a firing threshold could be detected. The firing threshold of an action potential was defined as a voltage at which dV/dt reached the level of $0.03 \times (dV/dt_{max} - dV/dt_{min}) + dV/dt_{min.}$ The spike width was analyzed at -20 mV.

3.2.7.2 Voltage-clamp recordings

Cells were held at -130 mV for at least 8 min to facilitate recovery of sodium channels from inactivation. Activation of sodium channels was measured with test depolarizations between -110 and 30 mV in steps of 10 mV, delivered every 10 s. The test pulse duration was 100 ms. Leak and capacitive currents were measured with a p/n method and subtracted online. Data were low-pass filtered at 3 kHz.

3.2.8 Quantification and statistical analysis

3.2.8.1 Quantification with CellProfiler

Whole cell culture coverslips stained for neuronal and glial markers were tile-scanned with 14 bit at a resolution of 0.454 µm/ pixel. Analysis of the large amount of data (5-6 GB per cover) was performed with CellProfiler (McQuin *et al*, 2018). Each cover scan was processed in a batch of tif-converted single-tile images.

Quantification of DAPI, Tuj1, Map2, GFAP, or Brn3a-positive cells was performed with the "IdentifyPrimaryObjects" module. Here, the minimum cross entropy thresholding method was used, where the lower bounds on the threshold needed to be adjusted manually for each cover scan to counteract staining variability. The RFP-positive area was defined with a manual threshold and the resulting mask was projected onto the marker staining (module: "MaskImage") to determine how many of the infected cells were positive for the respective marker. Results were exported to spreadsheets and further processed and visualized in python.

3.2.8.2 Analysis of calcium imaging signals

Calcium imaging videos of cells stimulated with either Capsaicin or AITC were analyzed in python. Region of interest (ROI) detection was performed with the open-source DL model StarDist2D (Schmidt *et al.*, 2018). First, the DsRed signal was segmented with StarDist2D to detect infected cells. Based on the resulting ROIs, calcium imaging signal traces were extracted for each infected cell. For uninfected cells, the DsRed-positive ROIs were removed from the calcium imaging video, and ROI detection and signal extraction was performed on the rest of the OGB1-stained cells. To identify the proportion of reacting cells, signal traces were low-pass filtered with a wavelet function. When the derivative of the low-pass filtered signal reached a uniform threshold, the cell was counted as reacting. The proportion of reacting infected cells was compared to the proportion of reacting uninfected cells. The analysis script is openly available (https://github.com/AmSchulte/Nociceptor).

3.2.8.3 Deep learning-based image analysis

For image feature segmentation, we followed guidelines for reproducible deep learning (DL)-based bioimage analysis (Segebarth *et al*, 2020) and adapted the method to image features of DRG tissue (Schulte *et al.*, 2022c). As depicted in Figure 3, DRG tissue from rats treated with SNI or sham surgery was immunofluorescence stained for neurofilament (NF), glutamine synthetase (GS), and GFAP in serial sections. Imaging in large-field tile scans resulted in czi-images that were converted to tiff files using python. 15 exemplary images of each marker were annotated by three experts using ImageJ. The ground truth of the segmentation masks

was estimated with the simultaneous truth and performance level estimation (STAPLE) method. Ground truth estimation and consecutive DL model training was performed with *deepflash2* (Griebel *et al.*, 2021). Before training, the dataset was split into 80% training and 20% testing dataset. One DL model ensemble was trained to segment neurons with the NF dataset, and one DL model ensemble was trained to detect ring-shaped glial cells based on the GS and GFAP dataset. Three consensus DL models formed a model ensemble. The Jaccard similarity coefficient score, also called intersection over union (IoU), served as a score to evaluate the performance of the models. For testing, predicted labels were compared with the annotated labels of the test dataset.

All acquired DRG images (2541) were segmented with the model ensembles. NF images of rats 4-6 7 d after SNI needed to be adjusted in brightness and contrast. DRG images and segmentation masks are openly available (Schulte *et al*, 2022b). Data analysis was programmed in python. To define the tissue area, NF images were binarized with the Li thresholding method (Li & Tam, 1998) and further dilated and eroded. Only neurons bigger or equal to the smallest annotated neuron (202 µm^2) were included in the analysis. The new parameter, the percentage of neurons in proximity to GFAP/GS-positive glial cells, was calculated by dilating both the NF mask and the glial cell mask by one pixel. If the overlap between a dilated neuron and the surrounding glial cell mask was bigger than 0, the neuron was counted to be in proximity to a glial cell. Calculated image parameters were averaged for each DRG. For details see: https://github.com/AmSchulte/DRG (Schulte *et al.*, 2022c).

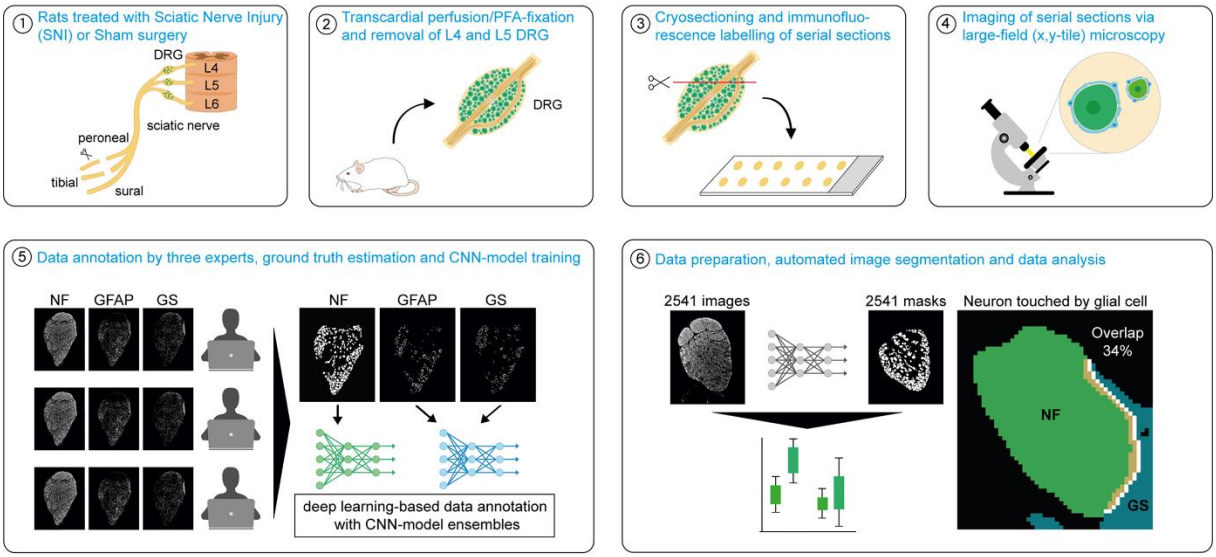

Figure 3. Schematic workflow and methods for systematic analysis of DRG in six steps. Rats underwent SNI or sham surgery. (2) After 7 or 14 d, transcardial perfusion with the fixative PFA was performed and ipsilateral and contralateral L4/L5 DRG were removed. (3) Serial sections were cut collecting every tenth slice with a thickness of 16 µm on one slide. (4) DRG slices were labelled and imaged via large-field (tile) microscopy. (5) Three human experts annotated 15 representative microscopy images for each label according to their individual criteria. These data were used for computing a consensus for ground truth estimation. 80% of the dataset was used to train deep learning (DL) model ensembles for NF, or GS and GFAP. 20% of the annotated images were used as the test

dataset. (6) Segmentation masks were predicted for a total of 2,541 images. Based on these, quantification and statistical analyses were conducted. Changes in GS and GFAP levels were analyzed by quantifying the amount and size of neurons in proximity to GS- or GFAP-positive glial cells (overlap > 0%). DRG, dorsal root ganglia; GFAP, glial fibrillary acidic protein; GS, glutamine synthetase; NF, neurofilament; SNI, spared nerve injury. Created by Annemarie Aue. Reproduced from (Schulte *et al.*, 2022c).

Similarly, the human DRG tissue stained for neurons with NF, and SGCs with Fatty Acid Binding Protein 7 (FABP7) and APOJ were analyzed, with minor modifications. Image feature annotation was performed on ten exemplary sections marked by NF by three experts using the QuPath software. Training of a new DL model ensemble (three models) was performed with eight of the ten exemplary sections using *deepflash2*, and two sections were used to test the model. Annotation overlap and the model's performance were evaluated with the Dice score. The Dice is defined as: $M_{Dice}(A,B) := \frac{2|A \cap B|}{|A|+|B|}$; where A and B are two sets of pixels. Then, the model ensemble was applied to predict the NF-positive neurons in human DRG images.

Masks for FABP7-positive SGCs were created with a thresholding method. Scikit-image filters were used for background reduction and sharpening (unsharp_mask function), as well as the calculation of an "optimal" threshold with the Otsu method. Pixels with fluorescence intensity above the Otsu Threshold were considered FABP7-positive. Thresholding was sufficient because FABP7 almost exclusively stained SGCs with a high signal-to-noise ratio (at least in fresh samples). Even though the filters accounted for a lot of the viability, the DRG images of one control needed to be excluded from the subsequent analysis because the thresholding method did not work adequately for images with a low signal-to-noise ratio.

Finally, the predicted areas of neurons and SGCs were used for image feature quantification. For this, python scripts were created (https://github.com/AmSchulte/DRGhuman). ROIs smaller than the smallest annotated NF-positive neuron (162 μm^2) were excluded from the analysis and some falsely detected ROIs outside of the neuron-rich areas were deleted manually. Then, the neuron-near area (NNA) was calculated through binary dilation (scikit-image morphology) of the NF segmentation. As another reference area, a convex hull was automatically drawn around the neuron-near area and defined as a neuronal polygon area (NPA). For SGC quantification, the area, and the proximity to neurons (percentage of neurons in proximity to FABP7-positive SGCs), were used. The intensity of the APOJ signal was determined inside FABP7-positive SGCs normalized to the rest of the APOJ intensity in the NNA or NPA. Calculated image parameters were averaged for each DRG.

3.2.8.4 Statistical analysis

Image quantifications were tested for significance using python as described (Schulte *et al.*, 2022c). The normal distribution of the data was assessed with the Shapiro test. Not normally distributed data were tested for significant differences with the Kruskal-Wallis H-test and post hoc Mann-Whitney rank test, or two-sided Mann-Whitney U test when just two groups were compared.

Normally distributed data were tested first for equal variance with the Bartlett's test. More than two groups were tested with the Alexander Govern test when the variance was unequal, or with the one-way ANOVA when the variance of the data was equal. Then, a post hoc T-test was performed. Two groups with unequal variance were compared with the Welch's t-test, or with the t-test when having an equal variance. Bonferroni correction was applied for multiple comparisons if not otherwise described. Data are presented as the mean ± standard error.

4 Results

4.1 *In vitro* reprogramming of glial cells from adult DRG into nociceptor-like neurons

4.1.1 Satellite glial cells become sensory progenitor-like cells *in vitro*

In the DRG cell culture of 4-8 weeks old wt C57BL/6 mice, we observed fast-dividing cells growing around DRG neurons. These cells are not visible immediately after plating but appear around single DRG neurons within a few days (Figure 4 B). In immunofluorescent stainings of DRG cultures at day *in vitro* (DIV) 3 and 7, cells showed the sensory progenitor and glial cell markers Sox2 and Sox10, as well as immunoreactivity to NG2 and PDGFRß, which are markers for glial cells and pericytes (Figure 4 C). To better characterize the cultured cells, we determined the mRNA-transcriptome (n = 6). The transcript per millions (TPM) gene count distribution was homogenous between individual cultures (Figure S1 A). Marker genes were chosen based on their differential expression and high abundance in the respective cell type (Avraham *et al.*, 2020; Jager *et al.*, 2020).

Cells abundantly expressed specific marker genes for satellite glial cells, such as *Fabp7* and *Kcnj10* (gene for Kir4.1) (Figure 4 D). The pericyte cell type was excluded, as other pericyte marker genes, such as *Pla1a*, were barely detectable in the transcriptome (Figure 4 D). Expression profiles also indicated a connective tissue cell type, but fibroblasts were excluded by negative staining to fibronectin (Figure 4 C, D). Also, the cells expressed βIII-Tubulin (gene: *Tubb3*), a microtubule element mainly expressed in neurons. Notably, genes for Sox2 and Sox10 were highly transcribed in the cells (Figure 4 E). Both proteins are found in neural-crest-derived progenitors of the PNS and are typically found in satellite glial and Schwann cell markers. This pointed to a sensory progenitor-like cell type originating from peripheral glial cells of the adult DRG. Further exploring the progenitor phenotype, differentially expressed marker genes of neural crest cells, especially those of boundary cap cells, were found (Figure S1 B). Expression of glial and progenitor marker genes was on the same level as housekeeping genes (Figure S1 C). Based on these transcriptome data, a reprogramming strategy for glial sensory progenitor (gSP) cells in direction of peripheral nociceptors was developed. We selected fate-determining transcription factors: Neurog1, Neurog2, Brn3a (*Pou4f1*), Prdm12, and Runx1; all these factors are known to be relevant for sensory neuron development. Furthermore, they were barely present in the 7 weeks old DRG cell cultures (Figure 4 F).

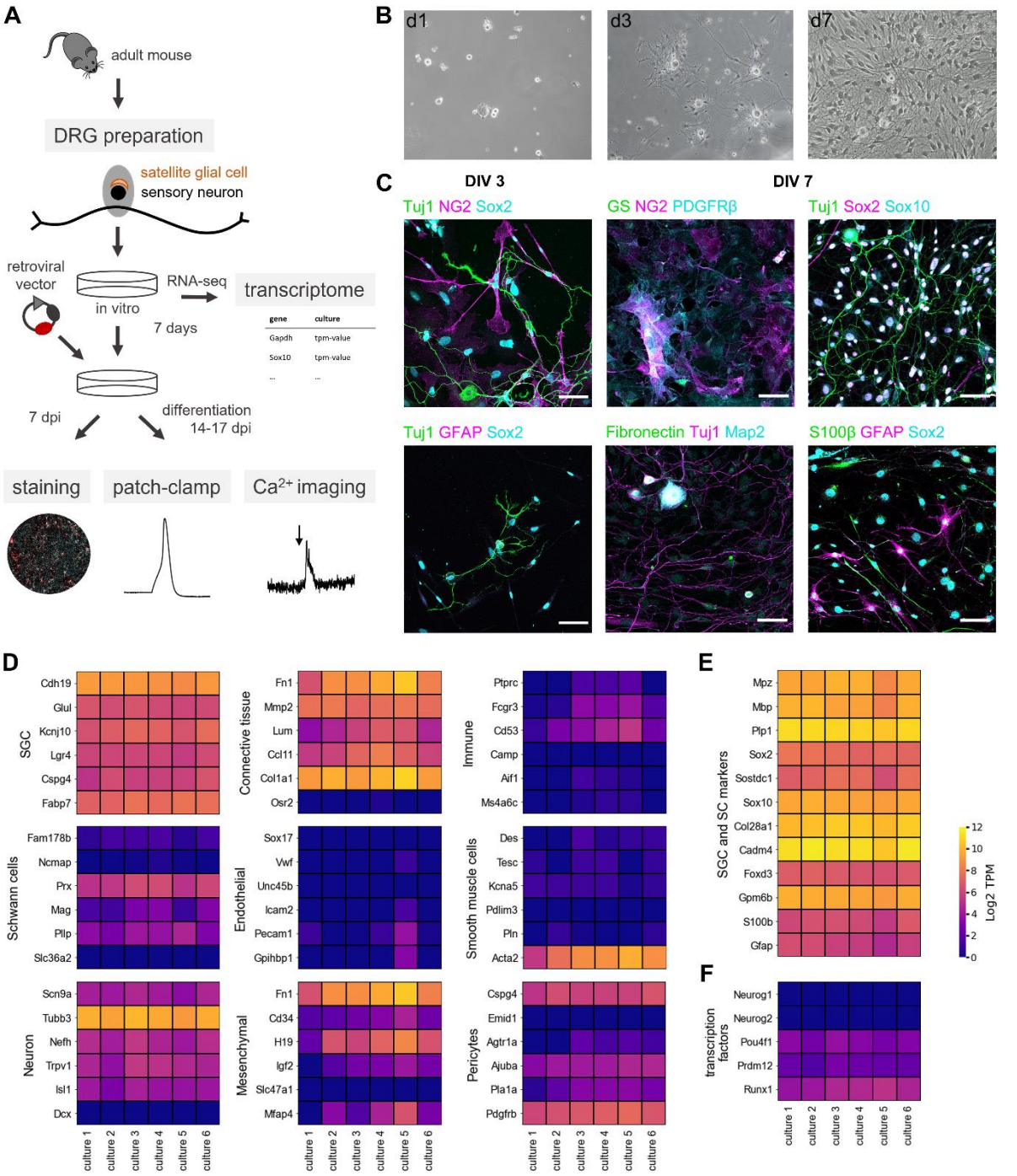

Figure 4. Fast-dividing sensory progenitor-like cells in DRG cell cultures from adult mice. (**A**) DRG cells were prepared from adult mouse DRG and cultured for 7 days to perform RNA-seq or split and infect them with a retroviral vector. Infected cells were analyzed with immunofluorescent stainings, patch-clamp, and calcium (Ca^{2+}) imaging. (**B**) Representative brightfield images of mouse cell culture at d 1, d 3, and d 7 *in vitro*. (**C**) Immunofluorescence images of DRG cell cultures at day *in vitro* (DIV) 3 or 7 stained for the glial and pericyte markers NG2 and PDGFRβ, the glial markers GFAP and S100β, Sox2 and Sox10, which are markers for progenitors as well as glial cells, and fibronectin, a fibroblast marker. Tuj1 (βIII-Tubulin) labels neurons. Scale bars: 50 µm. (**D-E**) Heatmaps visualize the expression profile of selected marker genes across samples for 9 cell types (satellite glial cells (SGC), Schwann cells (SC), neuron, connective tissue, endothelial, mesenchymal, immune, smooth muscle cells, pericytes). (**F**) Expression profile of transcription factors used for reprogramming. Each column represents a sample of a DRG cell culture (DIV 7) of adult wt mice (n = 6). Scale bar: Log_2 transcripts per million (TPM). DRG, dorsal root ganglia.

4.1.2 Retroviral vectors are validated in HEK293 cells

The sensory progenitor-like cells were dividing fast. Therefore, we used retroviral vector constructs for the expression of the selected transcription factors. Starting from a vector that was successfully used for reprogramming cortical glial cells into neurons (Blum *et al.*, 2011; Heinrich *et al.*, 2010) (Figure 5 A), vectors for forced expression of different combinations of Neurog1 (Ngn1), Neurog2 (Ngn2), Brn3a, Runx1, and Prdm12 were cloned (Table 1). To enable the distinction of different vector constructs in case of double infection, additionally to the DsRed-tagged vector backbone a similar GFP-tagged retroviral backbone was used (Zhao *et al.*, 2006). Codon-optimized transcription factor sequences were used. In bi- or tricistronic constructs, some of the factors were either tagged with Flag, Myc, or HA affinity tags. The retroviral vector constructs were validated in HEK293 cells. After transfection, HEK293 cells showed immunoreactivity for the respective single transcription factors (Figure 5). In summary, 15 different vector constructs were successfully developed.

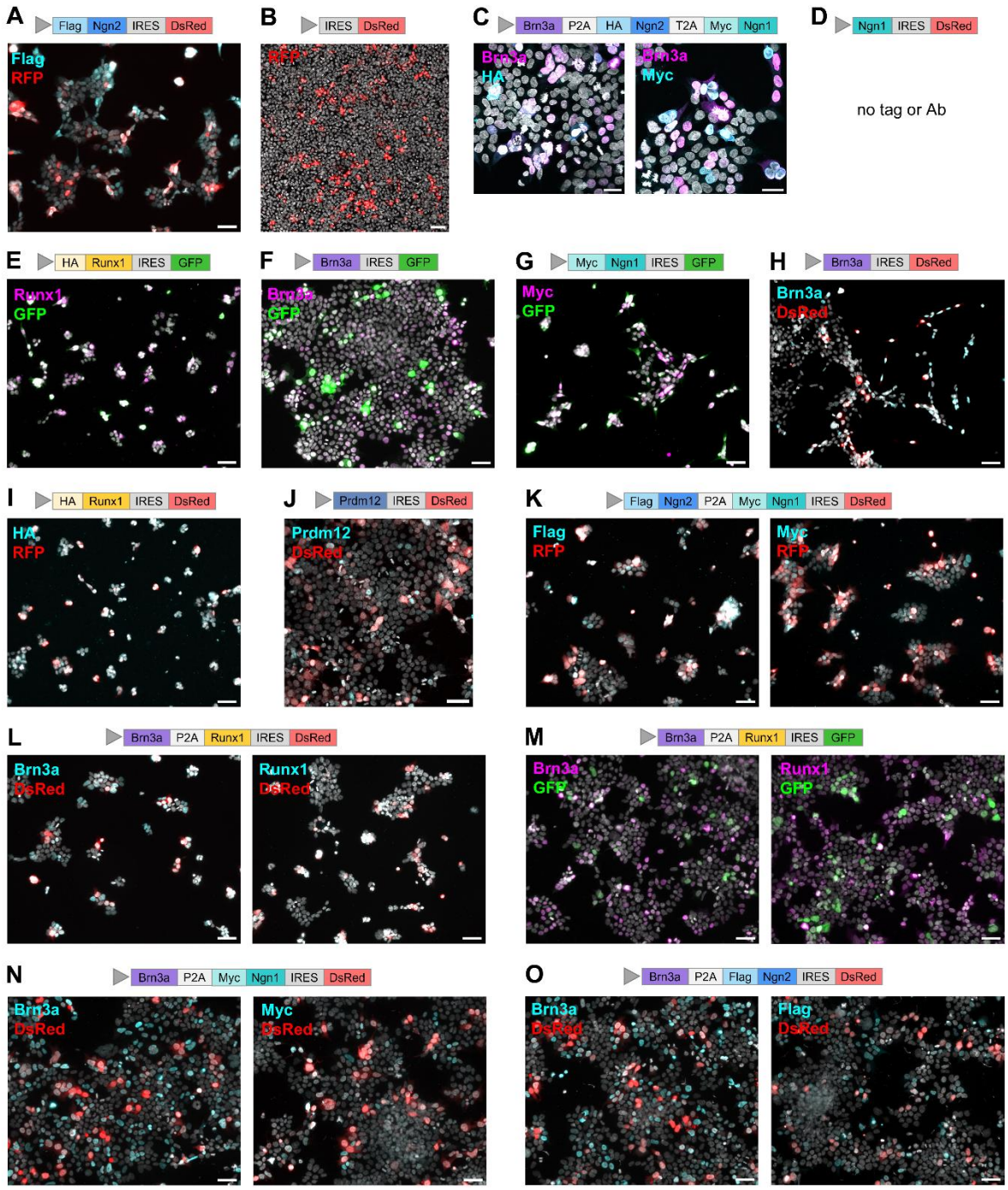

Figure 5. Retroviral vectors transfected and expressed in HEK293 cells. HEK293 cells expressing retroviral vectors were labeled 48-72h after transfection. (**A**) The CAG-IRES-DsRed backbone originated from the CAG-Flag-Ngn2-IRES-DsRed vector (Heinrich *et al.*, 2010; Zhao *et al.*, 2006) (**B**) and served as a control. (**C**) Except for the triple vector with Brn3a (violet), Neurog2 (Ngn2, HA-tagged, blue), and Neurog1 (Ngn1, Myc-tagged, cyan) sequences, mono- and bicistronic constructs contained DsRed or GFP as a fluorescent protein marker. (**D-I**) Neurog1, Runx1 (HA-tagged, yellow), and Brn3a were expressed with IRES-DsRed or IRES-GFP vectors. (**J**) CAG-Prdm12-IRES-DsRed enabled Prdm12 (grey-blue) expression in HEK293 cells. (**K-O**) HEK293 cells expressing the bicistronic constructs Flag-Ngn2-P2A-Myc-Ngn1, Brn3a-P2A-Runx1, Brn3a-P2A-Myc-Ngn1, or Brn3a-P2A-Flag-Ngn2. The grey arrowhead represents the CAG promotor. Scale bars: 50 µm (C: 25µm). GFP, green fluorescent protein; DsRed/RFP, red fluorescent protein.

4.1.3 Glial sensory progenitor (gSP) cells have a high reprogramming potential

To test if gSP cells can be reprogrammed into neurons, 7 d old gSP cells were infected with different combinations of the retroviral vectors. Within 7 dpi, gSP cells expressing either neurogenins (Neurog1 or Neurog2) or Brn3a developed a neuronal Map2-/Tuj1-positive phenotype (Figure 6 A). Bicistronic or tricistronic expression of Neurog1, Neurog2, and Brn3a induced neurons with even higher probability (Figure 6 A). Quantification in tile-scans of whole coverslips showed that all ^{IRES}DsRed-based vectors expressing neurogenin (Neurog1, Neurog2) and/or Brn3a induced significantly more neurons than the control vector (Figure 6 B-F). 10-20% of the infected cells expressing either Neurog1, Neurog2, or Brn3a became Tuj1-positive (Figure 6 C); about 5-10% of the cells were Map2-positive (Figure 6 E). Expression of multiple transcription factors increased this to about 40-50% Tuj1-positive and 20-30% Map2-positive cells. The triple (Brn3a-P2A-Ngn2-P2A-Ngn1) and the Ngn2-P2A-Ngn1 vector induced the highest number of neurons (Figure 6 C, E). Effects of the vector backbone on the gSP cells were excluded with the control vector (Figure 6 D, F).

For unknown reasons, ^{IRES}GFP-tagged retroviral vectors for Neurog1 and Brn3a expression did not effectively work in gSP cells (Figure S2 A). To test if the backbone was the reason for this, we exchanged the DsRed of the CAG-Brn3a-IRES-DsRed vector with GFP, but the CAG-Brn3a-IRES-GFP vector did still not work. Moreover, ^{IRES}GFP- and ^{IRES}DsRed-based retroviral vectors expressing Runx1 alone or together with Brn3a did not seem to induce neurons (Figure S2 B-D). However, while the Brn3a-P2A-Runx1 vector was able to express Runx1 (Figure 5 L), no immunoreactivity to Runx1 was detectable in the infected gSP cells (Figure S2 D). As Runx1 might be only necessary and expressed later during neuronal differentiation of DRG cell subpopulation (Kobayashi *et al.*, 2012; Kramer *et al.*, 2006), we double-infected gSP cells with Brn3a-P2A-Runx1 and Ngn2-P2A-Ngn1. No striking morphological changes compared to Ngn2-P2A-Ngn1 infection alone were seen (Figure S2 E). Therefore, we did not pursue this approach further. Moreover, Prdm12 did not induce a neuronal phenotype, but could neither be immunocytochemically detected in gSP cells (Figure S2 F). Retroviral vectors for coexpression of Brn3a with Neurog1 or Neurog2 (Brn3a-P2A-Ngn1, Brn3a-P2A-Ngn2) did not effectively induce neurons (Figure S2 G). This may be due to reduced packaging efficiency resulting in a low titer. Problems with these vectors were not further investigated because expression of neurogenins and Brn3a with some of the ^{IRES}DsRed-based vectors could already induce a sensory neuron-like phenotype.

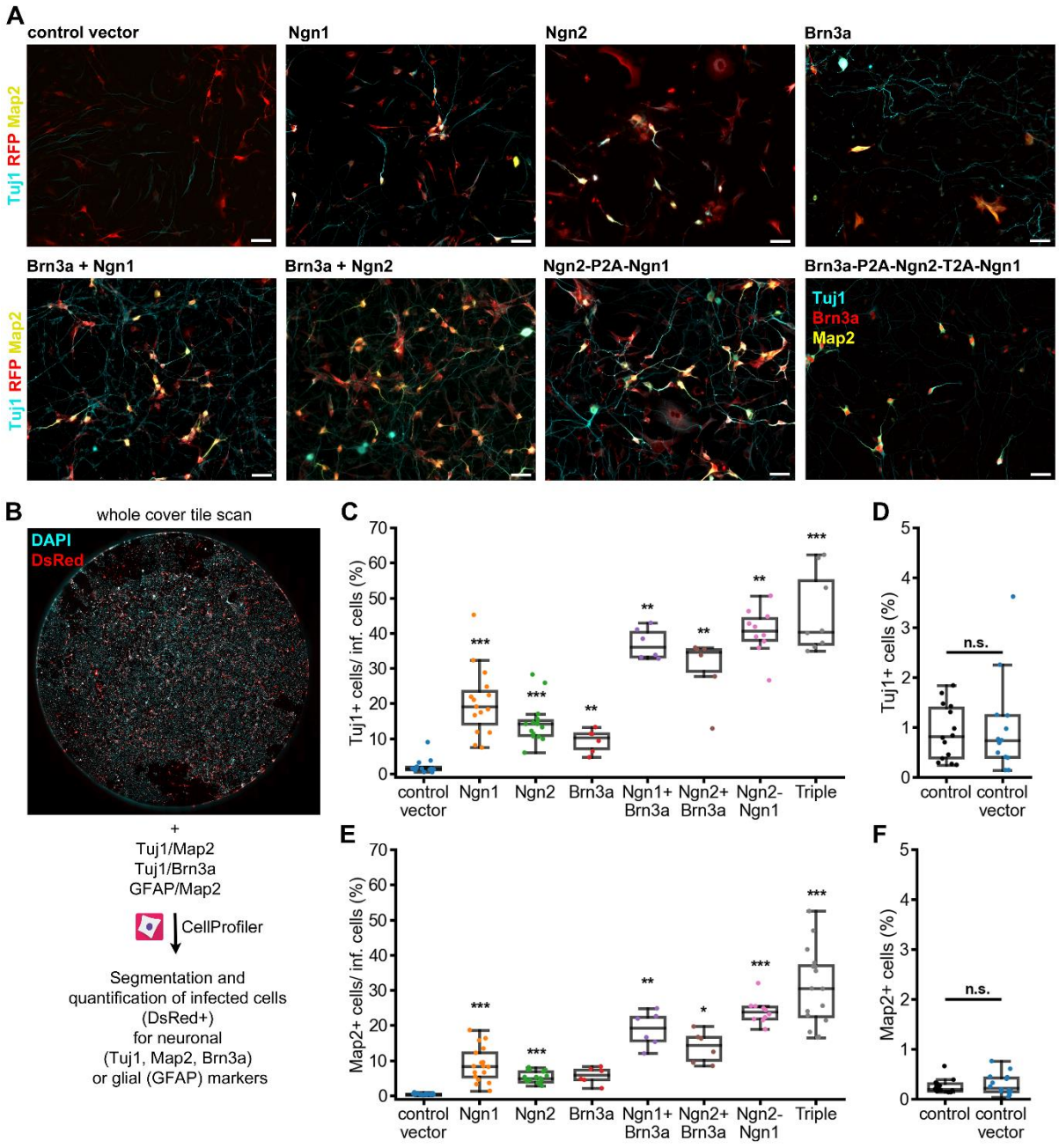

Figure 6. Reprogramming of glial sensory progenitor (gSP) cells with neurogenins and Brn3a. (**A**) Representative images of gSP cells infected with CAG-IRES-DsRed-based retroviral vectors at 7 dpi. Infected cells are labelled with ^{IRES}DsRed (stained: RFP, red) or Brn3a (red). βIII-Tubulin (Tuj1, cyan) and Map2 (yellow) mark neuronal properties in cells transduced with retroviral vectors expressing indicated transcription factors. Brn3a and neurogenin vectors (Ngn1, Ngn2) were also simultaneously infected (Brn3a+Ngn1, Brn3a+Ngn2). Scale bars: 50 µm. (**B**) Whole cover scans were segmented (threshold-based) and quantified with CellProfiler. The percentage of the infected cells positive for (**C-D**) Tuj1 and (**E-F**) Map2 are shown with bar graphs. The control vector was compared to an uninfected control based on all cells. Triple: Brn3a-P2A-Ngn2-T2A-Ngn1. Significant changes compared to the control vector are marked with: *p ≤ 0.05; **p ≤ 0.01; ***p ≤ 0.001; n.s.: not significant. DsRed/RFP, red fluorescent protein.

Due to the high reprogramming efficiency of Ngn2-P2A-Ngn1 (Figure 6), we asked whether additional Brn3a expression, e.g., with the triple vector (Brn3a-P2A-Ngn2-T2A-Ngn1), was even necessary. As suspected, Brn3a was already present in some of the neurogenin-expressing gSP cells 7 dpi (Figure 7 A-B). Especially Neurog1 and Neurog2 coexpression induced Brn3a expression, with about 30% of the infected gSP cells being Brn3a-positive (Figure 7 C). In contrast, Brn3a was barely present in uninfected or control-infected gSP cells (Figure 7 D). Therefore, Brn3a coexpression with neurogenins might be obsolete, and the reprogramming procedure was continued with Ngn2-P2A-Ngn1.

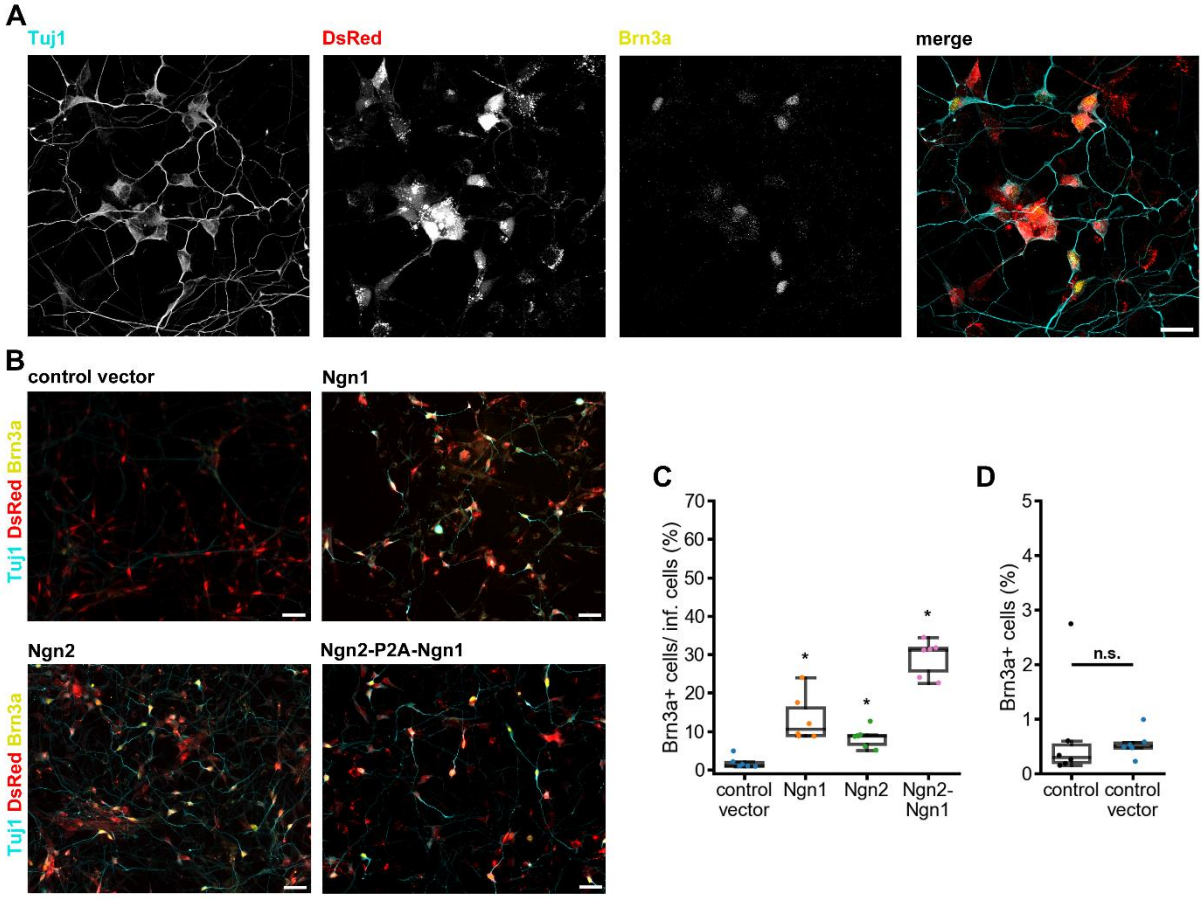

Figure 7. Brn3a expression in gSP cells induced by neurogenins. (**A**) Representative confocal image of Ngn2-P2A-Ngn1 transduced cells (7 dpi) and (**B**) fluorescent images of control- and neurogenin-transduced cells labeled for the neuronal marker βIII-Tubulin (Tuj1, cyan) and the transcription factor Brn3a (yellow). ^{IRES}DsRed marks infected cells. Scale bar: (A) 25 µm (B) 50 µm. (**C**) Percentage of Brn3a-positive cells in neurogenin (Neurog1 and/or Neurog2) infected cells (**D**) and in the controls (uninfected and infected). Significant changes compared to the control vector: *p ≤ 0.05; n.s.: not significant. DsRed, red fluorescent protein; gSP, glial sensory progenitor.

4.1.4 gSP cells can differentiate into glial cells by neurogenin expression

So far, gSP cells showed high reprogramming potential in direction of a neuronal phenotype when neurogenins and Brn3a are expressed (Figure 6). However, neurogenins (Neurog2) have been shown to promote the differentiation of peripheral progenitor cells not only into sensory neurons but also glial cells (Kim *et al*, 2011; Zirlinger *et al*, 2002). Indeed, forced expression of both Neurog1 and Neurog2 was sufficient to also induce a GFAP-positive cell phenotype (Figure 8 A-B), while expression of the proneuronal Brn3a prohibited the development of the glial-like cell phenotype (Figure 8 C). GFAP-positive cells were induced in about 20% of the neurogenin (Ngn1, Ngn2, Ngn2-P2A-Ngn1) infected cells (Figure 8 D), whereas controls only showed 0.5-1% GFAP-positive glial cells (Figure 8 E).

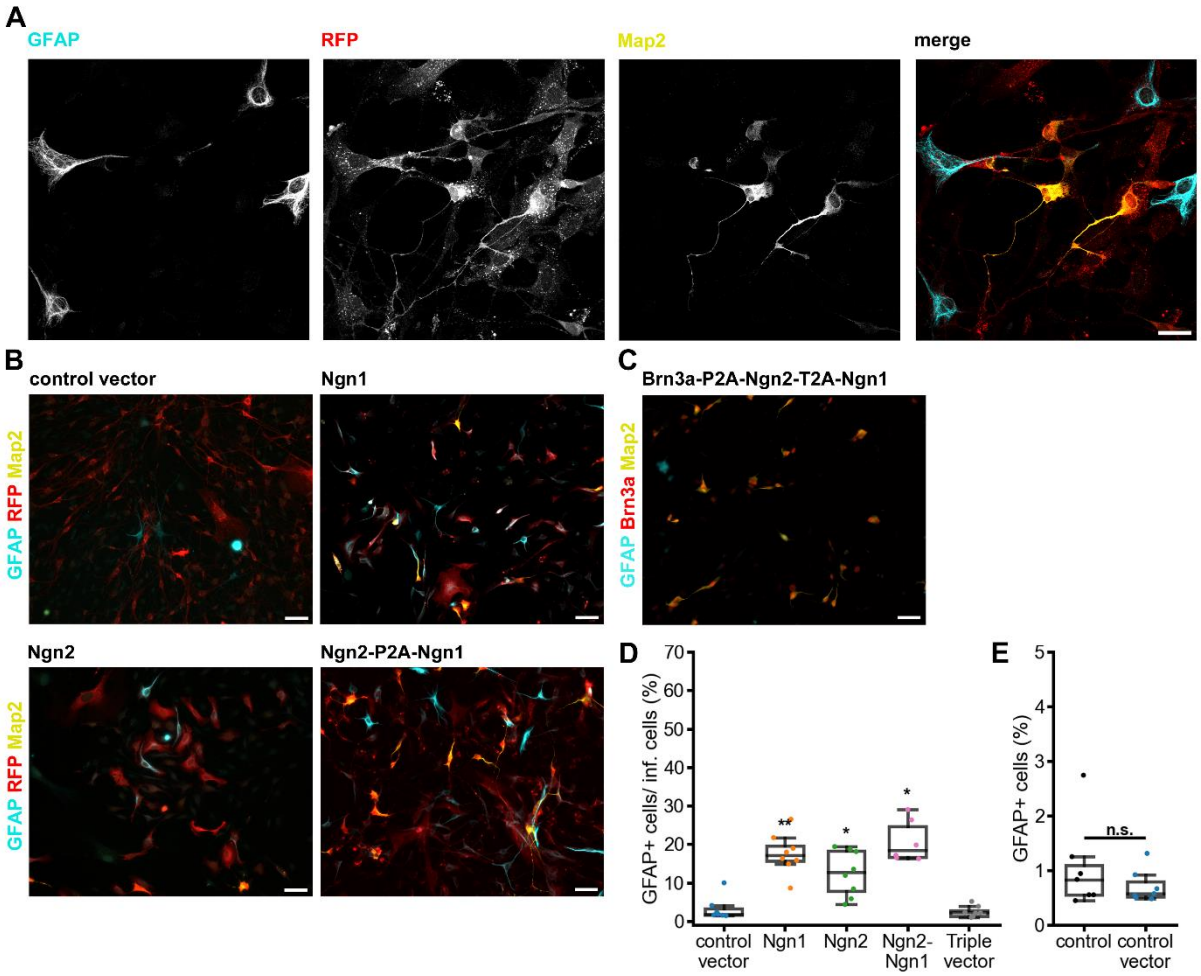

Figure 8. GFAP-positive glial cells induced by neurogenins (**A**) Representative confocal image of Ngn2-P2A-Ngn1 infected cells (7 dpi) labelled for the glial marker GFAP (cyan), the neuronal marker Map2 (yellow), and RFP (red). Scale bar: 25 µm. (**B**) GFAP (cyan) and Map2 (yellow) in control, neurogenin (Neurog1 and/or Neurog2), and triple vector transduced cells. RFP (red) labels ^{IRES}DsRed-positive, infected cells. (**C**) The triple vector contains Brn3a-P2A-Ngn2-T2A-Ngn1. Scale bar: 50 µm. (**D**) Percentage of GFAP-positive cells in neurogenin or triple vector infected cells (**E**) and the controls (uninfected and infected). Significant changes compared to the control vector: *p ≤ 0.05; **p ≤ 0.01; n.s.: not significant. DsRed/RFP, red fluorescent protein; GFAP, glial fibrillary acidic protein.

4.1.5 gSP-derived neurons show immunoreactivity to nociceptor markers

To further differentiate the gSP-derived neurons, 100 ng/ml nerve growth factor (NGF) was added to the cell culture. NGF is a neurotrophin and high-affinity ligand for TrkA (tropomyosin receptor kinase A) that promotes the differentiation of sensory neurons over TrkA signaling (Sharma *et al.*, 2020). When cultured for more than two weeks (14-16 dpi), gSP-derived neurons developed longer neurites, had a diameter of about 10-15 µm, and were able to form clusters of neurons (Figure 9 A-C). Moreover, cells showed immunoreactivity to marker proteins typical for nociceptors. The cells showed pronounced expression of the intermediate neurofilament peripherin, TrkA, and the TTX-resistant voltage-gated sodium channel $Na_V1.9$ (Figure 9 D-F). Also, gSP-derived neurons expressed the transient receptor potential channel TrpA1, the receptor for mustard oil, and TrpV1, the receptor for capsaicin (Figure 9 G-H).

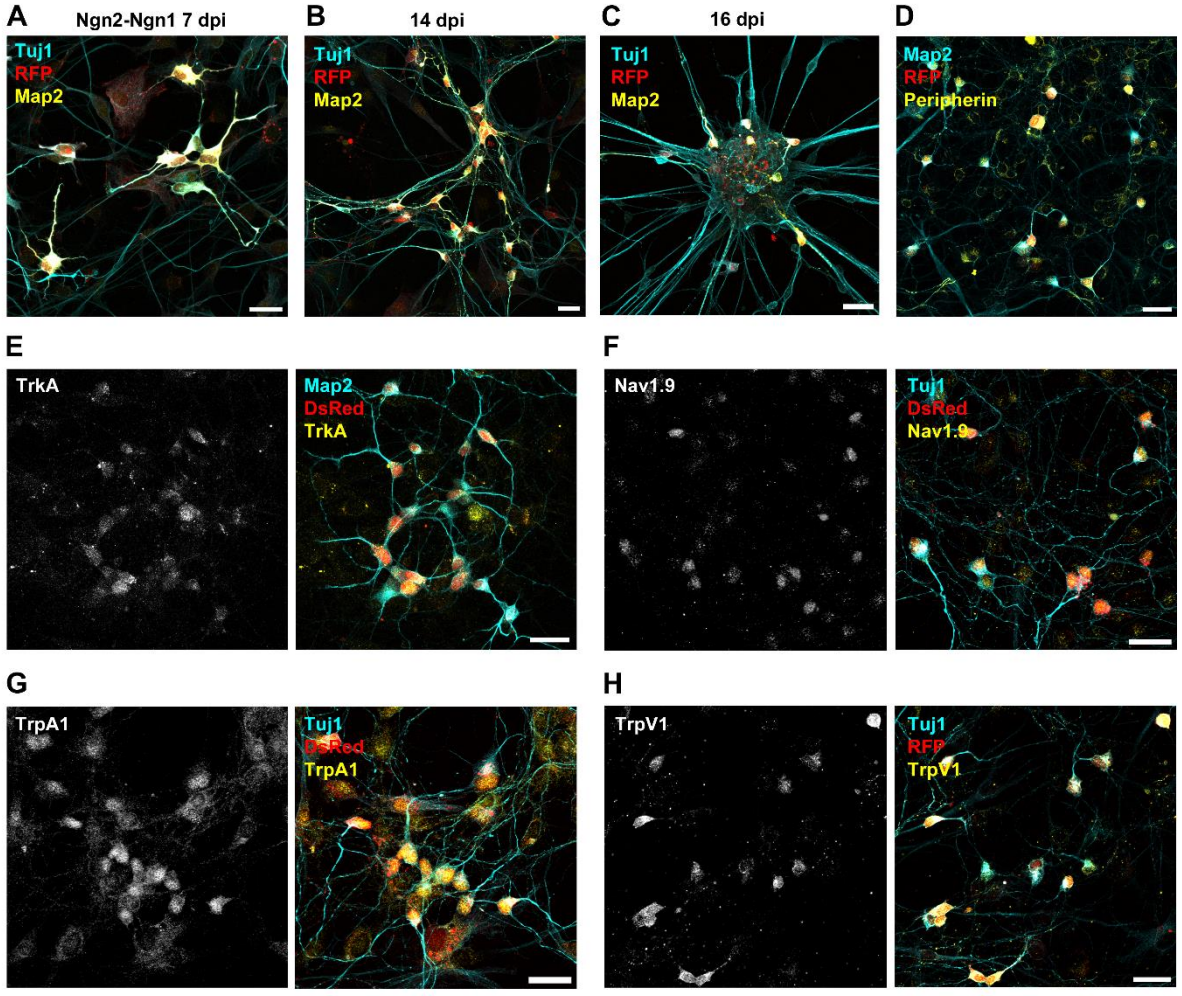

Figure 9. Nociceptor-like, sensory neuron hallmarks in gSP-derived neurons. Representative confocal images display gSP-derived neurons reprogrammed with Ngn2-P2A-Ngn1, as visualized with ^{IRES}DsRed (stained: RFP, red). Labelled are the neuronal markers βIII-Tubulin (Tuj1) and Map2 at (**A**) 7 dpi, (**B**) 14 dpi, and (**C**) 16 dpi. (**D**) Peripherin (yellow) and (**E**) TrkA (yellow) are shown together with Map2 (cyan). (**F**) The sodium channel $Na_V1.9$ (yellow), (**G**) the nociceptor markers TrpA1 (yellow), and (**H**) TrpV1 (yellow) are counterstained with Tuj1 (cyan). Scale bars: 25 µm. DsRed/RFP, red fluorescent protein; gSP, glial sensory progenitor.

4.1.6 gSP-derived neurons are sensitive to capsaicin and mustard oil

gSP-derived neurons were tested for calcium responses to the TrpV1 agonist capsaicin and the TrpA1 agonist mustard oil (allyl-isothiocyanate, AITC) at 14-15 dpi. Neurogenin-infected cells were identified by their coexpression of DsRed with the help of StarDist2D. Uninfected cells on the same coverslip served as a control (Figure 10 A). gSP-derived neurons responded with a cytosolic calcium transient in response to the acute application of capsaicin (10 µM for 10 s). Capsaicin responses were heterogenous in time and amplitude (Figure 10 B). Uninfected cells did barely respond to capsaicin (Figure 10 C). Overall, about 35% of the infected cells were capsaicin-sensitive (Figure 10 D). Stimulation of TrpA1 with 100 µM AITC also induced calcium responses (Figure 10 C). 11% of the neurogenin-DsRed-positive cells were sensitive to AITC (Figure 10 F-G).

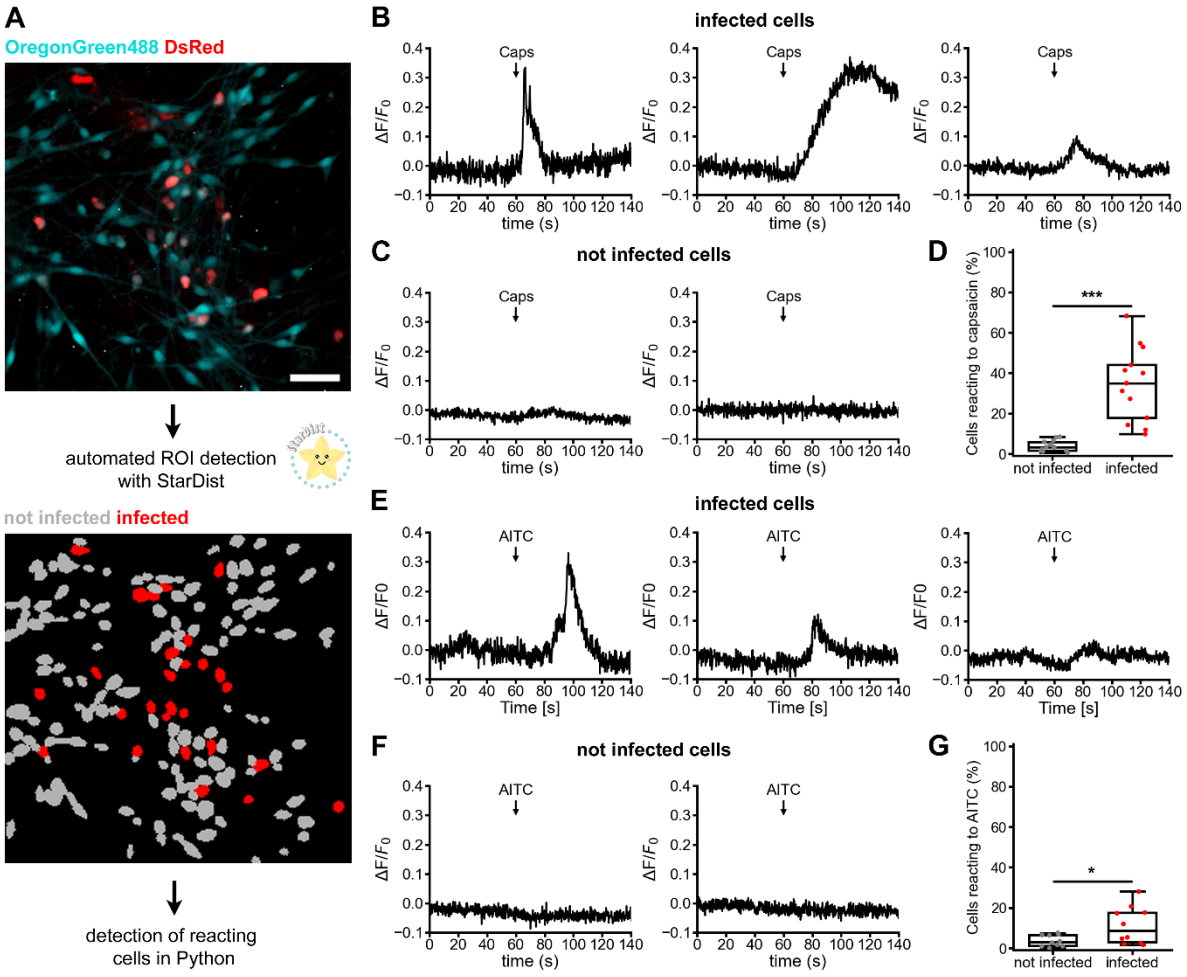

Figure 10. Sensitivity of gSP-derived neurons to the TrpV1 agonist capsaicin and the TrpA1-agonist AITC. (**A**) Workflow: Calcium signals were detected with Oregon Green 488 (cyan) in Ngn2-P2A-Ngn1 infected cells (14-16 dpi), labelled with ^{IRES}DsRed (red). Automatic region of interest (ROI) detection with StarDist2D separated not infected (grey) from infected (red) cells. The percentage of reacting cells was determined using python scripts. Scale bar: 50 µm. (**B-C**) Representative calcium signals of infected and uninfected cells stimulated for 10 s with 10 µM capsaicin (Caps). (**D**) Bar graph: Percentage of infected and uninfected capsaicin-sensitive neurons (n = 13 measurements). (**E-G**) Representative AITC-induced calcium signals and percentage of AITC-sensitive neurons (stimulation with 100 µM AITC for 10 s) (n = 10 measurements). Significant differences: *p ≤ 0.05; ***p ≤ 0.001. DsRed, red fluorescent protein; gSP, glial sensory progenitor; AITC, allyl-isothiocyanate.

4.1.7 Sensory progenitor derived neurons show neuronal properties that differ from those of naïve small-diameter DRG neurons

Next, we used whole-cell patch-clamp recordings to analyze the electrophysiological properties of the gSP-derived neurons compared to naïve small-diameter DRG neurons (Figure 11 A). We found pronounced inward and outward currents in 72 recorded gSP-derived neurons 14-17 dpi (Figure 11 B). Inward current densities were significantly smaller, but outward current densities, as well as the resting membrane potentials (RMP, mean: -46.95 ± 1.35 mV), were similar to naïve DRG neurons (Figure 11 C-E).

gSP-derived neurons were able to fire action potentials (Figure 11 F). The firing threshold (-28.18 ± 0.63 mV) was similar to naïve neurons (Figure 11 G), whereas the spike width at -20 mV (2.82 ± 0.08 ms) and the maximum (11.76 ± 0.91 mV) and minimum (-63.44 ± 0.33 mV) action potential amplitudes differed significantly (Figure 11 H-J).

The ability to fire multiple action potentials was seen in some of the gSP-derived neurons using 300 ms long current stimulations (Figure 11 K). Multiple action potentials (mostly 2-3) were found in 7 % of all neurons. 75% of all gSP-derived neurons fired only one action potential. In contrast, 69% of all naïve small-diameter DRG neurons showed multiple spike events (Figure 11 L-M). The rheobase (51.19 ± 3.32 pA) was comparable between SP-induced neurons and naïve neurons (Figure 11 N).

TTX-resistant currents are very characteristic of nociceptors. They are based on the sodium channels $Na_V1.9$ and $Na_V1.8$ (Dib-Hajj *et al*, 2002; Djouhri *et al*, 2003). Furthermore, $Na_V1.5$-mediated inward currents have been observed during sensory neuron development (Renganathan *et al*, 2002). To test for TTX-resistant, voltage-gated inward currents, gSP-derived neurons were analyzed by whole-cell patch clamp recording in presence of 500 nM TTX (Figure 11 O) (Leipold *et al*, 2013). Cells held at -130 mV reached about -200 pA TTX-resistant currents at a 0 mV test pulse (Figure 11 P). Under these conditions, TTX-resistant inward currents were seen in 84% of 31 gSP-derived neurons (Figure 11 Q). Neurons were counted as TTX-resistant when the minimal current density was smaller than -30 pA/pF.

In summary, gSP-derived neurons reprogrammed with Neurog1 and Neurog2 coexpression develop a nociceptor-like sensory neuron phenotype. These transdifferentiated neurons express functional TrpA1 and TrpV1 ion channels, show immunoreactivity to TrkA and $Na_V1.9$, and develop biphasic TTX-resistant sodium inward currents and fire action potentials. Still, the gSP-derived nociceptive neurons show differences in their phenotype (smaller size) and electrophysiological properties to naïve cultured small-diameter DRG neurons.

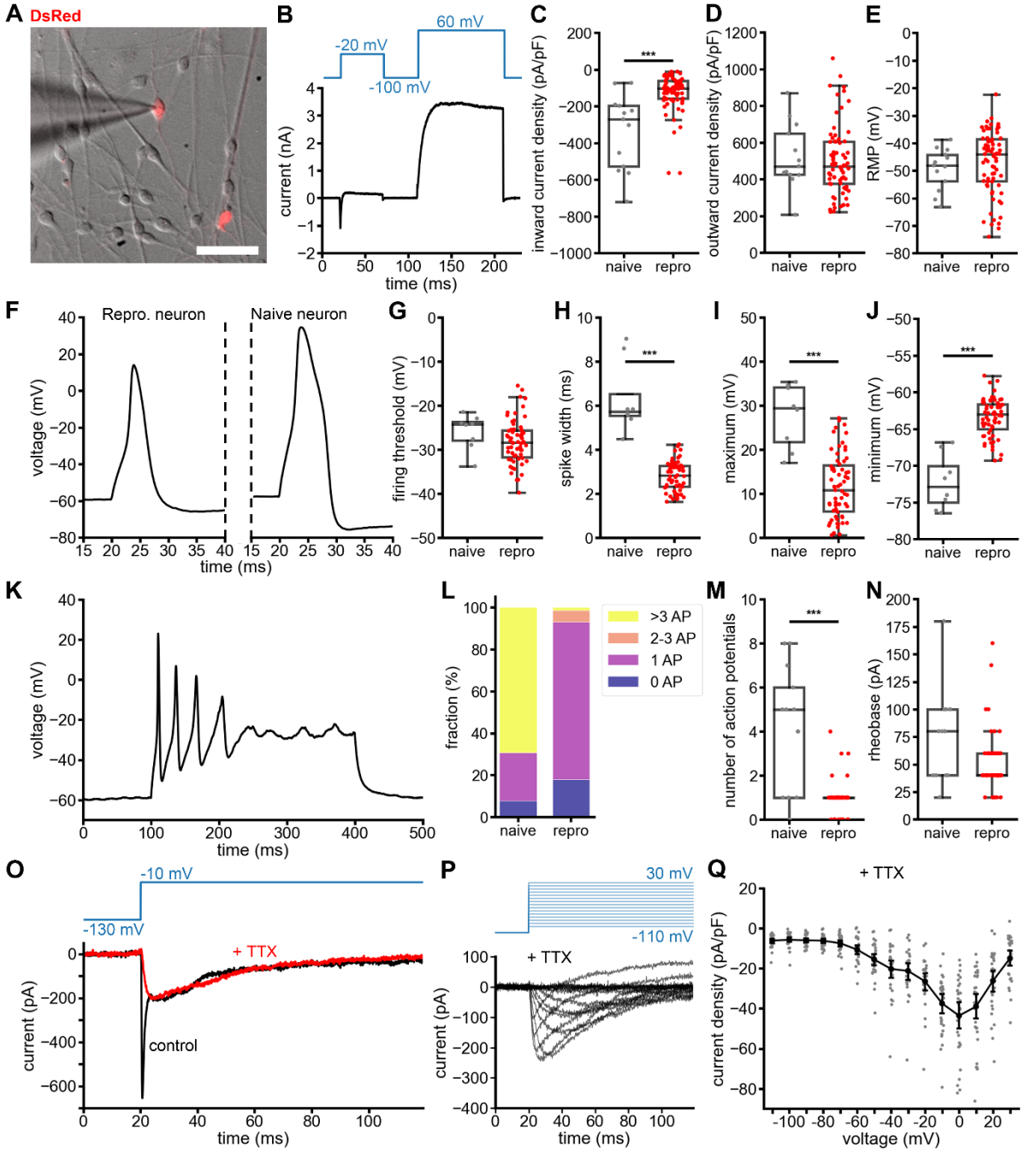

Figure 11. Electrophysiological properties of gSP-derived neurons. (**A**) Patch-clamp recording of a gSP-derived neuron at 17 dpi. Scale bar: 50 µm. (**B**) Representative currents of a gSP-derived neuron at -20 and 60 mV. (**C**) Inward and (**D**) outward current density, and (**E**) resting membrane potential (RMP) of gSP-derived neurons (repro, 14-17 dpi, n=72) were compared to those of 1-2d old naïve small-diameter DRG neurons (n=13). (**F**) Representative single action potentials (APs) of a gSP-derived neuron and naïve DRG neuron stimulated for 3 ms with 60 pA or 220 pA, respectively. (**G**) Firing threshold, (**H**) spike width at -20 mV, (**I**) maximum, and (**J**) minimum of single action potentials of naïve and gSP-derived neurons. (**K**) gSP-derived neuron firing multiple action potentials in response to a 300 ms current injection of 40 pA. (**L**) Fractions of naïve and gSP-derived neurons firing no, one, two, or three or more action potentials. (**M**) Number of action potentials and (**N**) rheobase of naïve and gSP-derived neurons are shown. (**O**) Inward currents of a representative gSP-derived neuron at -10 mV before and after application of 500 nM TTX. (**P**) Representative current traces of a gSP-derived neuron in presence of 500 nM TTX in response to 100 ms long depolarizing voltages ranging from -110 to 30 mV in steps of 10 mV. (**Q**) Mean peak inward current densities ± S.E.M. as a function of voltage of gSP-derived neurons in presence of 500 nm TTX. Dots represent peak current densities of individual cells (n=31). Significant differences: ***p ≤ 0.001. DsRed, red fluorescent protein; gSP, glial sensory progenitor; TTX, tetrodotoxin.

4.2 Unbiased analysis of cellular plasticity in the DRG after peripheral nerve injury

DRG cell cultures showed high cellular plasticity toward an SGC-like sensory progenitor *in vitro*. Therefore, we asked whether a similar plastic cell type can be found *in vivo*, possibly serving as an endogenous cell source for reprogramming into neurons after peripheral nerve injury. To assess the necessity of neuronal replacement therapy, we also investigated whether and to which extent neuronal loss occurs after peripheral nerve injury.

In a previous study, we acquired immunofluorescence microscopy images of DRG sections of rats after SNI and sham injury. The images showed characteristic features of the DRG: NF labelling visualized sensory neuron somata and fiber-rich regions, and the GS and GFAP signals surrounded the NF-labeled sensory neurons in a ring-like shape. As expected after SNI, DRG sections showed more GFAP signal (Schulte *et al.*, 2022c).

4.2.1 DRG sections can be analyzed by DL-based image segmentation

To objectively investigate SGC and neuronal changes in DRG of SNI-injured rats, we used a deep learning (DL)-based image segmentation approach previously described for brain tissue (Griebel *et al.*, 2021; Segebarth *et al.*, 2020) (Figure 3). Here, multiple experts (this study: three) annotated representative images. The matching annotations from all experts form an estimated ground truth that is used to train DL model ensembles (Segebarth *et al.*, 2020). We computed two DL model ensembles, one for NF-positive neuronal somata, and one for both GS- and GFAP-positive glial cells (Figure 3). With these DL models, a total of 2541 images of DRG sections (847 per marker) were segmented (Schulte *et al.*, 2022c).

The validity of the image segmentations was evaluated with the intersection over union (IoU) metric. The IoU measures how well two segmentations overlap with zero (0) meaning no overlap and one (1) meaning a perfect match. According to other studies, a mean IoU value of at least 0.50 indicates overlapping segmentations of two ROIs (Falk *et al*, 2019; Griebel *et al.*, 2021; Maška *et al*, 2014). The expert annotations for the estimated ground truth showed higher similarities for NF-positive image features (mean IoU = 0.86) than for GFAP- (mean IoU = 0.61) or GS-positive image features (mean IoU = 0.65) (Schulte *et al.*, 2022c). Likewise, the NF model ensemble performed with a mean IoU of 0.867 better than the GS/GFAP glial cell model ensemble (GFAP: mean IoU = 0.543; GS: mean IoU = 0.583) on the test images (Schulte *et al.*, 2022c). Nevertheless, all models achieved IoU values close to the performed similarity of the human experts. All images and their predicted segmentations are provided online (Schulte *et al.*, 2022b). Examples can be explored with an interactive data app (https://share.streamlit.io/amschulte/drg/main).

4.2.2 Satellite glial cells show cellular plasticity but no gliosis

To assess SGC plasticity after SNI, we analyzed the GFAP and GS segmentations based on their proximity to neurons (Figure 12 A) (Schulte *et al.*, 2022c). The GFAP area per neuronal area and the percentage of neurons in proximity to GFAP-positive cells increased after SNI, more so 7 d after injury than 14 d after injury (Figure 12 B-C). Twice as many medium-sized and large-sized neurons compared to small-sized neurons were in proximity to GFAP-positive glial cells after injury (Figure 12 D-E). Surprisingly, immunoreactivity to GS, a supposed stable SGC marker in rodents, was decreased in SGCs after SNI. The GS area and the percentage of neurons in proximity to GS-positive SGCs were decreased after SNI (Schulte *et al.*, 2022c). For the overall amount of SGCs, GFAP and GS segmentations were merged into one glial cell ring segmentation, and the area of the glial cell rings and the percentage of neurons in proximity to glial cells were determined (Figure 13 A). Moreover, the GS and GFAP segmentation overlap was analyzed relative to the GS or GFAP segmentation area, respectively (Figure 13 B). Instead of an increase, indicating gliosis, we found a small, significant reduction of glial cells after SNI using the markers GS and GFAP. The glial cell ring area per neuronal area was reduced at the contralateral (CL) side after SNI (Figure 13 C). In proximity to neurons, both the ipsilateral (IL) and CL sides showed a significant decrease of neurons in proximity to glial cells 7 d after SNI (Figure 13 D). 14 d after SNI, no change was seen (Schulte *et al.*, 2022c).

Lastly, we observed plasticity changes in the composition of the glial cell markers. Ipsilaterally, GS-positive glial cells also expressed more GFAP (Figure 13 E), whereas fewer of the GFAP-positive glial cells were also GS-positive after SNI (Figure 13 F). L4 and L5 DRG were affected to a similar extent by all of the described changes (Schulte *et al.*, 2022c).

Altogether, we saw no sign of gliosis, but a slight decrease in the number of GS- and/or GFAP-positive glial cells after SNI. SGCs shifted from a mainly GS-positive to a more GFAP- and less GS-positive cell phenotype (Schulte *et al.*, 2022c).

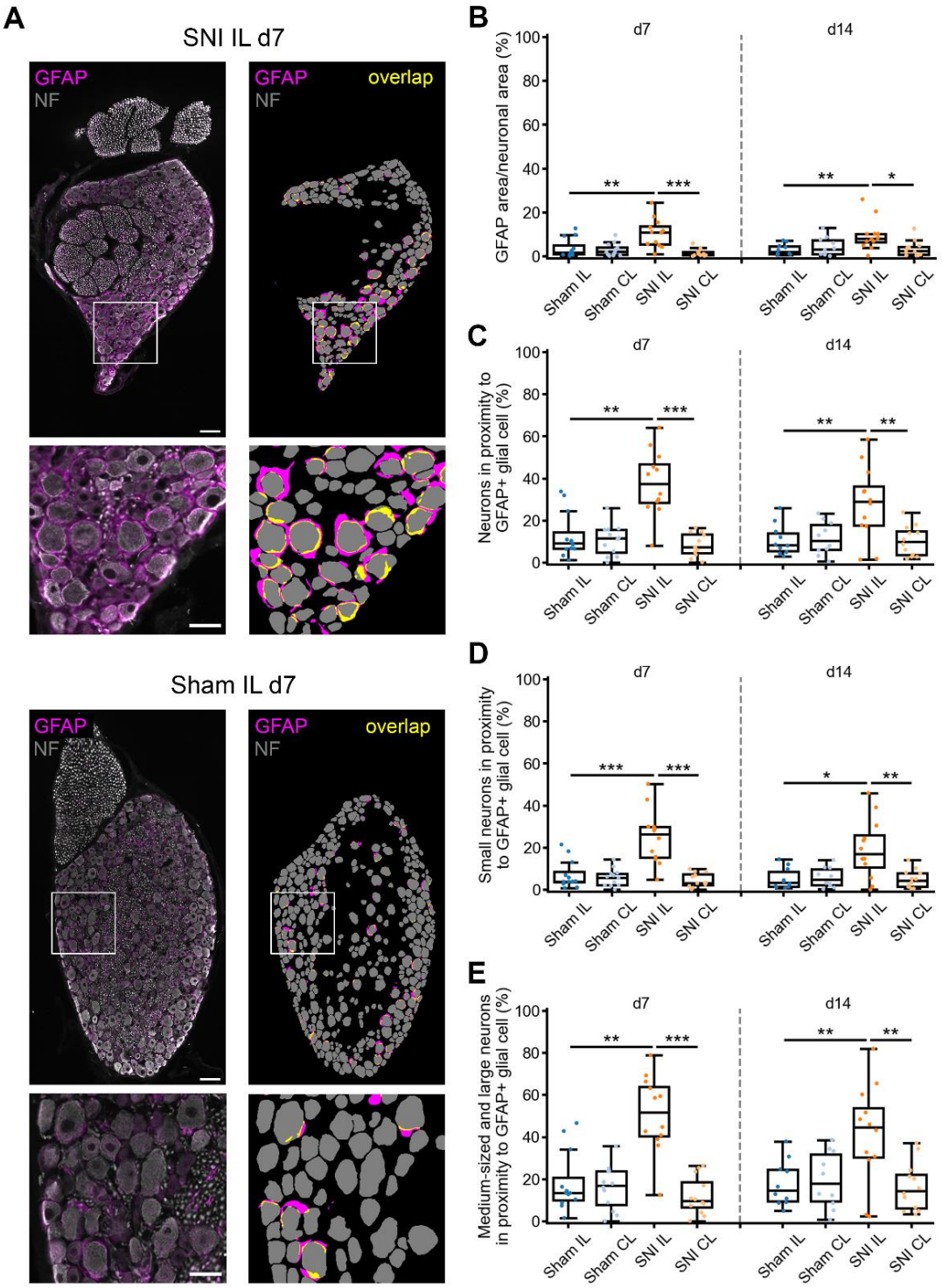

Figure 12. Increase of GFAP-positive SGCs around all types of neurons after SNI. (**A**) Representative immunofluorescent staining and corresponding DL-mediated segmentation of GFAP (magenta) and NF (gray) from SNI IL and sham IL injury sides. Yellow visualizes the overlap of GFAP-positive glial cells and neurons (scale bars: 100 µm/50 µm). (**B-E**) Image quantification displaying GFAP area per neuronal area (**B**, in %) as well as the percentage of all, small, and medium/large neurons that are in proximity to GFAP-positive glial cells. Sham IL, sham CL, SNI IL, and SNI CL 7 d (left), and 14 d (right) after injury (n = 10-12 DRG) are shown. Significant changes: *p ≤ 0.05; **p ≤ 0.01; ***p ≤ 0.001. GFAP, glial fibrillary acidic protein; SGC, satellite glial cell; SNI, spared nerve injury; IL, ipsilateral; CL, contralateral. Reproduced from (Schulte *et al.*, 2022c).

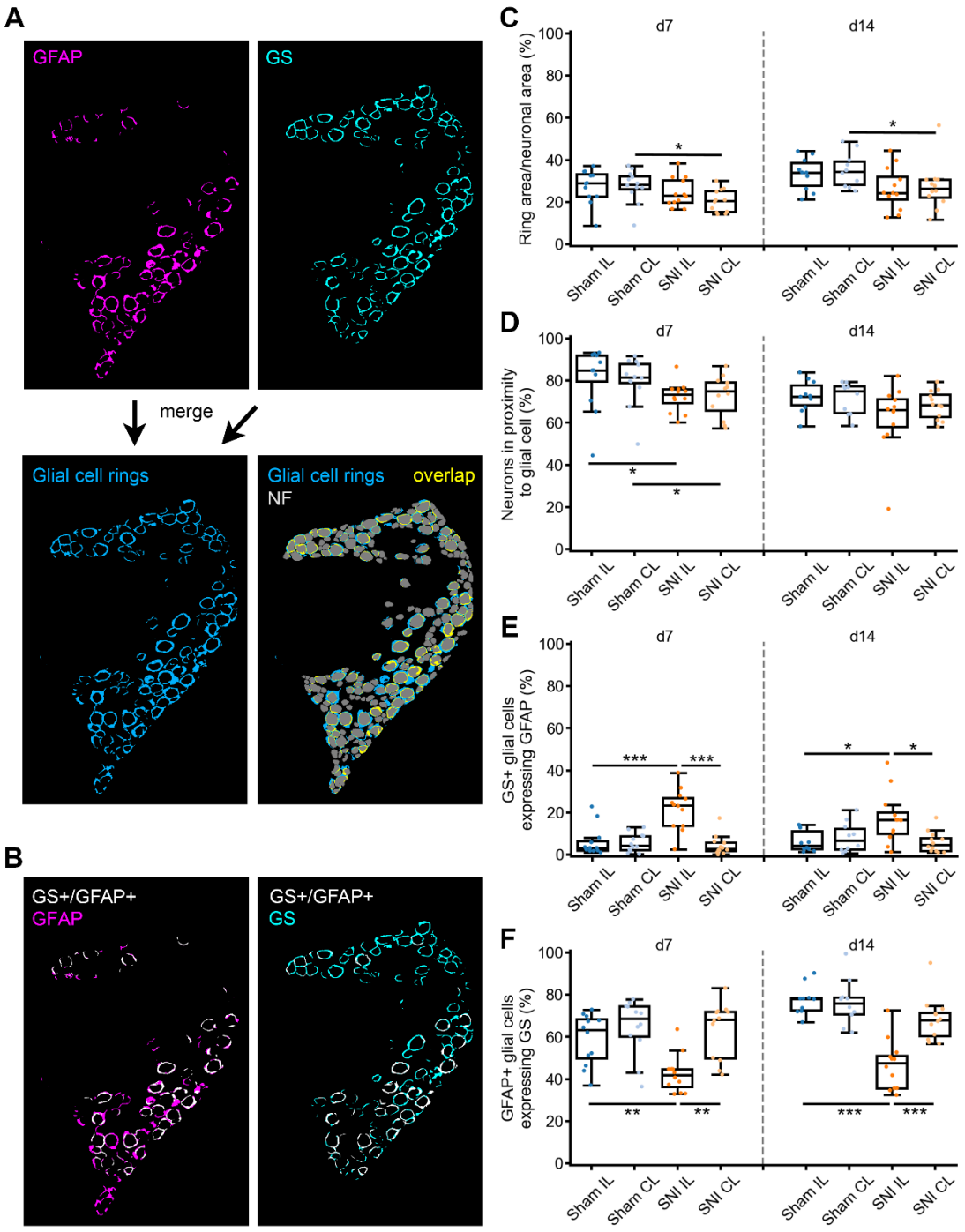

Figure 13. Cellular plasticity of SGCs after SNI. (**A**) Visualization of image analysis. GFAP (magenta) and GS (cyan) segmentation are merged into a glial cell ring segmentation (blue). NF-positive neurons that overlap with glial cell rings (yellow) are “neurons in proximity to glial cells”. (**B**) The overlap of GS- and GFAP-positive glial cells (white) was quantified in relation to all GFAP- (magenta + white) or GS- (cyan + white) positive glial cells. Image quantification for (**C**) glial cell ring area per neuronal area, (**D**) neurons in proximity to glial cells, (**E**) as well as GS-positive glial cells expressing GFAP-, and (**F**) GFAP-positive glial cells expressing GS are shown (in %). Compared were sham IL, sham CL, SNI IL, and SNI CL 7 d (left) and 14 d (right) after injury (n = 10-12 DRG). Significant changes: *p ≤ 0.05; **p ≤ 0.01; ***p ≤ 0.001. GFAP, glial fibrillary acidic protein; GS, glutamine synthetase; SGC, satellite glial cell; SNI, spared nerve injury; IL, ipsilateral; CL, contralateral. Reproduced from (Schulte *et al.*, 2022c).

4.2.3 The number of neurons is unchanged by SNI

Based on the NF segmentations of our large-scale dataset (Figure 14 A), we investigated if a neuronal loss occurs after peripheral nerve injury. Sensory neurons were composed of 50-60% (<700 µm²) small neurons (nociceptive, thermo-, and itch-sensitive), and 40-50% medium-sized and large neurons (≥700 µm², mechano- and proprioceptive). No significant change in this neuronal composition was seen after SNI (Figure 14 B-E). The total number of neurons, estimated in relation to the tissue area (Figure 14 F), was not changed at 14 d after injury (Figure 14 G) (Schulte *et al.*, 2022c).

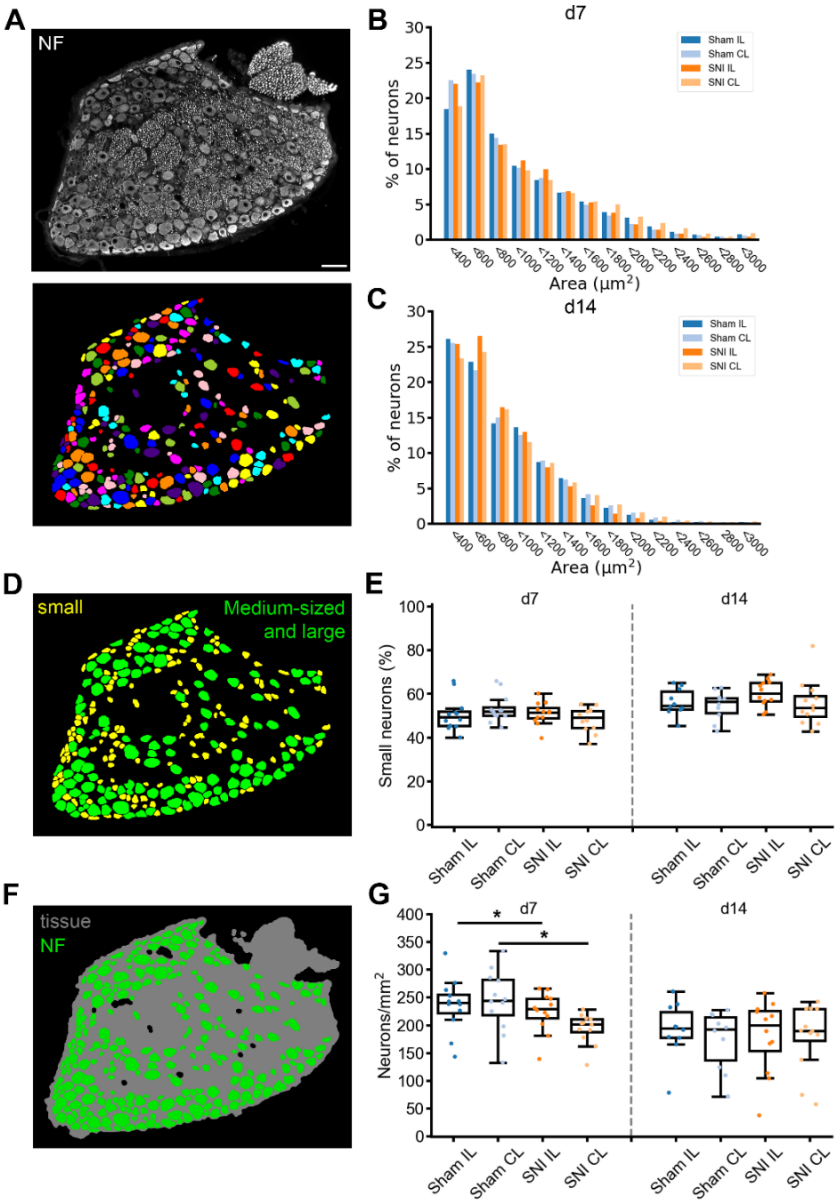

Figure 14. No loss of sensory neurons after SNI. (**A**) Segmentation of NF-stained DRG neurons (scale bar: 100 µm). (**B, C**) Size distribution of neurons 7 and 14 d after injury. (**D, E**) Relative number of small neurons (<700 µm²) (yellow) and medium-sized and large neurons (green). (**F, G**) Visualization and quantification of the cellular area including the number of neurons per mm² tissue area. The tissue area is based on the thresholded NF staining. Each dot represents the mean value of the images of one DRG from sham IL, sham CL, SNI IL, and SNI CL 7 d and 14 d after injury (n = 10-12). Significant changes: *p ≤ 0.05. NF, neurofilament; SNI, spared nerve injury; IL, ipsilateral; CL, contralateral. Reproduced from (Schulte *et al.*, 2022c).

4.3 Glial cells in human DRG after plexus injury

4.3.1 Either “neuronal loss” or “neuronal preservation” in DRG of patients with brachial plexus injury

As we could neither see sensory neuron loss nor gliosis after experimental peripheral nerve injury in rodents (Figure 15, Figure 16 (Schulte *et al.*, 2022c)), we asked whether a nerve injury would change the cellular composition of the neuron-SGC entity in the human DRG.

For this, we performed a collaborative study (Schulte *et al*, 2022a) and analyzed the cellular composition of a cohort of 13 patients after brachial plexus injury. In most cases, plexus injury was caused by a motorcycle accident. The nerve injury was diagnosed by magnetic resonance imaging (MRI). Most patients suffered from avulsion of two to three dorsal roots and all patients showed a pain phenotype (Schulte *et al.*, 2022a). The DRG of the patients, on average five months after brachial plexus injury, were removed during a nerve reconstruction surgery. DRG were fixed and investigated by hematoxylin and eosin (H&E) staining, immunohistochemistry, and large-scale tile microscopy (Schulte *et al.*, 2022a). For comparison, six control DRG were collected during forensic autopsy.

In one group of patients, H&E-staining confirmed typical neuron-rich regions with neuronal somata and surrounding SGCs (Figure 15 A, group: “neuronal preservation”). These intact DRG were surrounded by a thick protective layer and substantial connective tissue was seen between neuronal somata (Figure 15 A, C). Surprisingly, in 7 of the 13 patients, H&E staining showed a complete loss of the multicellular DRG unit (group: “neuronal loss”). Instead of DRG tissue, only fat cells and connective tissue was found in the corresponding tissue volume (Figure 15 B).

Human DRG with neurons were then prepared for cryosectioning and were labelled by immunofluorescent stainings against protein markers that are known to be expressed in human DRG neurons (neurofilament, NF) or satellite glial cells (FABP7) (Avraham *et al*, 2022). Now I asked whether the cellular composition of DRG with “neuronal preservation” is comparable to that of DRG controls.

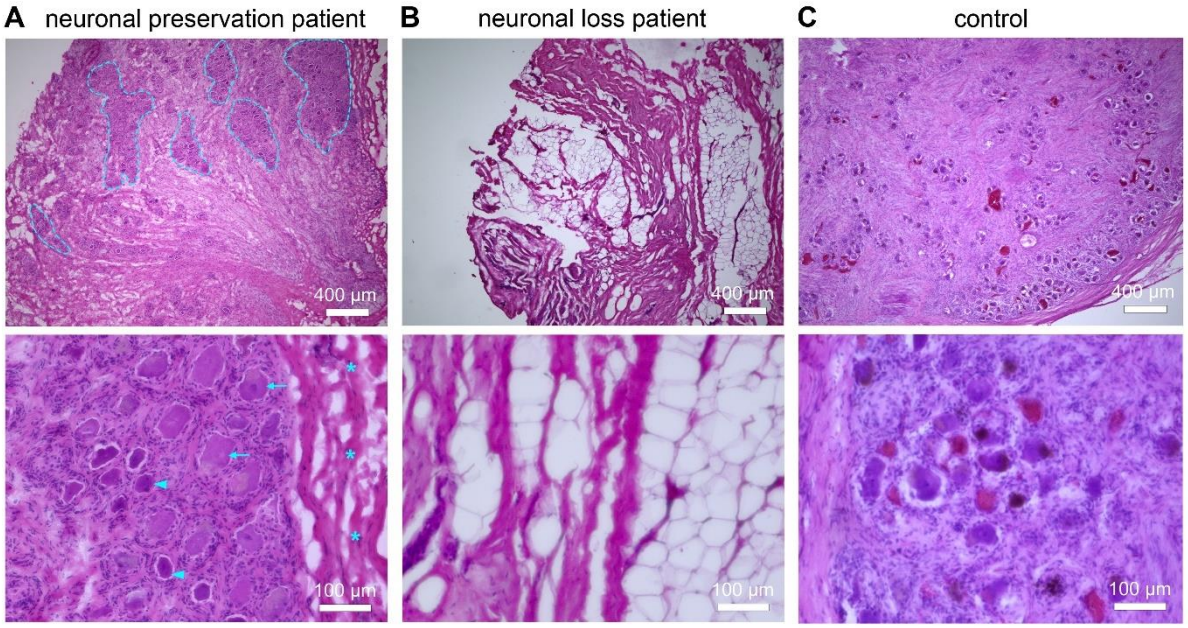

Figure 15. Classification of traumatic dorsal root avulsion patients based on DRG histology: neuronal loss and neuronal preservation. Representative images of H&E stained DRG sections from (**A-B**) patients after plexus injury during reconstructive surgery or (**C**) from controls during forensic autopsies. Arrowheads: small sensory neurons; arrows: large sensory neurons; asterisks: connective tissue; dotted line: neuron-rich area. Scale bars: 400/100 µm as indicated. DRG, dorsal root ganglia. Modified according to (Schulte *et al.*, 2022a). Image data by Dr. Annemarie Aue and Johannes Degenbeck.

4.3.2 Analyzing human DRG with DL-based image segmentation

To objectively investigate differences between the DRG of plexus injury patients and controls, we used our DL-based image segmentation approach on NF-positive neurons in human DRG, as previously described for rat DRG (Schulte *et al.*, 2022c). NF-positive neurons were annotated by three experts and expert annotations overlapped highly with the resulting ground truth estimation (Table 2). The DL models, which were validated with different image data sets, reached a mean dice score of 0.875 (Table 3). Testing of the DL-model ensemble was performed on annotated images that were not previously seen by the DL-model. This control test showed that the trained DL-model predicted segmentations of NF-positive neurons in the human DRG with human expert-like performance (Figure 16).

Thereby, neurons in the DRG of control and patients could be automatically segmented, despite the high variability between the different DRG, for example, in the abundance of autofluorescent lipofuscin aggregates in the neurons (Figure S3).

Table 2: Ground truth estimation performance

expert	average dice score	std dice score
1	0.945	0.013
2	0.931	0.015
3	0.856	0.030
mean	***0.911***	***0.019***

Table 3: Model validation performance

file	model no.	dice score	uncertainty score
0003.tif	1	0.810	0.047
0007.tif	1	0.865	0.042
0002.tif	2	0.929	0.027
0009.tif	2	0.930	0.030
0004.tif	3	0.845	0.040
0006.tif	3	0.870	0.039

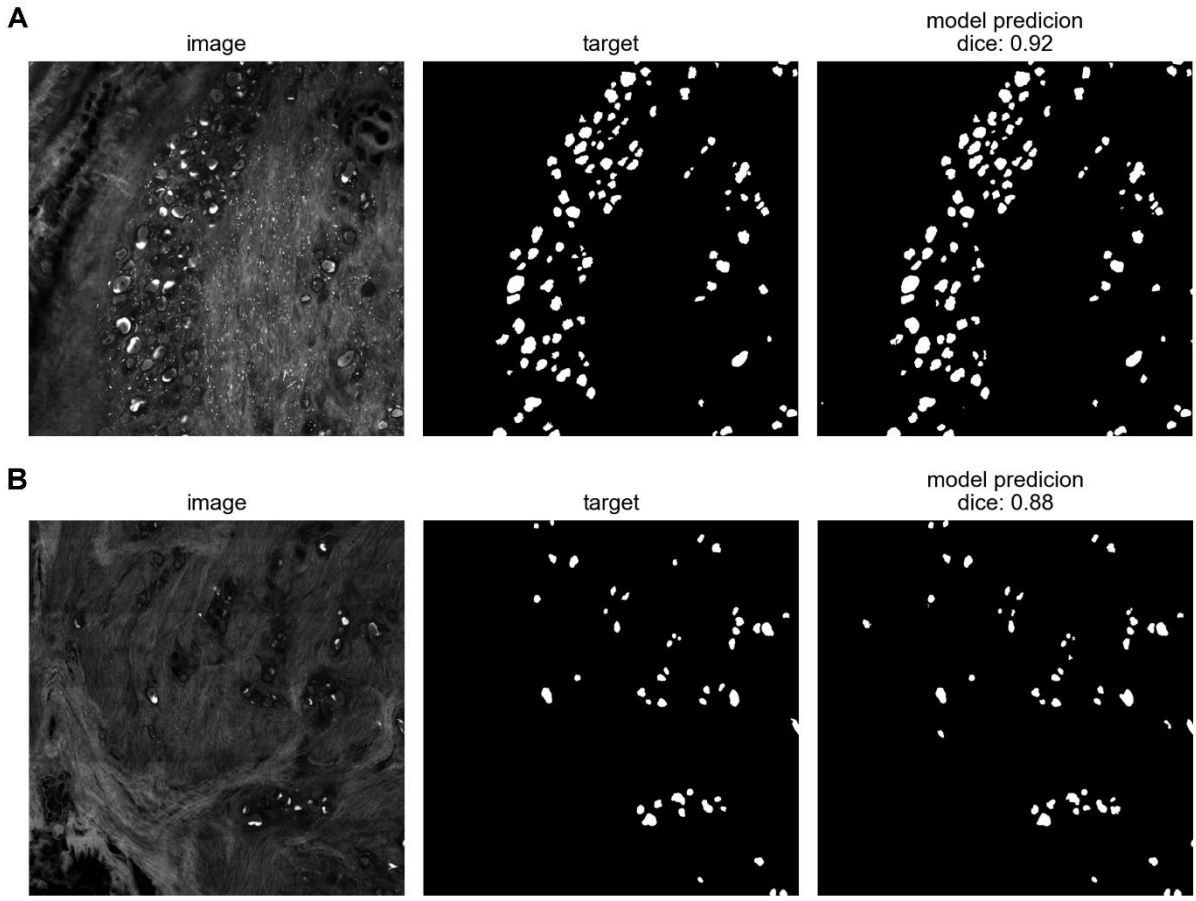

Figure 16. Performance of DL-model on test images. (**A-B**) Two NF images, their expert annotated segmentation target (ground truth), and the model prediction. The similarity of target and model prediction was evaluated with the dice score. DL, deep learning.

Next, I analyzed the DRG sections for SGC plasticity close to neurons and tested them for gliosis (Figure 17). Changes in SGC abundance were computed based on FABP7 immunolabels. Furthermore, anti-APOJ immunoreactivity was used as a plasticity marker because its gene (*CLU*) was shown to be upregulated after nerve injury (Avraham *et al.*, 2020). In line with other studies (Avraham *et al.*, 2022), the typical rodent SGC marker proteins, GS and GFAP, did not label the majority of SGCs well in the human DRG (Schulte *et al.*, 2022a). FABP7 was stained with a high signal-to-noise ratio and was almost exclusively targeting the human SGCs (Figure 17). Therefore, a thresholding method was considered sufficient to segment the human DRG for SGCs. Based on the FABP7-positive area, the intensity of the APOJ signal in SGCs was determined. As a reference size, a convex polygon was automatically drawn around the neurons. This region defined the neuron-rich region of interest (neuronal polygon area; NPA). Moreover, the neuronal NF segmentation was dilated to enable the quantification of anti-FABP7 and APOJ immunoreactivity within and in relation to the neuron near area (NNA). Neurons in proximity to FABP7-positive SGCs were quantified based on the overlap between 1 pixel-dilated neuronal and FABP7 segmentations (Figure 17) (proximity measure as shown in Figure 3). With this procedure, new parameters for quantifying neuronal and glial changes in human DRG were identified.

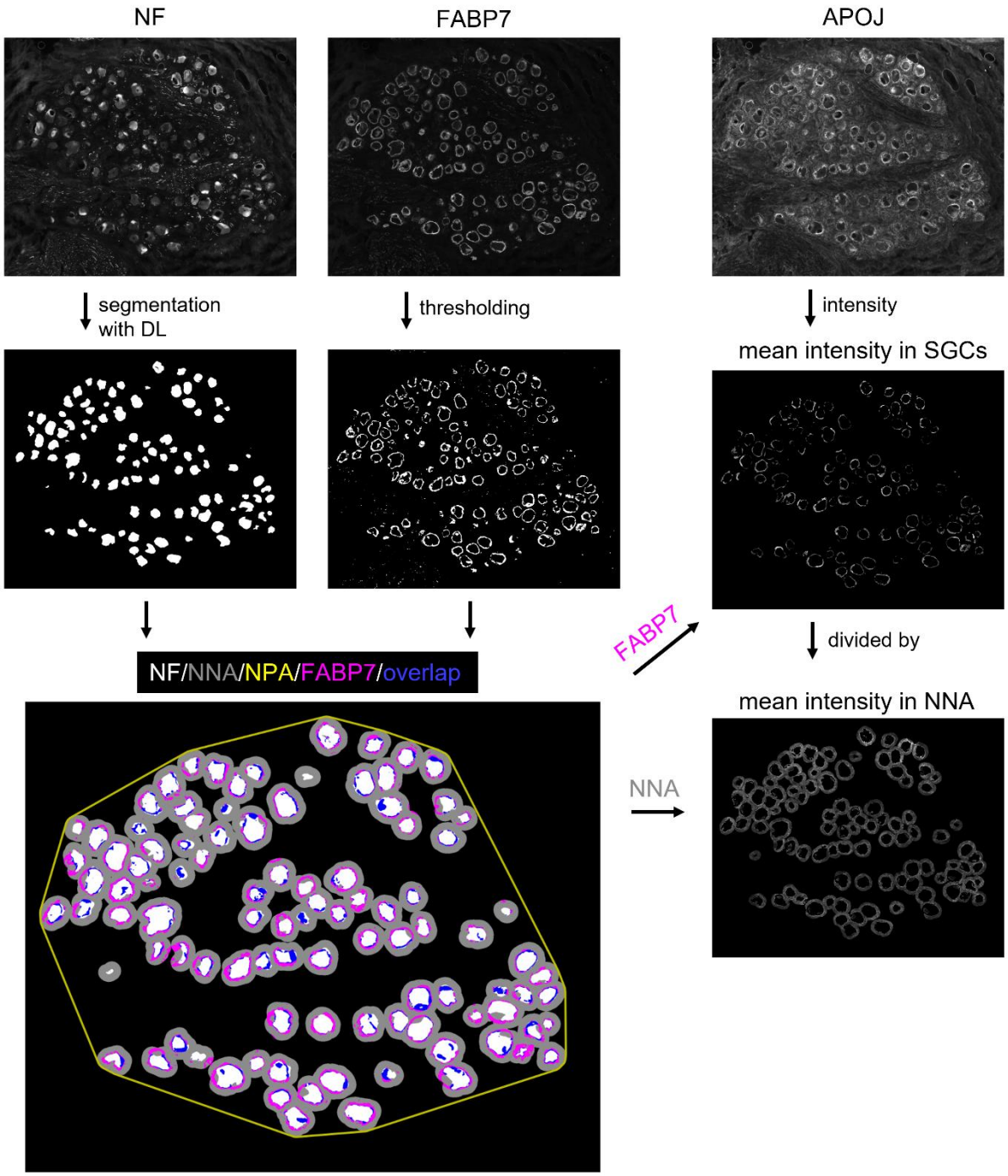

Figure 17. Analysis procedure for human DRG sections. SGC labeled sections were analyzed for the FABP7 area and APOJ intensity. NF-positive neurons were segmented with a DL model ensemble and FABP7-positive SGCs with a thresholding method. NF-positive neurons (white) were quantified in relation to the neuronal polygon area (NPA, yellow). For FABP7, the area per neuron near area (NNA) and per NPA, and the percentage of neurons in proximity to FABP7-positive SGCs, quantified based on the overlap (blue), were determined. The APOJ intensity was calculated by dividing the mean intensity in FABP7-positive SGCs by the mean intensity in the NNA and the NPA. APOJ, apolipoprotein J; DL, deep learning; DRG, dorsal root ganglia; FABP7, fatty acid binding protein 7; NF, neurofilament; SGC, satellite glial cell.

4.3.3 Neurons and satellite glial cells are unchanged in DRG with neuronal preservation

Neuronal somata, well segmented with the DL-based feature extraction approach (Figure 18 A), were slightly smaller in the DRG sections of the control group than in the DRG of patients (Figure 18 B). This might be explained by differences in tissue and staining quality (Figure S3) (Schulte *et al.*, 2022a). The number of neurons did not differ between control and neuronal preservation patients (Figure 18 C). Moreover, similar numbers of FABP7-positive cells occupied the neuron near and neuronal polygon area, while about 95% of all NF-positive neurons were in proximity to FABP7-positive SGCs (Figure 18 D-F). Also, the normalized APOJ intensity in FABP7-positive cells was unchanged between control and neuronal preservation patients (Figure 18 G-H).

In summary, objective annotation of the neuron-satellite glial cell entity in human DRG with nerve injury (group: neuronal preservation) shows neither substantial neuronal loss nor signs of gliosis. In striking contrast, about half of the patients (group: neuronal loss) show a complete loss of the whole cellular DRG unit.

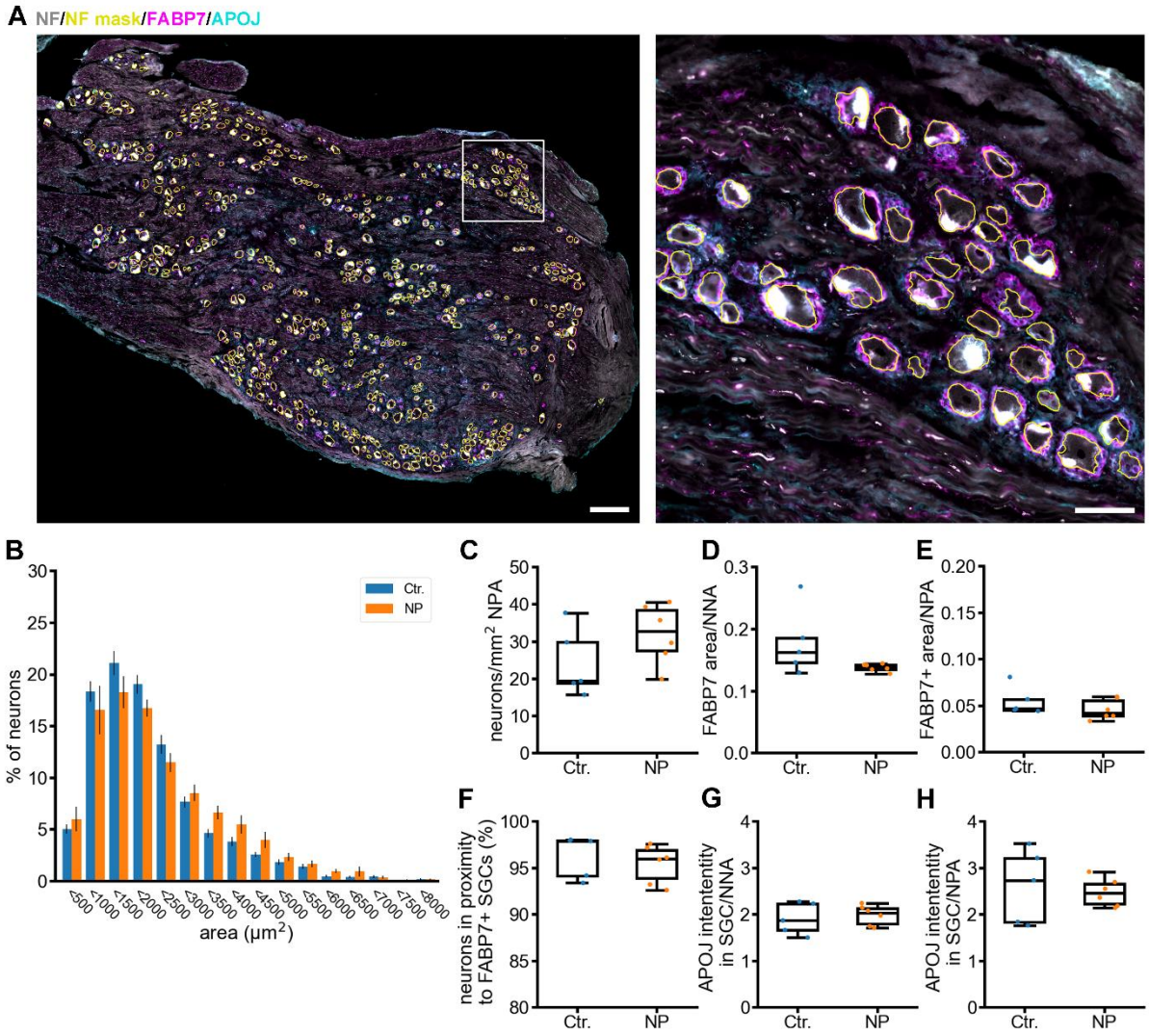

Figure 18. Similar cellular composition of DRG from patients with neuronal preservation vs. control. DL-based unbiased immunohistochemical analysis comparing control (Ctr., n = 5) versus neuronal preservation DRG (NP, n = 6). (**A**) Representative image and enlarged section of a patient DRG with neurons (NF, gray). NF labelling (grey) was annotated with a DL model (NF mask, yellow). FABP7 (magenta) and APOJ (cyan) mark satellite glial cells (SGCs). Scale bar: 400 / 100 µm. (**B**) Soma size distribution of neurons, gray lines depict the standard error of the mean. (**C**) Number of neurons detected per mm^2 of the neuronal polygon area (NPA). (**D-E**) Proportion of FABP7-positive area per neuron near area (NNA) or NPA. (**F**) Percentage of neurons in proximity to FABP7-positive SGCs. (**G-H**) Intensity of the APOJ signal in SGCs normalized to the intensity of the APOJ signal in the NNA or NPA. All p > 0.05 after Bonferroni correction. APOJ, apolipoprotein J; DL, deep learning; DRG, dorsal root ganglia; FABP7, fatty acid binding protein 7; NF, neurofilament.

5 Discussion

In this study, we investigated the reprogramming potential of SGCs of the adult DRG and asked whether this endogenous cell source is a candidate for regenerative medicine. We found that SGCs have the potential to dedifferentiate into sensory progenitor cells, at least *in vitro*. Surprisingly, the early fate-determining transcription factors Neurog1 and Neurog2 were sufficient to induce nociceptor-like neurons, as well as glial cells from these sensory progenitors. *In vivo*, in humans with painful plexus injury, we either found SGC plasticity with neither gliosis nor neuronal loss, or complete loss of the SGC-neuron entity. Therefore, at least two translational research directions might be followed for regenerative medicine concepts in the human DRG: reafferentation of existing DRG units or full replacement of the entire multicellular DRG structure using SGC-like progenitors as a cell source.

5.1 *In vitro* reprograming of glial progenitor-like cells from adult DRG

First, we found that adult mouse DRG harbor cells that have the genetic plasticity to dedifferentiate into glial progenitor-like cells *in vitro*. These glial sensory progenitor (gSP) cells expressed Sox2 and Sox10, and markers for SGCs (e.g. *Cdh19*, *Fabp7*), Schwann cells, and boundary cap cells. We suspect that they originate from SGC cell rings around DRG neurons because cell growth started around single, cultured sensory neurons (Figure 4 B). SGCs tightly wrap around neurons (Pannese, 1981; Pannese, 2010). Typical tissue dissection protocols cannot fully separate the SGC cell ring from isolated DRG neurons, suggesting that these cells, when taken out of their niche, start to rejuvenate and proliferate. Previous studies suggested that SGCs are like SC precursors whose further development have been arrested, because they express precursor markers, show similarities to Schwann cells, and were able to myelinate purified sensory neurons *in vitro* (George *et al.*, 2018). Partly, this could be due to the culturing process, as these precursor-like cells differ from *in vivo* characterized cells (Jager *et al.*, 2022). Still, SGCs seem to have the potential to develop multipotential glial precursor properties (Svenningsen *et al*, 2004).

Using ^{IRES}DsRed-based retroviral vectors (Heinrich *et al.*, 2010) for expression of developmental transcription factors, coexpression of Neurog1 and Neurog2 was sufficient to induce a sensory neuron differentiation process in gSP cells. Neuronal induction was further enhanced using both neurogenins compared with the use of single factors. Notably, neurogenins induced Brn3a expression, making the additional retroviral expression of Brn3a obsolete. This is in line with previous studies, where Brn3a follows neurogenin (Neurog1, Neurog2) expression (Newbern, 2015).

Moreover, both neurogenins induced GFAP-positive glial cells. For Neurog2, this was to be expected (Zirlinger *et al.*, 2002), but not for Neurog1, which was shown promote differentiation

of neural stem cells into solely neuronal fates (Kim *et al.*, 2011; Sun *et al*, 2001; Velkey & O'Shea, 2013). Thus, Neurog1 function might vary between different cell populations. Interestingly, additional expression of Brn3a with the triple vector abolished the induction of GFAP-positive glial cells, likely because Brn3a represses non-neuronal genes (Lanier *et al*, 2009).

Other interesting transcription factors for reprogramming were Runx1 and Prdm12. Runx1 was shown to induce differentiation of boundary cap cells towards sensory neurons *in vitro* and after transplantation (Aldskogius *et al*, 2009). Prdm12 drives nociceptor sensory development over TrkA expression and maintenance of Neurog1 and Neurog2, as also shown with expression in human iPSCs (Bartesaghi *et al.*, 2019; Desiderio *et al.*, 2019; Lanier *et al.*, 2009). Here, reprogramming with Runx1 and Prdm12 encoding retroviral vectors was not successful. However, both transcription factors were absent or undetectably expressed. It cannot be completely excluded that technical problems, such as a low titer, are the cause, but the vectors themselves were readily expressed in transfected HEK293 cells. Therefore, we suspect that rather the gSP cells themselves suppressed the transcription factors.

Nevertheless, Neurog1 and Neurog2 expression – together with the addition of NGF – was sufficient for induction of nociceptor-like neurons. Two weeks after infection, neurons showed immunoreactivity to nociceptor markers such as $Na_V1.9$ and TrkA, as well as expression and functionality of TrpV1 and TrpA1. Overall, our data suggest that 10-30% of the Ngn2-P2A-Ngn1 infected cells could be nociceptors, though electrophysiological properties are not completely similar to naïve small-diameter DRG neurons. gSP-derived neurons mainly fired single action potentials instead of multiple and action potentials were smaller in spike width and amplitude. Strikingly, the majority of gSP-derived neurons showed TTX-resistant currents, an important feature of nociceptors (Cummins *et al*, 1999; Rush *et al*, 2007). This raises the question of why early fate-determinants of the sensory neuron lineage drive gSP cells in direction of a neuronal cluster with nociceptor-like phenotypes. According to an unbiased classification of DRG neurons, TrkA/$Na_V1.9$-positive cells belong to the cluster of peptidergic and non-peptidergic nociceptors (Usoskin *et al.*, 2015). Typically, $Na_V1.9$ is barely (if at all) found in other DRG neuron subtypes (Bennett *et al*, 2019). Possibly, neurogenins together with factors in the cell culture medium establish criteria for nociceptor differentiation. However, it could also be that Neurog1 and Neurog2 themselves instruct, among the glial lineage, a default differentiation program in direction to nociceptor-like cells, meaning that other subtypes of neurons are specified by other, yet unknown factors.

In principle, reprogramming of SGCs to sensory neurons with small molecules was already shown with the so-called Chambers protocol (Chambers *et al.*, 2012; Wang *et al.*, 2021). This protocol is often used to direct the differentiation of human pluripotent stem cells into sensory neurons. The reprogramming system is useful for *in vitro* modeling of biological processes from

living donors; for *in vivo* applications, the protocol is not suited. Furthermore, the system is still prone to high molecular and functional variation and has limited potential for modelling subtype-specific nociceptors (Schwartzentruber *et al.*, 2018).

Instead, we chose retroviral expression of Neurog1 and Neurog2 to generate a nociceptor-like phenotype because the use of viral vectors is also a promising strategy *in vivo*. Reprogramming of intrinsic cell sources using viruses (Bocchi & Götz, 2020; Li & Chen, 2016), or grafting of well-defined young neurons or pre-defined progenitors into the nervous system (Falkner *et al*, 2016) could help to regenerate a damaged peripheral nervous system. Because it is unclear which cell types, particularly SGCs, should be targeted after trauma and peripheral nerve lesion, we had a closer look at the cellular composition of the DRG after nerve injury.

5.2 Rodent DRG after peripheral nerve injury

Though it has been postulated that sensory neurons are lost (Kuo *et al.*, 2005) or SGCs proliferate (Donegan *et al*, 2013) after peripheral nerve injury, we saw no signs of gliosis or neuronal death after SNI in rats. Instead, we found pronounced cellular plasticity after peripheral nerve injury, characterized by more GFAP-positive and less GS-positive SGCs (Schulte *et al.*, 2022c). This is consistent with a recent study that did not detect SGC proliferation after nerve injury (Jager *et al.*, 2020). Upregulation of GFAP, an activation marker, is robustly shown following peripheral nerve injury in rats (Donegan *et al.*, 2013; Hanani & Spray, 2020; Woodham *et al.*, 1989). Downregulation of GS, on the other hand, was not expected. Usually, GS is used as a stable immunohistochemical SGC marker (Hanani, 2005; Miller *et al*, 2002), though others suggest that it might only represent a subset of SGC and might not entirely be specific to SGC (Avraham *et al.*, 2020). Thus, GS expression may also be modified by injury signaling, undermining SGC plasticity.

Concerning SGC plasticity markers, it is important to note that GFAP is not only a pure marker for SGC reactivity (Escartin *et al*, 2021), but is also expressed in progenitor cells and immature Schwann cells (Jessen & Mirsky, 2005; Kriegstein & Alvarez-Buylla, 2009). A de-differentiation response of SGCs, as indicated by GFAP-upregulation, could be an interesting biomarker to define a starting point for regenerative medicine, even in the absence of SGC proliferation. Yet, it is not clear whether neuronal death and reactive gliosis might appear later after injury, at time points not covered by our study (over 7 d and 14 d). Therefore, long-term studies and maybe other pain models could be helpful to evaluate the full potential of neural crest-derived glial cells as an endogenous cell source in the DRG.

5.3 Human DRG after brachial plexus lesion

Lastly, we had the chance to investigate the human DRG of representative plexus injury patients for signs of neuronal loss and SGC plasticity. Surprisingly, we found a dichotomic response: either preservation or complete loss of multicellular DRG units. DRG with neuronal preservation showed no striking differences in neuronal and SGC composition compared to control DRG (Schulte *et al.*, 2022a).

In human DRG, peripheral injury responses seem to be different from the CNS. Neuronal loss was not accompanied by gliotic responses, which would have enabled repair with endogenous glial cells similar to the CNS (Buffo *et al.*, 2008). Instead, SGCs, being in such close contact with the neurons (Hanani & Spray, 2020), were lost along with the neurons. Possibly, more severe injuries resulted in hematoma formation, disruption of blood supply, more inflammation and scarring, mitochondrial collapse, or anoxic death. Alternatively, due to the loss of connection to the spinal cord, growth factors necessary for neuronal survival could be lost, e.g., nerve growth, glia-derived neurotrophic, or ciliary neurotrophic factors (Aldskogius & Kozlova, 2021; Hoeber *et al.*, 2015). However, the first seems more plausible since half of the patients still have multicellular DRG tissue after brachial plexus injury. In this context, it is also important to note that adult sensory neurons seem to need neurotrophic factors for proper function but not survival (Pezet & McMahon, 2006).

In DRG with neuronal preservation, we did not find clear signs of SGC plasticity. About 95% of all NF-positive neurons were in proximity to FABP7-positive SGCs, but SGCs did not change their area, nor their expression of APOJ (Schulte *et al.*, 2022a). With GS/GLUL and GFAP not being an appropriate markers in human DRG (Avraham *et al.*, 2022), additional markers for SGC reactivation or other methods such as transcriptomic analysis of human DRG (Hall *et al*, 2022) might be needed to investigate SGC plasticity after nerve injury. Moreover, as DRG were removed on average five months after brachial plexus injury, possible SGC responses might no longer be detectable.

5.4 Restoring DRG function: translational research directions

For restoring DRG function after plexus injury, at least two translational research directions might be needed: reafferentation of existing DRG units or full replacement of the entire multicellular DRG structure. When DRG still exist, the promotion of reconnection to the spinal cord (Hoeber *et al.*, 2015) or pathfinding support using bioprinting could be beneficial (Aldskogius & Kozlova, 2021). Maybe, even the generation of new neurons that have more growth potential could be helpful. For the replacement of entire DRG structures, first, a suitable cell source is needed.

This study now raised the option to use reactive SGC-like progenitors for local *in vivo* reprogramming into sensory neurons and their corresponding glial cells, for instance after an

injury-induced loss of sensory neuron/SGC entities. However, it remains questionable whether fast-dividing glial sensory precursor cells can also be found in adult DRG *in vivo* after injury. Our data could not confirm the presence of a fast-dividing glial cell source in the DRG after injury, neither in rodents after spared nerve injury, nor in humans after plexus injury (Schulte *et al.*, 2022a; Schulte *et al.*, 2022c). Perhaps, to generate sensory neurons and corresponding glial cells, neural crest cells generated from human fibroblast (Kim *et al*, 2014) could serve as an alternative starting point. The expression of Neurog1 and Neurog2 may then induce both neurons and glial cells, which could be grafted into severely damaged DRG to replace the multicellular DRG structure.

Yet, no animal model represents the human plexus injury phenotypes. Though technically difficult and a huge burden for the animals, dorsal root avulsion (Chew *et al*, 2011; Hoeber *et al.*, 2015) could be suitable. Such a model could help to clarify which pathomechanism is causally responsible for the loss of neuron/SGC units after traumatic nerve injury. Still, differences between rodent and human sensory neurons, especially of small diameter nonpeptidergic neurons (Nguyen *et al*, 2021), could complicate the application in humans. Thus, research on human DRG is also essentially needed. Acquiring human DRG of good tissue quality, especially in Germany, is challenging but essential for investigating injury effects. Additionally, non-invasive imaging methods, for example, magnetic resonance neurography at a higher resolution, would be very helpful for a better *in vivo* evaluation of the plexus injury and maybe even be able to resolve whether neuron/SGC units are lost or not.

Important for this study was the use of open-source data analysis tools such as deepflash2, StarDist2D, and CellProfiler and self-programmed python scripts. They enabled the analysis of a huge amount of image data (thousands of bioimages with hundreds of thousands of image features). In line, in our open science community, data and tool sharing allowed us to establish a new level of analysis of the DRG cell composition, in rodent and human tissue. Importantly, shared data, such as bioimages and segmentation masks, can be used for algorithm evolution in the future. Deep learning-assisted data analysis, when used in a scientifically appropriate way, is certainly the future of biomedical research (Laine *et al*, 2021; Schulte *et al.*, 2022c; Segebarth *et al.*, 2020). Here, DL-based image feature extraction was essentially needed, as experimenter blinding was not possible because experimental conditions were visible to the experimenter, making unbiased, heuristic bioimage analysis virtually impossible. Moreover, it enabled a more complex and detailed analysis of the DRG, with parameters such as “neurons in proximity to glial cells “.

5.5 Limitations

A limitation of this study might be that it is not ultimately clear if reprogrammed cells truly originated from rejuvenated SGCs. The transcriptome indicates an SGC progenitor-like cell type, but theoretically, a less abundant cell type could be infected as well. To solve this question, a transgenic mouse line with genetically labeled SGCs would be necessary. However, such a mouse line does not exist. Still, adult mouse DRG harbor cells that can be reprogrammed into nociceptor-like neurons. Furthermore, the maturation stage of the gSP-derived neurons could not fully be described. For instance, differentiation into subclasses of peptidergic and non-peptidergic neurons is unclear, from early TrkA+/Runx1+ to late Ret or TrkA lineages (Lallemend & Ernfors, 2012; Usoskin *et al.*, 2015). Additionally, it would be interesting to see how heterogeneous the induced neurons are (Schwartzentruber *et al.*, 2018). To completely characterized gSP-derived neurons, single-cell sequencing is needed (and ongoing).

A major limitation of the human DRG study was the different processing times of patient and control DRG. Patient DRG were harvested during surgery and processed immediately, whereas control DRG were collected at autopsy after an unnatural death, so up to five days could elapse before autopsy and DRG biopsy. During this time interval, autolysis could have been active, probably causing the neuronal somata of the control DRG to shrink. Moreover, the variability of the control group was very high, microscopy settings needed to be adjusted and one control DRG had to be excluded. This questions the comparability of the two groups. To counteract this, we have developed an – at least on the image level – objective analysis procedure. Human DRG tissue samples are so valuable that such objective and largely automatized analyses are helpful research tools on the way to new therapies.

5.6 Conclusions

In summary, this study offers important insights into the use of endogenous peripheral satellite glial cells for regenerative medicine. Glial cells from adult DRG of mice seem to acquire progenitor properties *in vitro*, favoring reprogramming into nociceptor-like neurons and glial cells with the early developmental factors Neurog1 and Neuog2. Whether this offers a new therapy strategy after peripheral injury *in vivo*, even in the absence of gliosis and neuronal loss, remains to be elucidated. Patients affected by plexus injury would need a two-tailored therapy: one for reafferentation of existing DRG neurons, and one for rebuilding complete neuron/SGC units. *In vivo*, SGC plasticity could be useful in developing corresponding regenerative therapies.

6 References

Aldskogius H, Berens C, Kanaykina N, Liakhovitskaia A, Medvinsky A, Sandelin M, Schreiner S, Wegner M, Hjerling-Leffler J, Kozlova EN (2009) Regulation of boundary cap neural crest stem cell differentiation after transplantation. *Stem Cells* 27: 1592-1603

Aldskogius H, Kozlova EN (2021) Dorsal Root Injury—A Model for Exploring Pathophysiology and Therapeutic Strategies in Spinal Cord Injury. *Cells* 10: 2185

Anderson DJ (1999) Lineages and transcription factors in the specification of vertebrate primary sensory neurons. *Current Opinion in Neurobiology* 9: 517-524

Assinck P, Duncan GJ, Hilton BJ, Plemel JR, Tetzlaff W (2017) Cell transplantation therapy for spinal cord injury. *Nature Neuroscience* 20: 637-647

Avraham O, Chamessian A, Feng R, Yang L, Halevi AE, Moore AM, Gereau RWI, Cavalli V (2022) Profiling the molecular signature of satellite glial cells at the single cell level reveals high similarities between rodents and humans. *PAIN*: 10.1097/j.pain.0000000000002628

Avraham O, Deng P-Y, Jones S, Kuruvilla R, Semenkovich CF, Klyachko VA, Cavalli V (2020) Satellite glial cells promote regenerative growth in sensory neurons. *Nat Commun* 11: 4891

Avraham O, Feng R, Ewan EE, Rustenhoven J, Zhao G, Cavalli V (2021) Profiling sensory neuron microenvironment after peripheral and central axon injury reveals key pathways for neural repair. *eLife* 10: e68457

Bankhead P, Loughrey MB, Fernández JA, Dombrowski Y, McArt DG, Dunne PD, McQuaid S, Gray RT, Murray LJ, Coleman HG *et al* (2017) QuPath: Open source software for digital pathology image analysis. *Scientific reports* 7: 16878

Bartesaghi L, Wang Y, Fontanet P, Wanderoy S, Berger F, Wu H, Akkuratova N, Bouçanova F, Médard J-J, Petitpré C *et al* (2019) PRDM12 Is Required for Initiation of the Nociceptive Neuron Lineage during Neurogenesis. *Cell Reports* 26: 3484-3492.e3484

Basbaum AI, Bautista DM, Scherrer G, Julius D (2009) Cellular and molecular mechanisms of pain. *Cell* 139: 267-284

Bennett DL, Clark AJ, Huang J, Waxman SG, Dib-Hajj SD (2019) The Role of Voltage-Gated Sodium Channels in Pain Signaling. *Physiological Reviews* 99: 1079-1151

Bertelli JA, Ghizoni MF (2010) The possible role of regenerating axons in pain persistence after brachial plexus grafting. *Microsurgery* 30: 532-536

Blanchard JW, Eade KT, Szucs A, Lo Sardo V, Tsunemoto RK, Williams D, Sanna PP, Baldwin KK (2015) Selective conversion of fibroblasts into peripheral sensory neurons. *Nat Neurosci* 18: 25-35

Blum R, Heinrich C, Sanchez R, Lepier A, Gundelfinger ED, Berninger B, Gotz M (2011) Neuronal network formation from reprogrammed early postnatal rat cortical glial cells. *Cereb Cortex* 21: 413-424

Bocchi R, Götz M (2020) Neuronal Reprogramming for Brain Repair: Challenges and Perspectives. *Trends Mol Med* 26: 890-892

Buffo A, Rite I, Tripathi P, Lepier A, Colak D, Horn A-P, Mori T, Götz M (2008) Origin and progeny of reactive gliosis: A source of multipotent cells in the injured brain. *Proc Natl Acad Sci U S A* 105: 3581-3586

Chambers SM, Qi Y, Mica Y, Lee G, Zhang XJ, Niu L, Bilsland J, Cao L, Stevens E, Whiting P *et al* (2012) Combined small-molecule inhibition accelerates developmental timing and converts human pluripotent stem cells into nociceptors. *Nature biotechnology* 30: 715-720

Chen C-L, Broom DC, Liu Y, de Nooij JC, Li Z, Cen C, Samad OA, Jessell TM, Woolf CJ, Ma Q (2006) Runx1 Determines Nociceptive Sensory Neuron Phenotype and Is Required for Thermal and Neuropathic Pain. *Neuron* 49: 365-377

Chew DJ, Carlstedt T, Shortland PJ (2011) A comparative histological analysis of two models of nerve root avulsion injury in the adult rat. *Neuropathology and Applied Neurobiology* 37: 613-632

Cranfill SL, Luo W (2022) Nerve regrowth can be painful. *Nature* 606: 32-33

Crawford LK, Caterina MJ (2020) Functional Anatomy of the Sensory Nervous System: Updates From the Neuroscience Bench. *Toxicologic Pathology* 48: 174-189

Cummins TR, Dib-Hajj SD, Black JA, Akopian AN, Wood JN, Waxman SG (1999) A novel persistent tetrodotoxin-resistant sodium current in SNS-null and wild-type small primary sensory neurons. *J Neurosci* 19: Rc43

Cummins TR, Sheets PL, Waxman SG (2007) The roles of sodium channels in nociception: Implications for mechanisms of pain. *PAIN* 131: 243-257

Desiderio S, Vermeiren S, Van Campenhout C, Kricha S, Malki E, Richts S, Fletcher EV, Vanwelden T, Schmidt BZ, Henningfeld KA *et al* (2019) Prdm12 Directs Nociceptive Sensory Neuron Development by Regulating the Expression of the NGF Receptor TrkA. *Cell Reports* 26: 3522-3536.e3525

Dib-Hajj S, Black JA, Cummins TR, Waxman SG (2002) NaN/Nav1.9: a sodium channel with unique properties. *Trends in Neurosciences* 25: 253-259

Dib-Hajj SD, Choi JS, Macala LJ, Tyrrell L, Black JA, Cummins TR, Waxman SG (2009) Transfection of rat or mouse neurons by biolistics or electroporation. *Nature Protocols* 4: 1118-1127

Dimou L, Götz M (2014) Glial Cells as Progenitors and Stem Cells: New Roles in the Healthy and Diseased Brain. *Physiological Reviews* 94: 709-737

Djouhri L, Fang X, Okuse K, Wood JN, Berry CM, Lawson SN (2003) The TTX-Resistant Sodium Channel Nav1.8 (SNS/PN3): Expression and Correlation with Membrane Properties in Rat Nociceptive Primary Afferent Neurons. *The Journal of Physiology* 550: 739-752

Donegan M, Kernisant M, Cua C, Jasmin L, Ohara PT (2013) Satellite glial cell proliferation in the trigeminal ganglia after chronic constriction injury of the infraorbital nerve. *Glia* 61: 2000-2008

Dykes IM, Tempest L, Lee SI, Turner EE (2011) Brn3a and Islet1 act epistatically to regulate the gene expression program of sensory differentiation. *J Neurosci* 31: 9789-9799

Eberhardt E, Havlicek S, Schmidt D, Link Andrea S, Neacsu C, Kohl Z, Hampl M, Kist Andreas M, Klinger A, Nau C *et al* (2015) Pattern of Functional TTX-Resistant Sodium Channels Reveals a Developmental Stage of Human iPSC- and ESC-Derived Nociceptors. *Stem Cell Reports* 5: 305-313

Ernst A, Frisen J (2015) Adult neurogenesis in humans- common and unique traits in mammals. *PLoS Biol* 13: e1002045

Escartin C, Galea E, Lakatos A, O'Callaghan JP, Petzold GC, Serrano-Pozo A, Steinhäuser C, Volterra A, Carmignoto G, Agarwal A *et al* (2021) Reactive astrocyte nomenclature, definitions, and future directions. *Nature Neuroscience* 24: 312-325

Falk T, Mai D, Bensch R, Cicek O, Abdulkadir A, Marrakchi Y, Bohm A, Deubner J, Jackel Z, Seiwald K *et al* (2019) U-Net: deep learning for cell counting, detection, and morphometry. *Nature methods* 16: 67-70

Falkner S, Grade S, Dimou L, Conzelmann KK, Bonhoeffer T, Gotz M, Hubener M (2016) Transplanted embryonic neurons integrate into adult neocortical circuits. *Nature* 539: 248-253

Faure L, Wang Y, Kastriti ME, Fontanet P, Cheung KKY, Petitpré C, Wu H, Sun LL, Runge K, Croci L *et al* (2020) Single cell RNA sequencing identifies early diversity of sensory neurons forming via bi-potential intermediates. *Nat Commun* 11: 4175

Gallaher ZR, Johnston ST, Czaja K (2014) Neural proliferation in the dorsal root ganglia of the adult rat following capsaicin-induced neuronal death. *J Comp Neurol* 522: 3295-3307

Gangadharan V, Zheng H, Taberner FJ, Landry J, Nees TA, Pistolic J, Agarwal N, Männich D, Benes V, Helmstaedter M *et al* (2022) Neuropathic pain caused by miswiring and abnormal end organ targeting. *Nature* 606: 137-145

Gascon S, Masserdotti G, Russo GL, Gotz M (2017) Direct Neuronal Reprogramming: Achievements, Hurdles, and New Roads to Success. *Cell Stem Cell* 21: 18-34

Gehrmann J, Monaco S, Kreutzberg GW (1991) Spinal cord microglial cells and DRG satellite cells rapidly respond to transection of the rat sciatic nerve. *Restorative neurology and neuroscience* 2: 181-198

George D, Ahrens P, Lambert S (2018) Satellite glial cells represent a population of developmentally arrested Schwann cells. *Glia* 66: 1496-1506

Grade S, Götz M (2017) Neuronal replacement therapy: previous achievements and challenges ahead. *NPJ Regen Med* 2: 29

Griebel M, Segebarth D, Stein N, Schukraft N, Tovote P, Blum R, Flath CM (2021) Deep-learning in the bioimaging wild: Handling ambiguous data with deepflash2. *ArXiv* abs/2111.06693

Haldane C, Frost G, Ogalo E, Bristol S, Doherty C, Berger M (2022) A systematic review and meta-analysis of patient-reported outcomes following nerve transfer surgery for brachial plexus injury. *PM&R* n/a

Hall BE, Macdonald E, Cassidy M, Yun S, Sapio MR, Ray P, Doty M, Nara P, Burton MD, Shiers S *et al* (2022) Transcriptomic analysis of human sensory neurons in painful diabetic neuropathy reveals inflammation and neuronal loss. *Scientific reports* 12: 4729

Hanani M (2005) Satellite glial cells in sensory ganglia: from form to function. *Brain Research Reviews* 48: 457-476

Hanani M, Spray DC (2020) Emerging importance of satellite glia in nervous system function and dysfunction. *Nature Reviews Neuroscience* 21: 485-498

Heinrich C, Blum R, Gascon S, Masserdotti G, Tripathi P, Sanchez R, Tiedt S, Schroeder T, Gotz M, Berninger B (2010) Directing astroglia from the cerebral cortex into subtype specific functional neurons. *PLoS Biol* 8: e1000373

Hoeber J, Trolle C, Konig N, Du Z, Gallo A, Hermans E, Aldskogius H, Shortland P, Zhang SC, Deumens R *et al* (2015) Human Embryonic Stem Cell-Derived Progenitors Assist Functional Sensory Axon Regeneration after Dorsal Root Avulsion Injury. *Sci Rep* 5: 10666

Holzer A-K, Karreman C, Suciu I, Furmanowsky L-S, Wohlfarth H, Loser D, Dirks WG, Pardo González E, Leist M (2022) Generation of Human Nociceptor-Enriched Sensory Neurons for the Study of Pain-Related Dysfunctions. *Stem Cells Translational Medicine* 11: 727-741

Inoue K-i, Shiga T, Ito Y (2008) Runx transcription factors in neuronal development. *Neural Development* 3: 20

Jager S, Pallesen L, Lin L, Izzi F, Pinheiro A, Villa-Hernandez S, Cesare P, Vaegter C, Denk F (2022) Comparative transcriptional analysis of satellite glial cell injury response [version 1; peer review: 2 approved]. *Wellcome Open Research* 7

Jager SE, Pallesen LT, Richner M, Harley P, Hore Z, McMahon S, Denk F, Vægter CB (2020) Changes in the transcriptional fingerprint of satellite glial cells following peripheral nerve injury. *Glia* 68: 1375-1395

Jessen KR, Mirsky R (2005) The origin and development of glial cells in peripheral nerves. *Nature Reviews Neuroscience* 6: 671-682

Jessen KR, Mirsky R (2019) The Success and Failure of the Schwann Cell Response to Nerve Injury. *Frontiers in Cellular Neuroscience* 13

Ji RR, Chamessian A, Zhang YQ (2016) Pain regulation by non-neuronal cells and inflammation. *Science* 354: 572-577

Kim EJ, Hori K, Wyckoff A, Dickel LK, Koundakjian EJ, Goodrich LV, Johnson JE (2011) Spatiotemporal fate map of neurogenin1 (Neurog1) lineages in the mouse central nervous system. *J Comp Neurol* 519: 1355-1370

Kim Yong J, Lim H, Li Z, Oh Y, Kovlyagina I, Choi In Y, Dong X, Lee G (2014) Generation of Multipotent Induced Neural Crest by Direct Reprogramming of Human Postnatal Fibroblasts with a Single Transcription Factor. *Cell Stem Cell* 15: 497-506

Kim YS, Anderson M, Park K, Zheng Q, Agarwal A, Gong C, Saijilafu, Young L, He S, LaVinka PC *et al* (2016) Coupled Activation of Primary Sensory Neurons Contributes to Chronic Pain. *Neuron* 91: 1085-1096

Kleggetveit IP, Namer B, Schmidt R, Helås T, Rückel M, Ørstavik K, Schmelz M, Jørum E (2012) High spontaneous activity of C-nociceptors in painful polyneuropathy. *PAIN* 153

Kobayashi A, Senzaki K, Ozaki S, Yoshikawa M, Shiga T (2012) Runx1 promotes neuronal differentiation in dorsal root ganglion. *Molecular and Cellular Neuroscience* 49: 23-31

Kramer I, Sigrist M, de Nooij JC, Taniuchi I, Jessell TM, Arber S (2006) A Role for Runx Transcription Factor Signaling in Dorsal Root Ganglion Sensory Neuron Diversification. *Neuron* 49: 379-393

Kriegstein A, Alvarez-Buylla A (2009) The glial nature of embryonic and adult neural stem cells. *Annu Rev Neurosci* 32: 149-184

Kuo LT, Simpson A, Schanzer A, Tse J, An SF, Scaravilli F, Groves MJ (2005) Effects of systemically administered NT-3 on sensory neuron loss and nestin expression following axotomy. *J Comp Neurol* 482: 320-332

Kupari J, Usoskin D, Parisien M, Lou D, Hu Y, Fatt M, Lönnerberg P, Spångberg M, Eriksson B, Barkas N *et al* (2021) Single cell transcriptomics of primate sensory neurons identifies cell types associated with chronic pain. *Nature communications* 12: 1510

Laine RF, Arganda-Carreras I, Henriques R, Jacquemet G (2021) Avoiding a replication crisis in deep-learning-based bioimage analysis. *Nature Methods* 18: 1136-1144

Lallemend F, Ernfors P (2012) Molecular interactions underlying the specification of sensory neurons. *Trends in Neurosciences* 35: 373-381

Lanier J, Dykes IM, Nissen S, Eng SR, Turner EE (2009) Brn3a regulates the transition from neurogenesis to terminal differentiation and represses non-neural gene expression in the trigeminal ganglion. *Developmental Dynamics* 238: 3065-3079

Leipold E, Hanson-Kahn A, Frick M, Gong P, Bernstein JA, Voigt M, Katona I, Oliver Goral R, Altmüller J, Nürnberg P *et al* (2015) Cold-aggravated pain in humans caused by a hyperactive NaV1.9 channel mutant. *Nat Commun* 6: 10049-10049

Leipold E, Liebmann L, Korenke GC, Heinrich T, Gießelmann S, Baets J, Ebbinghaus M, Goral RO, Stödberg T, Hennings JC *et al* (2013) A de novo gain-of-function mutation in SCN11A causes loss of pain perception. *Nature Genetics* 45: 1399-1404

Li CH, Tam PKS (1998) An iterative algorithm for minimum cross entropy thresholding. *Pattern Recognition Letters* 19: 771-776

Li H, Chen G (2016) In Vivo Reprogramming for CNS Repair: Regenerating Neurons from Endogenous Glial Cells. *Neuron* 91: 728-738

Li HY, Say EHM, Zhou XF (2007) Isolation and Characterization of Neural Crest Progenitors from Adult Dorsal Root Ganglia. *STEM CELLS* 25: 2053-2065

Liu F-Y, Sun Y-N, Wang F-T, Li Q, Su L, Zhao Z-F, Meng X-L, Zhao H, Wu X, Sun Q *et al* (2012) Activation of satellite glial cells in lumbar dorsal root ganglia contributes to neuropathic pain after spinal nerve ligation. *Brain Research* 1427: 65-77

Maka M, Claus Stolt C, Wegner M (2005) Identification of Sox8 as a modifier gene in a mouse model of Hirschsprung disease reveals underlying molecular defect. *Developmental Biology* 277: 155-169

Mapps AA, Thomsen MB, Boehm E, Zhao H, Hattar S, Kuruvilla R (2022) Diversity of satellite glia in sympathetic and sensory ganglia. *Cell Reports* 38: 110328

Martin C, Stoffer C, Mohammadi M, Hugo J, Leipold E, Oehler B, Rittner HL, Blum R (2018) NaV1.9 Potentiates Oxidized Phospholipid-Induced TRP Responses Only under Inflammatory Conditions. *Front Mol Neurosci* 11: 7

Maška M, Ulman V, Svoboda D, Matula P, Ederra C, Urbiola A, España T, Venkatesan S, Balak DM, Karas P *et al* (2014) A benchmark for comparison of cell tracking algorithms. *Bioinformatics* 30: 1609-1617

McKay Hart A, Brannstrom T, Wiberg M, Terenghi G (2002) Primary sensory neurons and satellite cells after peripheral axotomy in the adult rat. *Experimental Brain Research* 142: 308-318

McQuin C, Goodman A, Chernyshev V, Kamentsky L, Cimini BA, Karhohs KW, Doan M, Ding L, Rafelski SM, Thirstrup D *et al* (2018) CellProfiler 3.0: Next-generation image processing for biology. *PLOS Biology* 16: e2005970

Menorca RM, Fussell TS, Elfar JC (2013) Nerve physiology: mechanisms of injury and recovery. *Hand Clin* 29: 317-330

Milichko V, Dyachuk V (2020) Novel Glial Cell Functions: Extensive Potency, Stem Cell-Like Properties, and Participation in Regeneration and Transdifferentiation. *Front Cell Dev Biol* 8: 809

Miller KE, Richards BA, Kriebel RM (2002) Glutamine-, glutamine synthetase-, glutamate dehydrogenase- and pyruvate carboxylase-immunoreactivities in the rat dorsal root ganglion and peripheral nerve. *Brain Research* 945: 202-211

Muratori L, Ronchi G, Raimondo S, Geuna S, Giacobini-Robecchi MG, Fornaro M (2015) Generation of new neurons in dorsal root Ganglia in adult rats after peripheral nerve crush injury. *Neural Plast* 2015: 860546-860546

Newbern JM (2015) Molecular control of the neural crest and peripheral nervous system development. *Curr Top Dev Biol* 111: 201-231

Nguyen MQ, von Buchholtz LJ, Reker AN, Ryba NJP, Davidson S (2021) Single-nucleus transcriptomic analysis of human dorsal root ganglion neurons. *eLife* 10: e71752

Nickolls AR, Lee MM, Espinoza DF, Szczot M, Lam RM, Wang Q, Beers J, Zou J, Nguyen MQ, Solinski HJ *et al* (2020) Transcriptional Programming of Human Mechanosensory Neuron Subtypes from Pluripotent Stem Cells. *Cell Reports* 30: 932-946.e937

Ogawa R, Fujita K, Ito K (2017) Mouse embryonic dorsal root ganglia contain pluripotent stem cells that show features similar to embryonic stem cells and induced pluripotent stem cells. *Biology open* 6: 602-618

Pannese E (1981) The satellite cells of the sensory ganglia. *Adv Anat Embryol Cell Biol* 65: 1-111

Pannese E (2010) The structure of the perineuronal sheath of satellite glial cells (SGCs) in sensory ganglia. *Neuron Glia Biology* 6: 3-10

Pezet S, McMahon SB (2006) NEUROTROPHINS: Mediators and Modulators of Pain. *Annu Rev Neurosci* 29: 507-538

Rasulić L, Savić A, Živković B, Vitošević F, Mićović M, Baščarević V, Puzović V, Novaković N, Lepić M, Samardžić M *et al* (2017) Outcome after brachial plexus injury surgery and impact on quality of life. *Acta Neurochirurgica* 159: 1257-1264

Renganathan M, Dib-Hajj S, Waxman SG (2002) Nav1.5 underlies the 'third TTX-R sodium current' in rat small DRG neurons. *Molecular Brain Research* 106: 70-82

Rodríguez FJ, Valero-Cabré A, Navarro X (2004) Regeneration and functional recovery following peripheral nerve injury. *Drug Discovery Today: Disease Models* 1: 177-185

Rush AM, Cummins TR, Waxman SG (2007) Multiple sodium channels and their roles in electrogenesis within dorsal root ganglion neurons. *J Physiol* 579: 1-14

Schmidt U, Weigert M, Broaddus C, Myers G, 2018. Cell Detection with Star-Convex Polygons, in: Frangi A.F., Schnabel J.A., Davatzikos C., Alberola-López C., Fichtinger G. (Eds.), Medical Image Computing and Computer Assisted Intervention – MICCAI 2018. Springer International Publishing, Cham, pp. 265-273.

Schneider CA, Rasband WS, Eliceiri KW (2012) NIH Image to ImageJ: 25 years of image analysis. *Nature Methods* 9: 671-675

Schulte A, Degenbeck J, Aue A, Schindehütte M, Schlott F, Schneider M, Monoranu CM, Bohnert M, Pham M, Antoniadis G *et al* (2022a) Human dorsal root ganglion after brachial plexus injury: either preservation or complete loss of the multicellular unit. *in preparation*

Schulte A, Lohner H, Degenbeck J, Segebarth D, Rittner H, Blum R, Aue A Data from: Unbiased analysis of cellular plasticity in the dorsal root ganglion after peripheral nerve injury (2022b) (http://dx.doi.org/10.5281/ZENODO.6546069) [DATASET]

Schulte A, Lohner H, Degenbeck J, Segebarth D, Rittner H, Blum R, Aue A (2022c) Unbiased analysis of the dorsal root ganglion after peripheral nerve injury: no neuronal loss, no gliosis, but satellite glial cell plasticity. *Pain*

Schwartzentruber J, Foskolou S, Kilpinen H, Rodrigues J, Alasoo K, Knights AJ, Patel M, Goncalves A, Ferreira R, Benn CL *et al* (2018) Molecular and functional variation in iPSC-derived sensory neurons. *Nature Genetics* 50: 54-61

Segebarth D, Griebel M, Stein N, von Collenberg CR, Martin C, Fiedler D, Comeras LB, Sah A, Schoeffler V, Lüffe T *et al* (2020) On the objectivity, reliability, and validity of deep learning enabled bioimage analyses. *eLife* 9: e59780

Sharma N, Flaherty K, Lezgiyeva K, Wagner DE, Klein AM, Ginty DD (2020) The emergence of transcriptional identity in somatosensory neurons. *Nature* 577: 392-398

Sommer C, Leinders M, Uceyler N (2018) Inflammation in the pathophysiology of neuropathic pain. *Pain* 159: 595-602

Subramanian N, Wetzel A, Dombert B, Yadav P, Havlicek S, Jablonka S, Nassar MA, Blum R, Sendtner M (2012) Role of Nav1.9 in activity-dependent axon growth in motoneurons. *Human Molecular Genetics* 21: 3655-3667

Sun Y, Nadal-Vicens M, Misono S, Lin MZ, Zubiaga A, Hua X, Fan G, Greenberg ME (2001) Neurogenin Promotes Neurogenesis and Inhibits Glial Differentiation by Independent Mechanisms. *Cell* 104: 365-376

Svenningsen ÅFEX, Colman DR, Pedraza L (2004) Satellite cells of dorsal root ganglia are multipotential glial precursors. *Neuron Glia Biology* 1: 85-93

Takahashi K, Yamanaka S (2006) Induction of Pluripotent Stem Cells from Mouse Embryonic and Adult Fibroblast Cultures by Defined Factors. *Cell* 126: 663-676

Tasdemir-Yilmaz OE, Druckenbrod NR, Olukoya OO, Dong W, Yung AR, Bastille I, Pazyra-Murphy MF, Sitko AA, Hale EB, Vigneau S *et al* (2021) Diversity of developing peripheral glia revealed by single-cell RNA sequencing. *Developmental Cell* 56: 2516-2535.e2518

Teixeira MJ, da Paz MGdS, Bina MT, Santos SN, Raicher I, Galhardoni R, Fernandes DT, Yeng LT, Baptista AF, de Andrade DC (2015) Neuropathic pain after brachial plexus avulsion - central and peripheral mechanisms. *BMC Neurology* 15: 73

Usoskin D, Furlan A, Islam S, Abdo H, Lönnerberg P, Lou D, Hjerling-Leffler J, Haeggström J, Kharchenko O, Kharchenko PV *et al* (2015) Unbiased classification of sensory neuron types by large-scale single-cell RNA sequencing. *Nature Neuroscience* 18: 145-153

Velkey JM, O'Shea KS (2013) Expression of Neurogenin 1 in Mouse Embryonic Stem Cells Directs the Differentiation of Neuronal Precursors and Identifies Unique Patterns of Downstream Gene Expression. *Developmental Dynamics* 242: 230-253

Wainger BJ, Buttermore ED, Oliveira JT, Mellin C, Lee S, Saber WA, Wang AJ, Ichida JK, Chiu IM, Barrett L *et al* (2015) Modeling pain in vitro using nociceptor neurons reprogrammed from fibroblasts. *Nat Neurosci* 18: 17-24

Wang D, Lu J, Xu X, Yuan Y, Zhang Y, Xu J, Chen H, Liu J, Shen Y, Zhang H (2021) Satellite Glial Cells Give Rise to Nociceptive Sensory Neurons. *Stem Cell Reviews and Reports*

Warwick RA, Hanani M (2013) The contribution of satellite glial cells to chemotherapy-induced neuropathic pain. *European Journal of Pain* 17: 571-580

Woodham P, Anderson PN, Nadim W, Turmaine M (1989) Satellite cells surrounding axotomised rat dorsal root ganglion cells increase expression of a GFAP-like protein. *Neuroscience Letters* 98: 8-12

Xiao D, Deng Q, Guo Y, Huang X, Zou M, Zhong J, Rao P, Xu Z, Liu Y, Hu Y *et al* (2020) Generation of self-organized sensory ganglion organoids and retinal ganglion cells from fibroblasts. *Science Advances* 6: eaaz5858

Zhang L, Xie R, Yang J, Zhao Y, Qi C, Bian G, Wang M, Shan J, Wang C, Wang D *et al* (2019) Chronic pain induces nociceptive neurogenesis in dorsal root ganglia from Sox2-positive satellite cells. *Glia* 67: 1062-1075

Zhao C, Teng EM, Summers RG, Ming G-l, Gage FH (2006) Distinct Morphological Stages of Dentate Granule Neuron Maturation in the Adult Mouse Hippocampus. *The Journal of Neuroscience* 26: 3

Zirlinger M, Lo L, McMahon J, McMahon AP, Anderson DJ (2002) Transient expression of the bHLH factor neurogenin-2 marks a subpopulation of neural crest cells biased for a sensory but not a neuronal fate. *Proc Natl Acad Sci U S A* 99: 8084-8089

7 Appendix

7.1 Supplementary figures

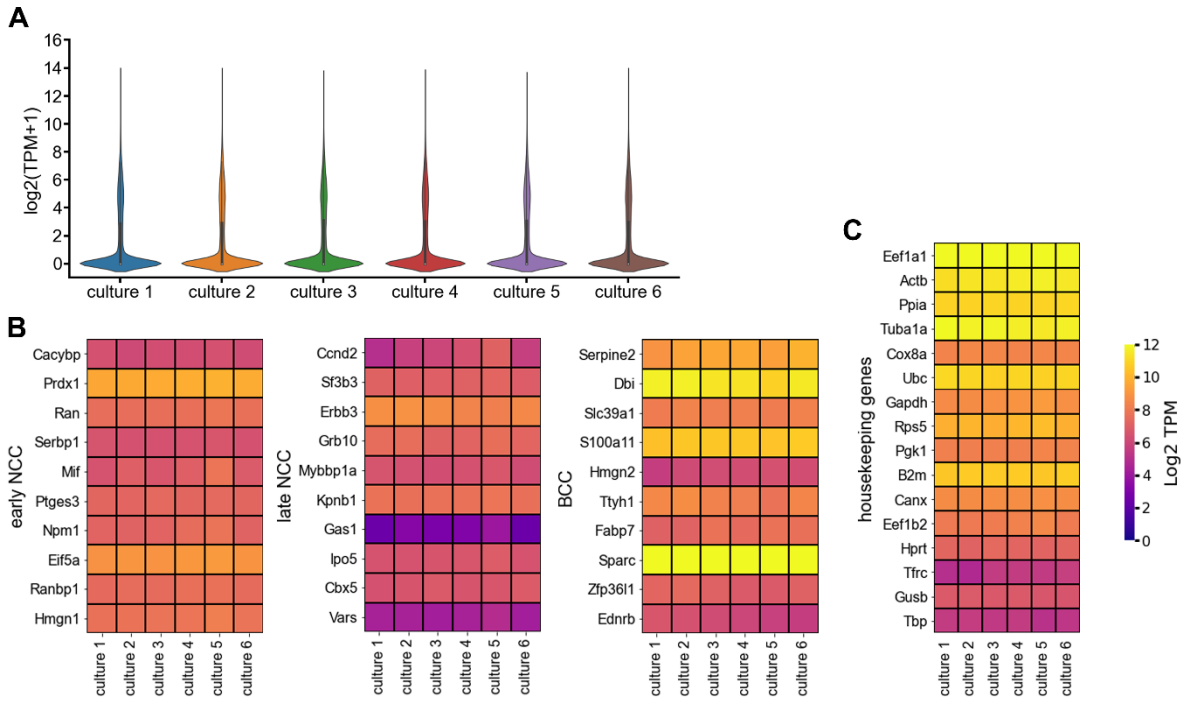

Figure S1. Sensory progenitor markers expressed at similar levels to housekeeping genes. (**A**) TPM count distribution for biological replicates of RNA sequenced 7 d old DRG cell culture shown as violin plots. (**B**) Heatmap of transcriptomic expression in 7 d old DRG cell culture of top 10 differentially expressed genes in early and late NCC (neural crest cells), and boundary cap cells (BCC) (Faure *et al.*, 2020), (**C**) and of housekeeping genes. Scale bar: Log_2 transcripts per million (TPM). DRG, dorsal root ganglia.

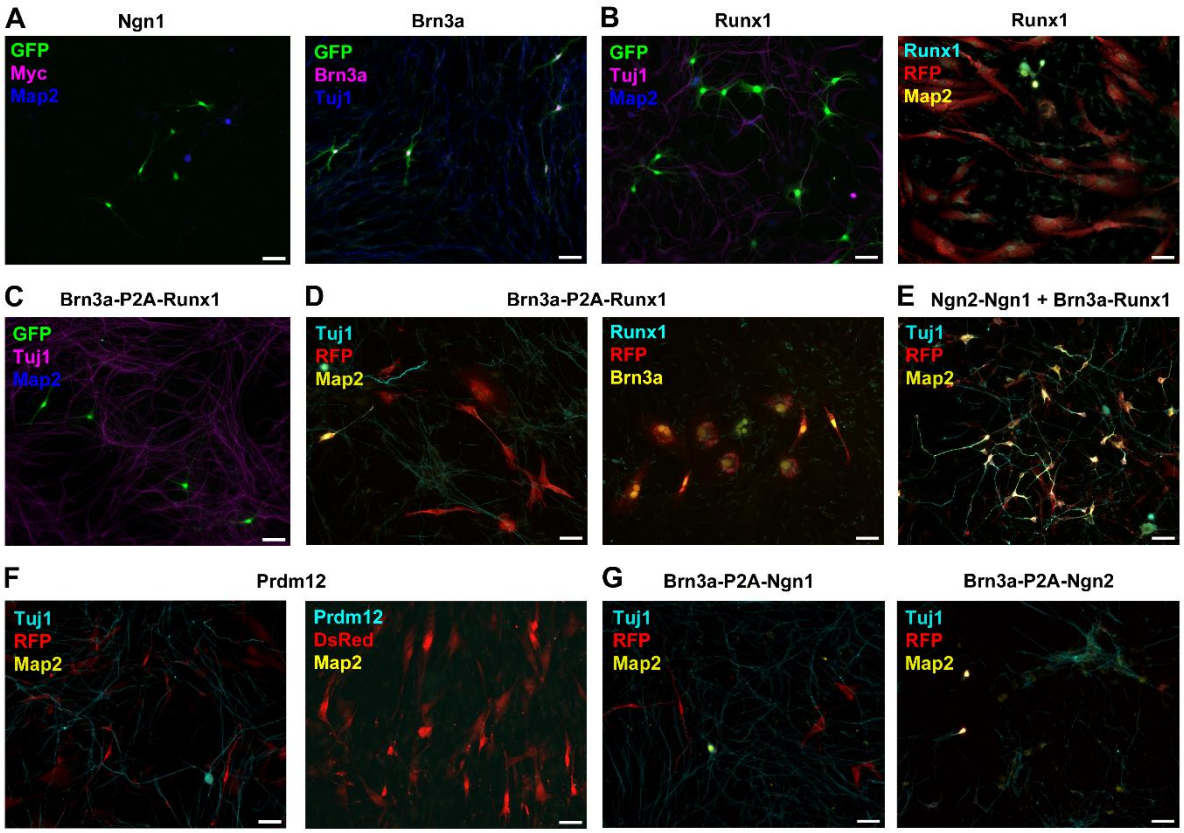

Figure S2. Retroviral vectors with no effect on gSP cells. Representative images of sensory progenitor-like cells infected with retroviral vectors at 7 dpi. (**A-C**) ^{IRES}GFP or (**B, D-G**) ^{IRES}DsRed (stained: RFP) served as infection markers. The neuronal markers βIII-Tubulin (Tuj1) and Map2 were used to visualize if a neuronal phenotype was induced. gSP cells were transduced with retroviral vectors expressing indicated transcription factors. Vectors were tested for expression of (**A**) Neurog1 (Ngn1, Myc-tagged, magenta) or Brn3a (magenta), (**B**) expression of Runx1 (cyan), (**C-D**) coexpression of Brn3a and Runx1, (**E**) also in combination with the Ngn2-P2A-Ngn1 vector, (**F**) expression of Prdm12 (cyan), (**G**) and coexpression of Brn3a with Neurog1 or Neurog2. Scale bars: 50 µm. DsRed/RFP, red fluorescent protein; GFP, green fluorescent protein; gSP, glial sensory progenitor.

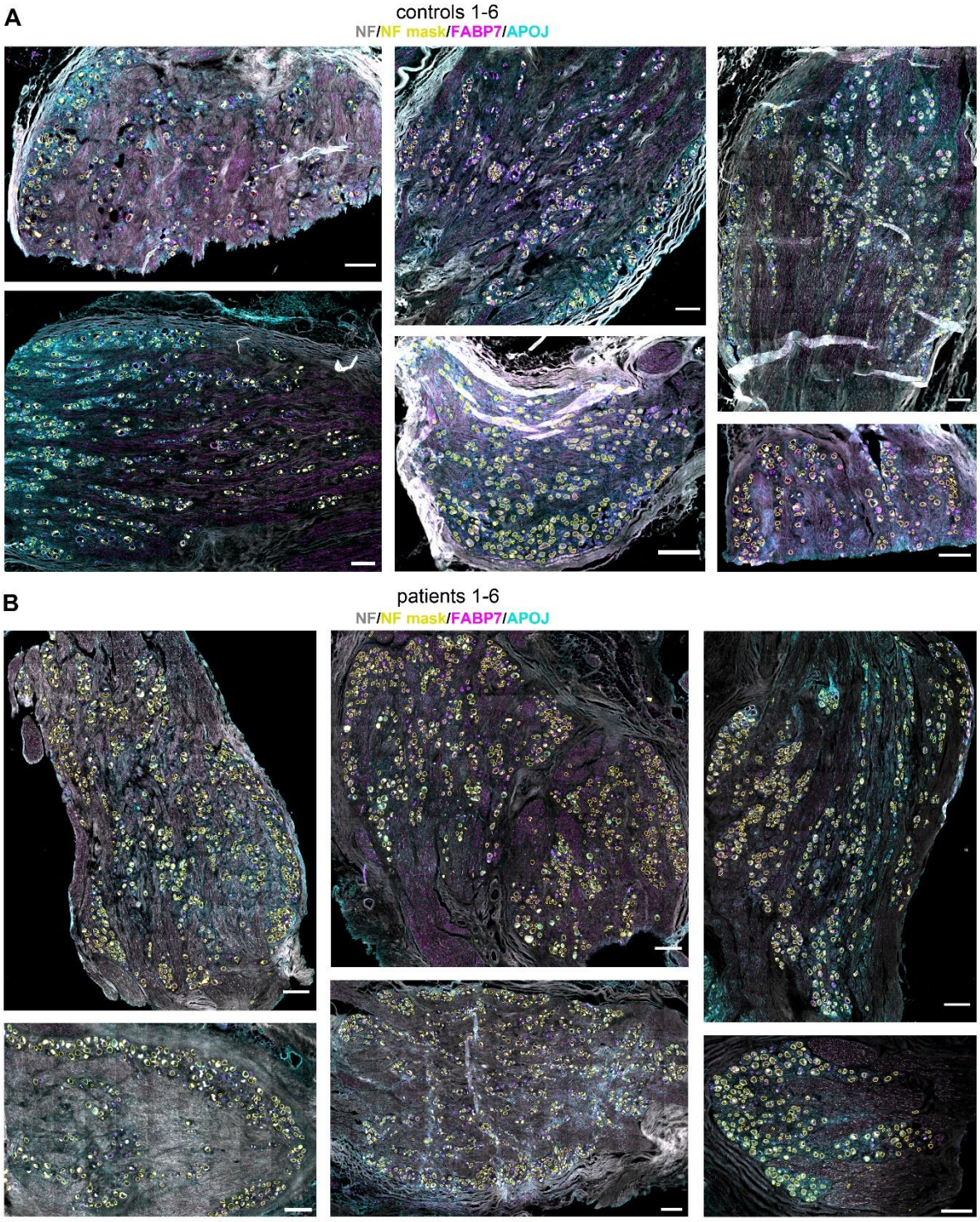

Figure S3. NF segmentation of DRG sections. Representative NF segmentations (NF mask, yellow) for each (**A**) control or (**B**) patient DRG. SGCs are labelled with FABP7 (magenta) and APOJ (cyan), neurons with NF (gray). The control DRG marked with an asterisk was excluded from image analysis due to bad signal to noise ratio. Scale bars: 400 µm. APOJ, apolipoprotein J; DRG, dorsal root ganglia; FABP7, fatty acid binding protein 7; NF, neurofilament; SGC, satellite glial cell.

7.2 List of figures

7.3 List of supplementary figures

7.4 List of tables

7.5 Abbreviations

ACSF	artificial cerebrospinal fluid
AITC	allyl-isothiocyanate
APOJ	apolipoprotein J
BCC	boundary cap cells
CL	contralateral
CNS	central nervous system
DIV	day *in vitro*
DL	deep learning
dpi	days post infection
DRG	dorsal root ganglia
DsRed/RFP	red fluorescent protein
EGF	epidermal growth factor
FABP7	fatty acid binding protein 7
FCS	fetal calf serum
FGF	fibroblast growth factor
GFAP	glial fibrillary acidic protein
GFP	green fluorescent protein
GS	glutamine synthetase
gSP	glial sensory progenitor
HEK293	human embryonic kidney-293
IL	ipsilateral
IoU	intersection over union
iPSCs	induced pluripotent stem cells
MMLV	moloney murine leukemia virus
NCC	neural crest cells
NF	neurofilament
NGF	nerve growth factor
Ngn1	Neurog1
Ngn2	Neurog2
NNA	neuron-near area
NPA	neuronal polygon area
OGB1	Oregon Green 488 BAPTA-1 AM
PBS	phosphate-buffered saline
PFA	paraformaldehyde
PLL	poly-L-lysine hydrobromide
PNS	peripheral nervous system
RefSeq	reference sequence
RMP	resting membrane potential
ROI	region of interest
SGC	satellite glial cell
SNI	spared nerve injury
TPM	transcript per millions
TTX	tetrodotoxin

7.6 Statement of individual author contributions to results in figures

Figure	**Author,** Responsibility decreasing from left to right			
4.1	In vitro reprogramming of glial cells from adult dorsal root ganglia into nociceptor-like neurons			
4	Annemarie Schulte	Nastaran Esfahani	Thorsten Bischler	
5	Annemarie Schulte	Niels Köhler	Nastaran Esfahani	Nina Schukraft
6	Annemarie Schulte			
7	Annemarie Schulte			
8	Annemarie Schulte			
9	Annemarie Schulte			
10	Annemarie Schulte			
11	Annemarie Schulte	Enrico Leipold		
S1	Annemarie Schulte	Thorsten Bischler		
S2	Annemarie Schulte			
4.2	Unbiased analysis of cellular plasticity in the dorsal root ganglion after peripheral nerve injury			
3	Annemarie Aue	Annemarie Schulte		
12	Annemarie Schulte	Annemarie Aue	Hannah Lohner	
13	Annemarie Schulte	Annemarie Aue	Hannah Lohner	
14	Annemarie Schulte	Annemarie Aue	Hannah Lohner	Johannes Degenbeck
4.3	Glial cells in human DRG after plexus injury			
15	Annemarie Aue	Johannes Degenbeck	Annemarie Schulte	
16	Annemarie Schulte	Johannes Degenbeck	Felicitas Schlott	
17	Annemarie Schulte	Johannes Degenbeck	Felicitas Schlott	
18	Annemarie Schulte	Johannes Degenbeck	Annemarie Aue	Felicitas Schlott
S3	Annemarie Schulte	Annemarie Aue	Johannes Degenbeck	Olivia Rudtke

Explanations:

The study in chapter 4.1 was conducted with the help and previous data of listed authors. The collaborative studies in chapter 4.2 and 4.3 were conducted together with Annemarie Aue (Postdoc) and medical/biomedical students (Hannah Lohner, Johannes Degenbeck, Felicitas Schlott), who particularly contributed to data collection, annotation, and analysis, under supervision by the supervisors Prof. Heike Rittner and PD Dr. Robert Blum.

I also confirm my primary supervisor's acceptance.

Annemarie Schulte 21.10.2022, Würzburg

Doctoral Researcher's Name Date Place Signature

7.7 List of publications

Schulte A, Lohner H, Degenbeck J, Segebarth D, Rittner H, Blum R, Aue A (2022) Unbiased analysis of the dorsal root ganglion after peripheral nerve injury: no neuronal loss, no gliosis, but satellite glial cell plasticity. Pain

Schulte A, Blum R (2022) Shaped by leaky ER: Homeostatic Ca2+ fluxes. Frontiers in Physiology 13

Bieniussa L, Kahraman B, Skornicka J, **Schulte A**, Voelker J, Jablonka S, Hagen R, Rak K (2022) Pegylated Insulin-Like Growth Factor 1 attenuates Hair Cell Loss and promotes Presynaptic Maintenance of Medial Olivocochlear Cholinergic Fibers in the Cochlea of the Progressive Motor Neuropathy Mouse. Frontiers in Neurology 13

Schulte A, Bieniussa L, Gupta R, Samtleben S, Bischler T, Doering K, Sodmann P, Rittner H, Blum R (2022) Homeostatic calcium fluxes, ER calcium release, SOCE, and calcium oscillations in cultured astrocytes are interlinked by a small calcium toolkit. Cell Calcium 101: 102515

Karl F, Colaço MBN, **Schulte A**, Sommer C, Üçeyler N (2019) Affective and cognitive behavior is not altered by chronic constriction injury in B7-H1 deficient and wildtype mice. BMC Neurosci 20: 16-16

7.8 Affidavit

Affidavit

I hereby confirm that my thesis entitled ***In vitro* reprogramming of glial cells from adult dorsal root ganglia into nociceptor-like neurons** is the result of my own work. I did not receive any help or support from commercial consultants. All sources and / or materials applied are listed and specified in the thesis.

Furthermore, I confirm that this thesis has not yet been submitted as part of another examination process neither in identical nor in similar form.

Place, Date Signature

Eidesstattliche Erklärung

Hiermit erkläre ich an Eides statt, die Dissertation ***In vitro* Reprogrammierung von Gliazellen aus adulten Spinalganglien in Nozizeptor-ähnliche Neurone** eigenständig, d.h. insbesondere selbständig und ohne Hilfe eines kommerziellen Promotionsberaters, angefertigt und keine anderen als die von mir angegebenen Quellen und Hilfsmittel verwendet zu haben.

Ich erkläre außerdem, dass die Dissertation weder in gleicher noch in ähnlicher Form bereits in einem anderen Prüfungsverfahren vorgelegen hat.

Ort, Datum Unterschrift

7.9 Acknowledgements

A PhD thesis is a long journey, with hopefully more ups than downs, a lot of scientific ideas, excitement, frustrations, creativity, effort, development, and, finally, success. I could not have done it without all the help I got from the people who have supported and accompanied me during this journey. Here, I would like to express my biggest gratitude to all of you.

First of all, PD Dr. Robert Blum, you are a true mentor, and I am forever grateful for your support and guidance. Thank you for showing me the way, but also the freedom to find my own. Your advice is always spot on. Thank you for being so honest, enthusiastic, supportive, helpful, and resourceful with research questions and so much more.

A special thanks also to you, Prof. Heike Rittner, for giving me the opportunity to start my career in pain research. Your clinical view helps to put the work of a neurobiologist in perspective, so I always know what I am working for. Thank you for integrating me in your research group. Your positive feedback and knowledge have been most helpful.

I would also like to express my gratitude to Prof. Dr. Erhard Wischmeyer for supporting my study as my 3rd supervisor. Moreover, big thanks Prof. Enrico Leipold from Lübeck, for teaching me important practical and theoretical electrophysiology skills and giving me useful feedback. Many thanks to Prof. Carmen Villmann and her group, for trusting me with their cell culture. And, very special thanks to Michi and Hilde, your technical assistance from getting the right water to having a high-quality retrovirus was so important for the success of my work.

In addition, I would like to thank the Graduate School of Life Science for teaching me useful scientific and transferable skills, and the Studienwerk Villigst for the financial and personal support during my PhD. Your scholarship has given me a new perspective for my career and for me as a person. The research focus on "Resilience factors in pain research" was most interesting, especially the interdisciplinary exchange of ideas.

Next, I would like to thank all my collaborators and colleagues. Especially, Annemarie Aue, Niels Köhler, Johannes Degenbeck, and Hannah Lohner, without you all this work would not have been possible. Thank you for the wonderful cooperation and assistance. A huge thanks to all the coming and going members of AG Blum: Feli, Niels, Rohini, Teresa, Yvi, Dennis, Cora, Manju, and Corinna. You are such a nice and intelligent group; I really enjoy working with you. Big thanks to AG Rittner, you are fun to work, discuss and spend evenings with. And lastly, to all my friends from the Institute of Clinical Neurobiology, you were great companions on my way to a doctorate. I wish you all the best for your future.

Last but not least, I want to thank my friends and family. Most of all, Phil, my partner and fiancé, your humor, intelligence, and support got me through this important time of my live. Also, our cats Nala and Morty, who we got right at the beginning of my PhD. They were so helpful in keeping the spirits up not only during the PhD, but also during the Corona times.

Thank you all!